POLARIZED ABSORPTION SPECTRA OF PURINES AND PYRIMIDINES

Thesis by

Robert Farrell Stewart

In Partial Fulfillment of the Requirements

For the Degree of

Doctor of Philosophy

California Institute of Technology

Pasadena, California

1963

Αρχιμήδει

δσίως

ζήτημα τοῦτυ

ACKNOWLEDGMENTS

I am grateful to Professor Norman Davidson for his counsel and guidance during my graduate studies here at the Institute. This gratitude cannot be overstated. I wish to thank Dr. Karst Hoogsteen for his cooperation and advice in the crystal work; I am indebted to Dr. Walter Huber for his many helpful suggestions concerning the various mathematical derivations throughout this investigation. The cooperation of the Geology Department in the optical measurements of the crystals is appreciated. Mr. William Schuelke's advice made the crystal grinding and microspectrophotometer possible. I am thankful to Dr. Philip Seeger and to Mr. Robert Deverill for their help in writing computer programs.

My general education at the Institute has been an invaluable experience. I am particularly grateful for the association with and advice from Professors Hammond and Robinson, and Dr. Vinograd. The National Institute of Health predoctoral fellowship and Institute Scholarship, which supported me in this work and general studies, are appreciated.

My wife's love and encouragement during my graduate studies have been invaluable; progress could not have been made without her.

ABSTRACT

The polarized absorption spectra for single crystals of 1-methylthymine and 9-methyladenine and a hydrogen-bonded complex of the two have been determined. A microspectrophotometer was constructed to carry out these measurements. A technique for preparing thin sections of the single crystals with thicknesses down to 10^{-5} cm has been developed. Special attention has been given to intensity determinations for the several ultraviolet absorption spectra.

TABLE OF CONTENTS

INTRODUCTION

Polarized absorption spectra of single crystals of purines and pyrimidines are of interest for the understanding of absorption spectra, exciton phenomena and other electronic properties of nucleic acids (27, 5, 24). With favorable crystal symmetries, dichroism measurements are useful for resolving absorption bands and for assigning transition dipole moment directions to electronically allowed transitions. To date ultraviolet dichroism measurements of purines and pyrimidines have been sparse. Lyons (14) measured the polarization of the first three ultraviolet transitions of 2-amino-4-chloro-6-methylpyrimidine and of 2-chloro-4,6-dimethylpyrimidine. No dichroic ratios were reported, but the polarizations were used for tentative assignments of the transitions. Seeds (25) has reported that the first near ultraviolet absorption band for 2-hydroxy-4,6-dimethylpyrimidine is in the plane of the pyrimidine ring. The experiments described in this research are polarization studies of single crystals of 1-methylthymine, 9-methyladenine, and a hydrogen bonded complex of 1-methylthymine and 9-methyladenine.

The major difficulty in polarization experiments of this nature lies in the preparation of thin, single crystals with cross-sectional dimensions of several hundred microns and a controlled thickness between 10^{-4} and 10^{-5} cm. In the past the technical problem has

been overcome by selecting thin sublimation flakes, by crystallizing between two closely spaced plates, or by doping a transparent crystal with a chromophore which has a fixed orientation. These techniques have limitations; sublimation and crystallization usually result in only one predominant form and doping is restricted to special cases. When one can prepare thin sections ($\sim 10^{-5}$ cm) of single crystals in an arbitrary crystallographic plane, then this technical problem in crystal absorption is solved.

This research has attempted to solve the problem by optically polishing tractable crystals to thicknesses of 10^{-5} cm. The technique has not been perfected for the general problem, but a major development in this direction has been made. Microtomes, developed for thin sectioning in electron microscopy, have made this advance possible. A crystal was optically polished by slicing small sections off of it with a diamond knife; the small increment of advancement for the microtome arm allowed grinding of the crystals down to a thickness of 10^{-5} cm without destroying it. The faces of the crystal were kept parallel by observing interference colors of the crystal between crossed polaroids. One crystal, the hydrogen bonded dimer, was successfully polished in a direction perpendicular to the molecular layers. The method employed in this work can probably be extended to the polishing of soft organic crystals in a direction of choice.

In the past the accuracy of intensity measurements from absorption has been difficult to estimate due to thickness uncertainty and reflections off the crystal face. Both problems have been given special attention in this work. Thicknesses were determined by measuring the retardation of the crystal under crossed Nicols with a quartz wedge and monochromator. The relatively high birefringences of the crystals made thickness measurements possible with the retardation technique. The reflection coefficients of the crystal can be calculated by the well known Fresnel formulae if the refractive indices and the absorption coefficients at the wavelengths of interest are known. The refractive indices in an absorption band of interest for the research presented here were calculated from a two term Drude dispersion expression with the help of a Kramers-Kronig transformation.

A more accurate method of determining crystal thickness has recently been applied in the field of crystal spectroscopy (1). By means of double beam interferometry Bree and Thirunamachanbran were able to determine the thickness of single naphthalene crystals within 5% to 10%. The interferometer technique made it possible, moreover, for these workers to determine refractive indices up to the edge of the absorption band.

Recent theories on the molecular interactions in crystals (4),

"aggregates" (15), and polymers (27, 24) have led to the concern for accurate intensity measurements. In particular, the nucleic acid polymers have interesting intensity behavior when compared to the nucleotide monomers. For DNA the observed absorptivity per nucleotide is 0. 6 of the sum of the molar absorptivities of the individual nucleotides in solution. The decrease in intensity (hypochromism) is uniform over the first ultraviolet absorption band of the polymer and shows no apparent wavelength shift from the overall absorption band due to the several nucleotide monomers. The phenomenon of hypochromism in the nucleic acids has been a subject of theoretical interest for the last few years. Tinoco and, independently, Rhodes have presented a first order dispersion theory to account for the intensity behavior of polynucleotides. In the absence of exchange, the perturbation interaction is coulombic; the potential energy operator has been expanded to give the first non-zero matrix elements. These elements are of a transition dipole-dipole interaction type. Therefore the geometry of the several, ordered nucleotides in the polymer is an important factor for determining the intensity behavior. There is a remote possibility that a good theory will make it possible to draw some conclusions about the base sequence in a nucleic acid from its hypochromism.

The crystalline purine and pyrimidine derivatives studied in this research are approximations to polynucleotides and are expected

to have similar interactions between chromophores. By determining transition dipole moment directions for the various absorption bands and by knowing the crystal structure one can test the Tinoco or Rhodes theory for intensity behavior in polymers. In practice, however, this work did not realize a rigorous test of the theory. Several sources of error led to intensity uncertainties of from 10% to 40%. Furthermore, only the transition dipole moment directions for the first ultraviolet absorption bands could be determined. As a result the experiments were limited to a qualitative comparison with the theory.

THE MICROSPECTROPHOTOMETER

General Description. The microspectrophotometer consists of a magnetically stabilized, high pressure xenon arc, two monochromators in tandem, a modified polarizing microscope, and a photomultiplier tube, the voltage of which is amplified by an A.C. coupled amplifier. A schematic drawing of the optical system is shown in Figure 1. The light source is continuous with an ultraviolet output, which is relatively flat from 400 mμ to 300 mμ. Below 300 mμ the output intensity falls off; at 225 mμ the intensity is too low to be of practical use. The instrument is ordinarily operated with a half-band width of 3.3 mμ. The spectral purity of the monochromatic light is sufficiently good to measure transmissions of one part in 10^5 at 270 mμ. The monochromatic light, reflected onto an aperture with a front surface aluminum mirror, has a total convergence angle of 13°. Because of the relatively high dielectric constants of the crystals, the incident light is essentially parallel to the normal of the crystal face. A Glan-Thompson polarizing prism is between the mirror and the aperture. The crystal is mounted over a selected, movable aperture (usually 50 μ in diameter); a second aperture of the same diameter serves as a reference. (The apertures move across a rotatable stage.) The light signal, detected with a photomultiplier tube, is chopped every two seconds with a slow turning, saw toothed wheel. The one-half

Figure 1. Schematic optical diagram of the microspectrophotometer.

XA	Xenon arc light source
H	Stainless steel housing
EM	Stabilizing electromagnet
L_1	Collimating lens
QP	Dispersive quartz prisms
L_2	Focusing lens
W	Light chopping wheel
S_1	Entrance slit of grating monochromator
M_1, M_3	Front surface, plane mirrors
M_2	Focusing mirror
G	Grating
S_2	Exit slit of grating monochromator
L_3	1:1 imaging lens
P	Polarizing prism
A	Aperture

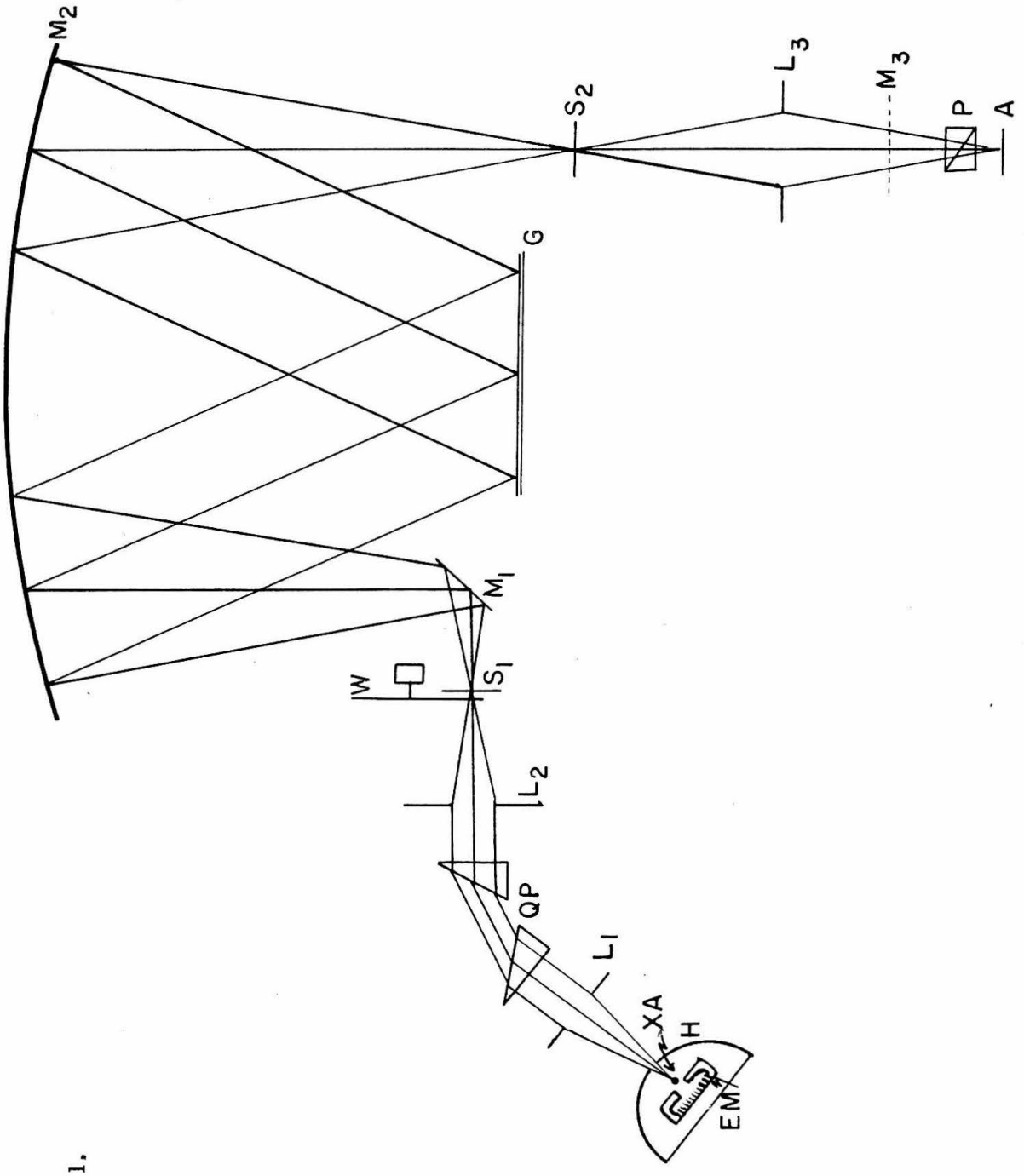

Figure 1.

cycle A. C. signal allows the filtering out of the higher frequency noise for high gain amplification and, moreover, eliminates the problem of D. C. drift. The A. C. signal is read on an oscilloscope grid; the smallest detectable absorbance is .02 units. The gain of the amplifier limits the high absorbance measurements to 5 at 270 mμ and to 3 at 230 mμ. A detailed discussion of the construction and operational features of the instrument is given below.

Components and Construction. The microspectrophotometer was constructed with two monochromators in tandem with near matched f-numbers in the ultraviolet. The premonochromator is a Bausch and Lomb quartz prism monochromator, Catalog No. 232. The instrument has two 30-60 quartz prisms which are symmetrically placed on a variable drum. As shown in the figure, the prisms have corresponding faces which are nearly perpendicular to the optic axis of the instrument. The two focusing lenses, which are crystalline quartz cut perpendicular to the optic axis, are mounted on racks and pinion gears, which have calibrated drums to correct for the chromatic aberration of the lenses. The focal lengths and diameter of the lenses are matched; these lengths were measured with a 436 mμ mercury arc line. They agree within 0.1 mm. The calculated linear dispersion, assuming near perpendicular incidence at 250 mμ is 4 mμ/mm. The focal lengths and f-numbers in the ultraviolet region

are listed in Table I. The values were calculated from the indices of refraction of quartz (9) and the diameter of the lenses, which are the entrance and exit pupils of the optical system. The device is mounted on a cast iron base which has three feet for vertical adjustment. The light source stands at the focal point of the entrance lens. The entrance slit of a second monochromator is placed at the focal point of the exit lens in the premonochromator.

TABLE I

λ = 436 mμ		f = 150.8 mm	
λ(mμ)	N_∞	f(mm)	f/no.
361	1.5635	148.3	4.8_3
330	1.5697	146.7	4.7_8
303	1.5770	144.8	4.7_2
275	1.5875	142.2	4.6_3
257	1.5962	140.2	4.5_7
245	1.6047	138.2	4.5_0
231	1.6140	136.1	4.4_3

The second monochromator is a Bausch and Lomb 500 mm focal length grating monochromator, Catalog Number 33-86-45-58. The grating is 100 mm X 100 mm grazed in the first order ultraviolet with 600 grooves/mm. The monochromator has a dispersion of 3.3 mμ/mm and an equivalent aperture ratio of f/4.4. The instrument was operated with the slits set at 1 mm. The wavelength drum

readings were calibrated with a low pressure mercury arc. Several strong lines from 4358 Å to 2537 Å were selected. The calibrated drum is accurate to within .5 mμ. Rocking the premonochromator back and forth 5 mμ about a mercury line, while the grating was fixed, attenuated the signal by a factor of about a hundred.

The light source is a 500 watt Osram xenon arc which approximates a point source. The arc is powered with a D. C. generator at 21 amps and 20 volts across the poles. To remove fluctuations in the D. C. generator seven 12 volt batteries are in parallel with the circuit, in a trickle charge configuration. The lamp is mounted on a ½-inch transite block and housed in stainless steel sheet metal. The transite base is perforated with 7/16-inch holes to allow cooling of the lamp with a blower. A 5 mm hole in the metal housing is centered about the optic axis of the instrument; the point source was assumed to be 1 mm above the cathode pole tip. The 5 mm aperture is a limiting stop for an f/4 instrument. So that a magnified image of the source can be projected onto a wall, a second aperture is situated at right angles to the light path. A low frequency jumping of the plasma about the burrs on the cathode pole created a serious difficulty with the arc. The problem was solved by placing near the cathode a weak magnetic field, which forces the plasma to sit on a particular burr at a minimum potential. The magnet is composed of two soft iron tips, held by an iron core, which is wound 200 times with 30 gauge enamelled copper

wire. The magnet draws several miliamps from two 1½-volt dry cells in series. The field strength is controlled by a 100 ohm variable resistor. When one edge of the parabolic image of the plasma is aligned along the axis of the poles, the arc is generally stable. In order to find the most stable configuration it is necessary to rotate the arc about its pole axis in the presence of the magnetic field. The arc usually has to be readjusted after several hundred hours of use.

The image of the source on the exit slit of the monochromator is focused by a stationary, fused quartz lens onto a small aperture. The lens, designed to minimize spherical aberration for one to one imaging, has a focal length of 9 cm for 260 mμ light. An iris is placed over the lens so that the angle of convergence can be varied. At full aperture the lens is f/4.4 and can be reduced to f/35. For normal operations the total angle of convergence is 13°. Incident light thus enters the crystal at a maximum angle of 6.5° with respect to the normal. The relatively high dielectric constants of the crystals bend the rays to angles of approximately 3.5° with respect to the normal. For the usual cases studied the light may be considered to have perpendicular incidence upon the crystal face. For more critical measurements the iris can be reduced, but with some loss of intensity.

Figure 2 is a photograph of the microspectrophotometer; it excludes the light source and monochromators. A front surface aluminum mirror reflects the incident light onto a small aperture. The

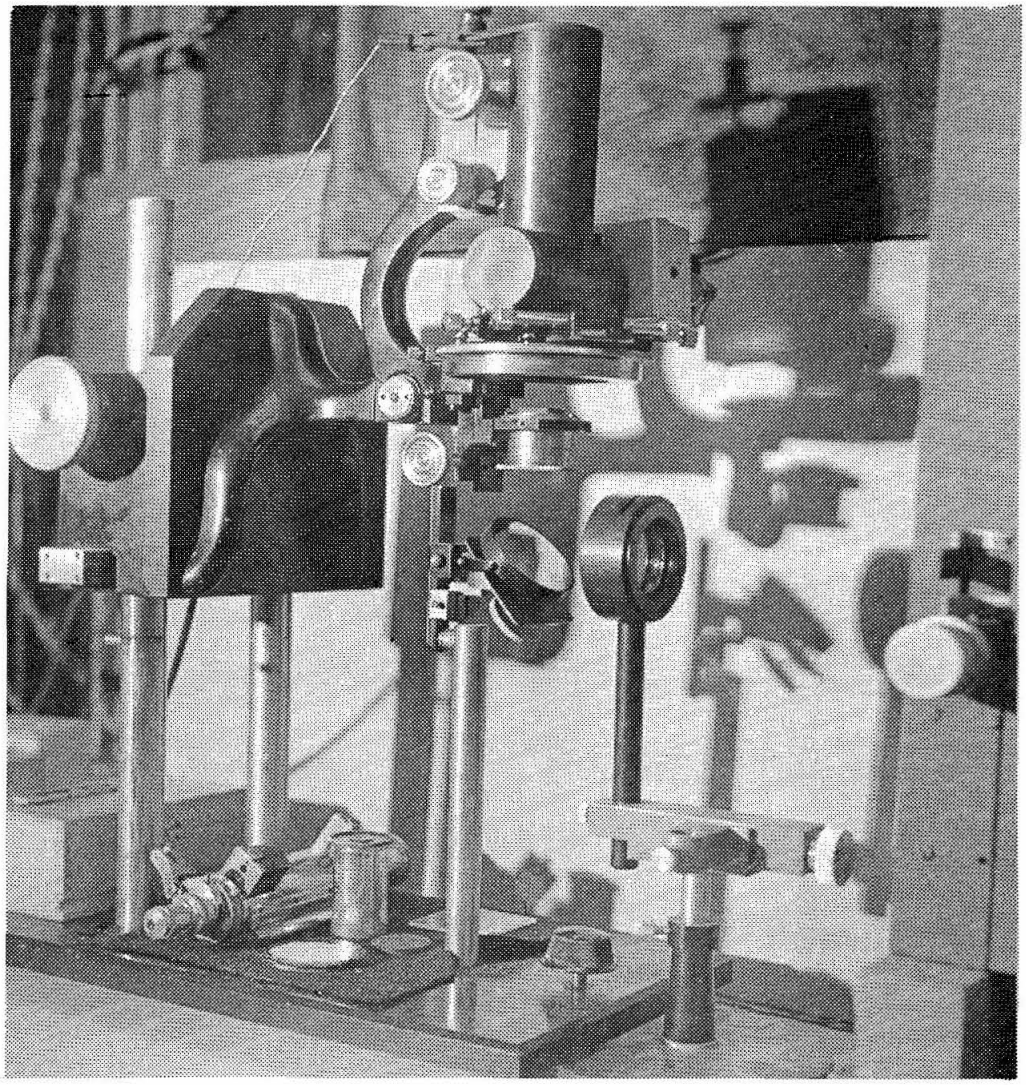

Figure 2. The microspectrophotometer. The premonochromator and light source are not visible. A panel on the grating monochromator is seen on the extreme right. See text for details.

mirror is attached to an adjustable yoke by two inset pins whose axis runs parallel to the plane of the mirror. Fine adjustment of the mirror about this axis is accomplished with a thumb screw and spring fixed to the yoke. The yoke's axis, which runs perpendicular to the inset pins, is attached to a fixed post with a flat-head pin. A small set screw and spring attached to the post permits a fine adjustment of the mirror about the yoke's axis.

A used, modified Leitz polarizing microscope completes the instrument. The Nicol polarizer and conoscope were removed, and a Glan-Thompson polarizing prism mounted in place of the Nicol. The transmission of the prism compared to air was recorded on a Cary Model 14 spectrophotometer from 360 mμ to 220 mμ. At 300 mμ the transmission is 17.5% and monotonically decreases to 2.5% at 220 mμ. The Glan-Thompson prism was rotated until it crossed the analyzer of the Leitz microscope. This rotation places the electric vector in a north-south position. The direction of vibration of the polarizer was also determined by extinguishing reflected light from a glass plate near Brewster's angle. The eccentricity of the polarized light was never determined, but a lower limit was established from transmission measurements of a crystal whose dichroic ratio is at least 38:1. An amplitude ratio of 28:1 was computed; thus the out of plane component, from an intensity point of view, is probably no more than one part in 800.

The base of the microscope was rotated to a 90° position with respect to the body tube and bolted to a mounting block, to which is attached a pinion gear box. Two fixed posts, one of which has a rack, provide support for the microscope. The mounting block is held to one post by a tight spring and to the other post through the gear box, which has a brake (See Fig. 2). The rack and pinion allows one to correct for the chromatic aberration of the 1:1 imaging lens. This correction is made by moving the microscope along the posts to a region of maximum signal for a particular wavelength. The two supporting posts and the mirror post are bolted to a rectangular stand which is supported by three adjustable feet.

The rotatable stage on the microscope is calibrated in one degree units. The center piece is fitted with a new disc which has a 1/16-inch hole in the middle. Mounted on the stage is an American Optical mechanical stage with lateral and to and fro motion; respective vernier scales read to the nearest 0.1 mm. The bulk of the mechanical stage allows rotation of the main stage only through 270°. The mechanical stage accommodates 3" X 1" X 1/8" anodized brass blocks which have two 1/16"-holes drilled in them. The two holes, aligned with the long axis of the rectangular block, are separated by 6 mm, each 3 mm off the short axis of the block. Platinum apertures are cemented over these holes. The several pairs include aperture diameters of 25 μ, 50 μ, 85 μ, and 100 μ. These, with the exception of the 85 μ aperture, are standard apertures used on electron microscopes.

The 85 μ apertures were punched out of 50 μ apertures with a sharp tungsten pick. All pairs of apertures are aligned along the long axes of the brass blocks within 50 μ. Thus for the transmission measurements, it is only necessary to move the apertures laterally with a fixed to and fro position. One of the apertures serves as a reference; the other has a crystal over it. The preparation of the crystals will be described later. The crystals are mounted on the nipple end of a cylindrical, fused quartz block. The block is supported by a small, brass sleeve with the nipple end over the aperture. A copper spring holds the brass sleeve onto the platinum disc.

A light-tight horn fits snugly over the anodized brass blocks. The horn allows free movement along the long axis of the blocks. The circular collar of the horn, one inch in diameter, is coupled to a photomultiplier housing with a tight fitting, felt ring. The felt ring restricts movement in the to and fro direction. The body tube of the microscope may be removed; a housing for an RCA 1P-28 photomultiplier tube fits in its place. A 7/16" hole at the bottom of the housing provides an adequate opening into the photomultiplier tube.

Voltage is applied to the dynodes of the photomultiplier by means of a voltage divider consisting of 80 K ohm resistors between each stage. The load resistor can be switched from 10 Meg ohms, which is built into the A. C. coupled amplifier, to 100 K ohms in parallel with the 10 Meg ohm resistor. The photomultiplier is driven

with negative voltage from a Keithley Model 240 power supply. The output signal is amplified by an A. C. coupled high gain amplifier. A Type E plug-in unit for the Type 535 Tektronix oscilloscope is an adequate amplifier; its linearity covers a range from 10 MV/cm to 0.05 MV/cm. At the entrance slit of the second monochromator a slow turning, saw-tooth wheel chops the light signal at one-half cycle frequency. The signal, displayed on a cathode ray tube, is a near square wave curve. The peak heights read to the nearest millimeter on a centimeter scale. A set of capacitors, in parallel with the load resistor of the photomultiplier tube, can be selected to filter out high frequency noise. The set ranges from 1 μf to .005 μf.

Operational Features. One major feature of the microspectrophotometer is a half cycle signal, which is used to enable filtering out the noise from high gain measurements. Most of the noise from the power supply and photomultiplier tube has frequencies larger than one hundred cycles. A capacitor which provides a response time of 0.1 seconds was selected for all measurements. Hence, even sixty cycle pickup was attenuated for the high gain measurements. The A. C. signal, with a half cycle, dark current reference, is advantageous; it eliminates the problem of D. C. drift, which is often encountered with D. C. circuit, high gain spectrophotometers.

There is essentially no problem of stray light with the two monochromators in tandem. The instrument was first compared to the Cary Model 14 spectrophotometer. The absorption spectrum of a 1 mm pyrex filter was measured from 390 mμ to 270 mμ on the Cary. At 270 mμ the absorbance was 4.92. By placing the filter over the exit slit of the second monochromator the transmission was then measured with the microspectrophotometer and the computed absorbance compared to the Cary measurement. From 340 mμ to 270 mμ, the absorbance measured with the two instruments agreed within 0.02. The signal on the oscilloscope can be read to within two percent at best. Thus absorbances less than .02 cannot be measured. (For crystal absorption the error is ± .04 absorbance units due to the correction for the quartz block.) A more critical stray light test was conducted with a 1-methylthymine crystal. A sufficiently thick section transmitted one part in ten thousand of the reference signal at 275 mμ. Putting the pyrex filter into the light path attenuated the signal beyond detection. Thus any light of wavelengths greater than 300 mμ must be less than one part in 10^5. The transmission of a Hoogsteen dimer crystal at 230 mμ was similarly tested. The transmittance was 0.01; the pyrex filter attenuated the signal beyond detection. Since the absorption of the crystal itself was an adequate filter for wavelengths from 280 mμ down to 235 mμ, stray light of wavelength greater than 240 mμ must be less than one part in 10^3. These stray light studies

indicate that absorbances as high as 5.0 at 270 mμ can be measured with confidence. It is important in the design of this system that the rated equivalent aperture of the grating monochromator not be exceeded. In our preliminary studies stray light was a major problem, because the grating was overfilled. Vignetting the grating monochromator reduced the stray light appreciably, but it was necessary to use a pre-monochromator in order to measure transmissions of the order of one part in 10^5.

The instrument was usually operated with a full scale signal on the oscilloscope for the reference aperture. The image of the source at the exit slit of the second monochromator was focused onto the reference aperture. With the 100 K ohm load resistor in parallel with the 10 Meg ohm resistor, the power supply was increased until a 60 millivolt signal appeared.

By switching out the 100 K ohms resistor a gain of 101 is introduced; a further gain of 200 can be achieved with the amplifier. (When changing the load resistor, it is necessary to reduce the capacitor in order to maintain a constant response time.) Even higher gains can be accomplished by increasing the voltage on the power supply, but this is usually impractical. Hence, the practical upper limit for transmission detection is one part in 10^5 to 10^4 at wavelengths above 240 mμ. Due to the relatively low intensity output of the xenon arc in the 240 mμ to 230 mμ region, and due also to the

absorption of the polarizer, the reference signal from the apertures used was too weak to measure transmissions less than one part in a thousand. The maximum voltage from the power supply is 1000 volts; the limit for the photomultiplier is about 100 volts per stage. At this level of gain signals were too noisy to read below 0.01 millivolts. Reference signals were about 10 millivolts. Below 230 mμ reference signals were not within a practical limit of detection.

The uncertainty of an intensity measurement is determined essentially by the smallest absolute reading on the grid over the oscilloscope tube. Gains were increased so that the largest possible reading was displayed. In this way the relative error was kept approximately constant. Every transmission measurement has a corresponding, constant absorbance error of ± .02 units. For quartz blank transmissions the crystal was dissolved off with water. Crystal absorbances have an error of ±.04 units. Intensity readings are reproducible when the apertures are moved to a position of maximum signal. The field seems to be uniform over a region 75 μ in diameter. The vernier scale on the mechanical stage is not adequate for reproducible settings. With care the apertures can be aligned so that their rotation does not change the signal.

The major limiting feature of the instrument is probably the polarizer. As mentioned earlier, the out of plane component is believed to be one part in 800 of the in plane energy. For transmissions

in the direction of weak absorption, the out of plane component is unimportant, because, at worst, only one part in eight hundred of the reference signal is removed by the principal direction of strong absorption. But for transmissions in the direction of strong absorption, the out of plane component is critical. The analysis presented immediately below shows that in the case of very large dichroic ratios, a transmission of about one part in a hundred is the limit of confidence. The error in the measured absorbance is

$$\Delta A = A\left(1 - \frac{1}{D}\right) + \log_{10}\left(\frac{I\,10^{-A} + 10^{-A/D}}{10^{-A} + I\,10^{-A/D}}\right)$$

where D is the dichroic ratio, A is the true absorbance in the direction of strong absorption, and I is the ratio of the in plane intensity to the out of plane intensity. Figure 3 is a plot of the error as a function of A for different dichroic ratios and for I = 800. From the functional behavior of the absorbance error, it is concluded, in general, that absorbances less than 2 are reliable for measurements in the principal direction of strong absorption. For crystals with a dichroic ratio of 2 or less, absorbances up to 4 can be measured within the error of ±.04 absorbance units. The situation could be improved by placing a second Glan-Thompson polarizer in series with the first. The limit of confidence is thus raised up to absorbances of about 4. However, the loss of intensity near the low wavelength region is an undesirable feature.

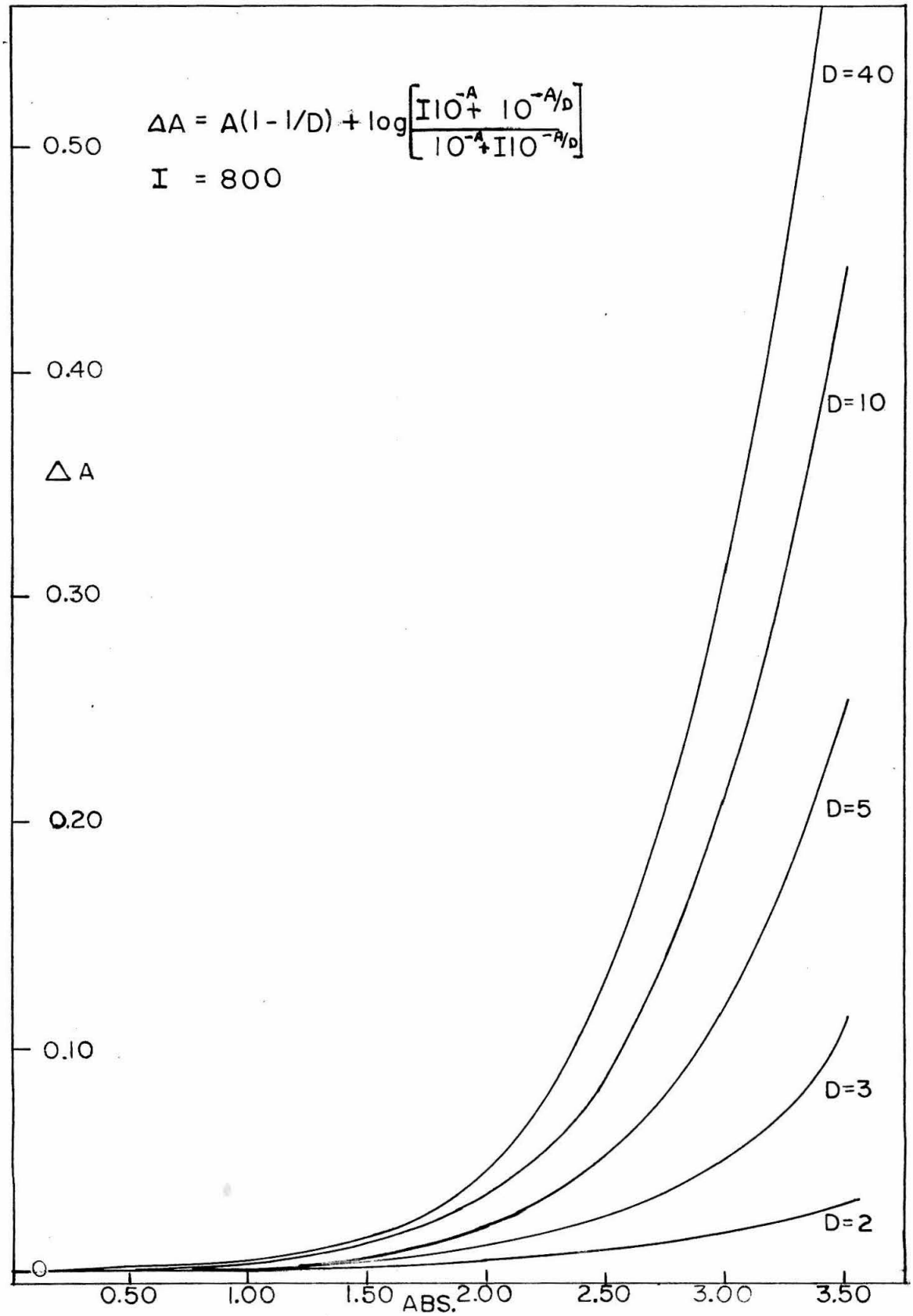

Figure 3. Absorbance error due to eccentricity of polarized light. See text for discussion.

Because of the 1 mm slit width settings for the grating monochromator, the width of the wavelength band of the output light is rather large, about 3.3 mμ. There is, therefore, an error in the absorbance measurements in a wavelength region where the absorption coefficients vary markedly with wavelength in that for a thick crystal the average wavelength of the transmitted light will be different from that of the incident light. This problem can be treated in the following way. The transmission measured is:

$$I/I_o = \frac{\int_{\lambda_1}^{\lambda_2} e^{-\varepsilon(\lambda)K} I_o(\lambda)d\lambda}{\int_{\lambda_1}^{\lambda_2} I_o(\lambda)d\lambda}$$

where $I_o(\lambda) = P(\lambda)S(\lambda)$.

$P(\lambda)$ is the intensity output function of the xenon arc plus the polarizer. $S(\lambda)$ is the slit function of the monochromator. The slit function is assumed to be triangular.

$$S(\lambda) = \frac{\lambda - \lambda_o}{\Delta\lambda} + 1 \text{ for } \lambda_1 \leq \lambda \leq \lambda_o$$

$$\frac{\lambda_o - \lambda}{\Delta\lambda} + 1 \text{ for } \lambda_o \leq \lambda \leq \lambda_2$$

$$S(\lambda) = 0 \quad \lambda \leq \lambda_1 \quad \lambda \geq \lambda_2$$

$\Delta\lambda$ is the half-band width of the monochromator. We expand $\epsilon(\lambda)$ about λ_o and $P(\lambda)$ about λ_o.

Case I.

$$P(\lambda) = P_o, \text{ a constant from } \lambda_1 \text{ to } \lambda_2$$

$$\epsilon(\lambda) = \epsilon(\lambda_o) + (\lambda - \lambda_o)\ \epsilon'(\lambda_o)$$

Then

$$I/I_o = 10^{-ak}\ \frac{\sinh^2\left(\frac{\beta\Delta\lambda}{2}\right)}{\left(\frac{\beta\Delta\lambda}{2}\right)^2}$$

or

$$A_{OBS} = A(\lambda_o) - \log_{10}\ \frac{\sinh^2\left(\frac{\beta\Delta\lambda}{2}\right)}{\left(\frac{\beta\Delta\lambda}{2}\right)^2}$$

where $\beta = 2.303\ \frac{dA}{d\lambda}\ (\lambda_o)$

Figure 4 is a plot of the correction term as a function of $\left|\frac{dA}{d\lambda}\ (\lambda_o)\right|$ for a band width of 3.3 mμ. The crystal's absorbance slope must have an absolute value of about 0.15 $m\mu^{-1}$ or less for a reliable transmission measurement. For most cases of interest the crystal had to be about 1 μ thin in order to determine meaningful toe absorption.

Case II.

$$P(\lambda) = P_o + (\lambda - \lambda_o)\ P'(\lambda_o)$$

$$\epsilon(\lambda) = \epsilon(\lambda_o) + (\lambda - \lambda_o)\ \epsilon'(\lambda_o)$$

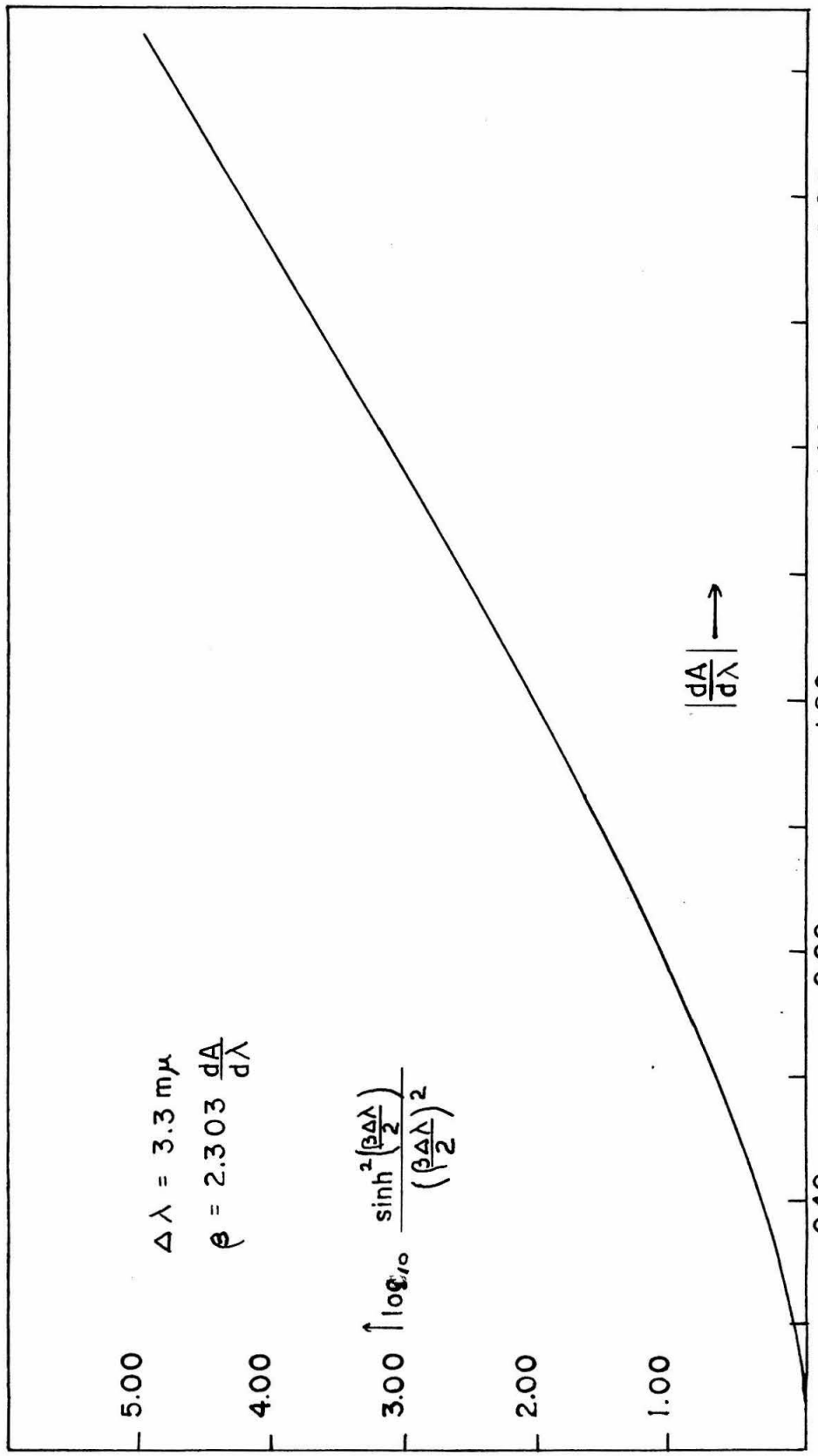

Figure 4. Absorbance correction for non-monochromicity.

$$\text{Then } I/I_o = 10^{-ak}\left\{\frac{\sinh^2\left(\frac{\beta\Delta\lambda}{2}\right)}{\left(\frac{\beta\Delta\lambda}{2}\right)^2} + \frac{P'(\lambda_o)}{2\beta P(\lambda_o)}\left[\frac{\sinh^2\left(\frac{\beta\Delta\lambda}{2}\right)}{\left(\frac{\beta\Delta\lambda}{2}\right)^2} - 2\,\frac{\sinh(\beta\Delta\lambda)}{\beta\Delta\lambda}\right]\right\}$$

The output function of the xenon arc is shown on a logarithm plot in Figure 5. The polarizer does not affect the contour down to a wavelength of about 300 mμ.

Around 300 mμ, $\frac{P'(\lambda)}{P(\lambda)}$ is $\sim 3 \times 10^{-2}$ mμ^{-1}. This is a small correction which justifies the simpler theory of Case I for establishing confidence limits.

In summary, the major advantages of the microspectrophotometer are the slow A.C. signal, which makes high gain measurements possible, and the absence of stray light to within one part in 10^5. The eccentricity of the polarized light limits transmission measurements in the direction of strong absorption, for dichroic ratios larger than five, to one part in several hundred. The non-monochromicity of the incident light limits absorption measurements to a crystal which has an absorbance change no more than 0.15 absorbance units per millimicron.

Retardation Measurements. The general principles for retardation measurements are outlined below. When a crystal is fixed with one of its extinction directions at an angle of 45° with respect to the electric vector of plane polarized, parallel light, the electric vector

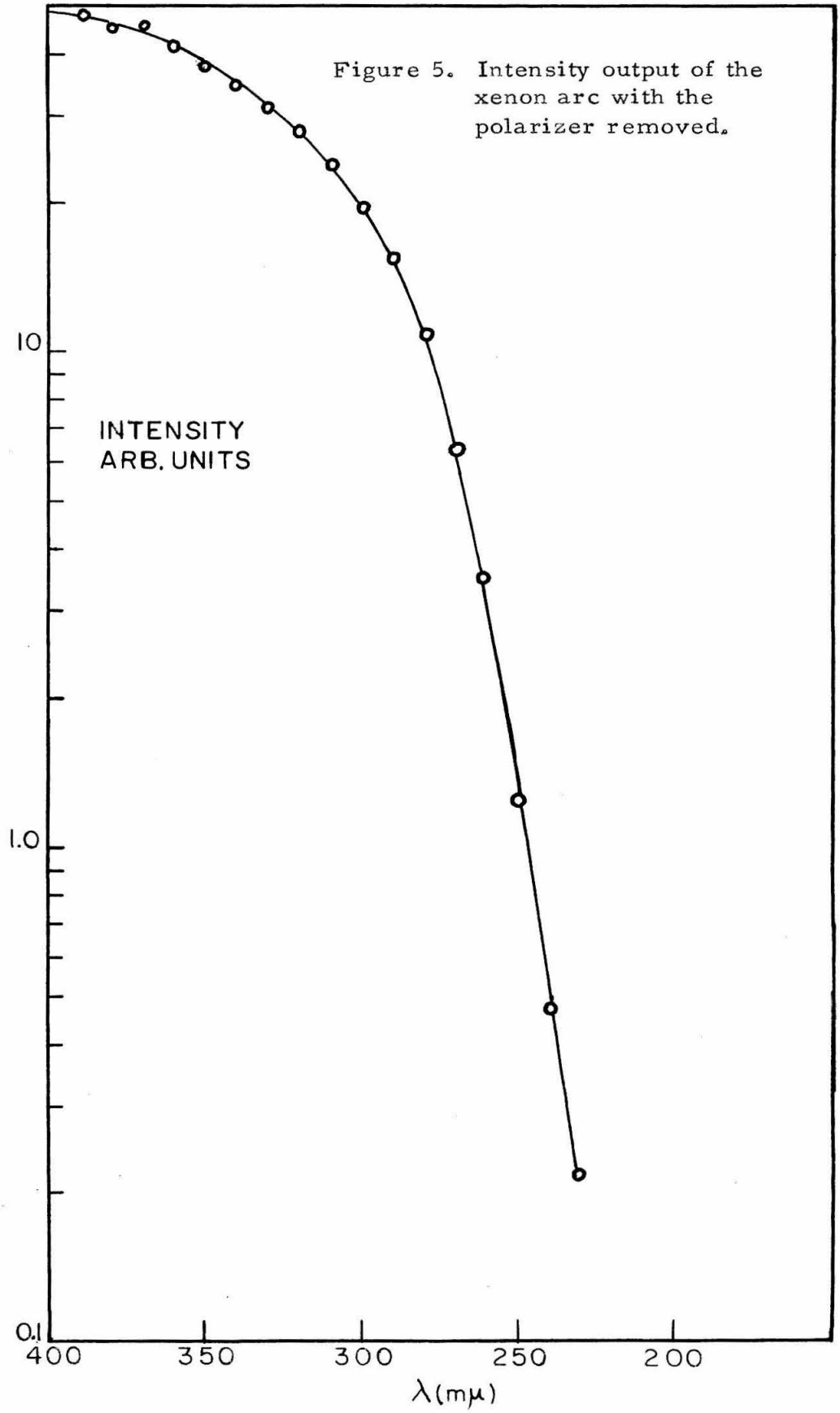

Figure 5. Intensity output of the xenon arc with the polarizer removed.

projects its amplitude equally onto the two extinction directions. As the ray proceeds through the transparent crystal, one component lags behind the other due to the different refractive indices along each extinction direction. The emerging light will, in general, be elliptically polarized. If quartz, or any other birefringent material, is placed over the crystal with extinction directions aligned, the retardation produced by the crystal will be either advanced or retarded depending on the alignment of the refractive indices of the two birefringent materials. If the high refractive index (slow ray direction) of quartz is colinear with the low refractive index (fast ray direction) of the crystal, then the quartz retards the phase difference introduced by the crystal. By using a wedge of quartz, a material of constant birefringence with varying thicknesses, it is possible to vary the advancement or retardation of the two components of the elliptically polarized light. When the total retardation of the light is some integral multiple of the wavelength for the light incident on the crystal, then the light emerges from the quartz as plane polarized light which is parallel to the plane of polarization of the polarizer. Thus the final emergent light has a plane of polarization at right angles to the vibration direction of the analyzer. A dark fringe will appear across the field of view because no light is transmitted by the analyzer.

If the crystal is removed and the quartz wedge is kept fixed, then the light passing through the wedge will be elliptically polarized

with components which will project themselves onto the vibration direction of the analyzer and will add to give a non-zero value. Thus light will appear across the field of view. The wavelength can be changed until a dark fringe appears again; at this point the retardation of the quartz is an integral multiple of the new wavelength.

Figure 6 is a two dimensional representation illustrating the retardation phenomenon discussed above. The dashed-line waves are vibrating at right angles to the plane of the paper. The wavelength for cases A and B is 589 mμ. The quartz wedge has its fast ray component over the fast ray component of the crystal. The quartz wedge advances the fast component from the crystal to one full wavelength ahead of the slow component of the crystal. For case B the resultant wave, not shown, is elliptically polarized. In case C the wavelength is 393 mμ, where the slow ray of the quartz is retarded one full wavelength behind the fast ray of the quartz.

For case A the retardation of the crystal plus the quartz wedge is 589 mμ; that is,

$$\Delta n_c t_c + \Delta n_q t_q = 589 \text{ m}\mu \qquad (1)$$

where Δn_c = the difference of refractive indices in a principal plane of the crystal; t_c = the physical thickness of the crystal; Δn_q = the birefringence of the quartz; t_q = the physical thickness of the quartz at the position of interference.

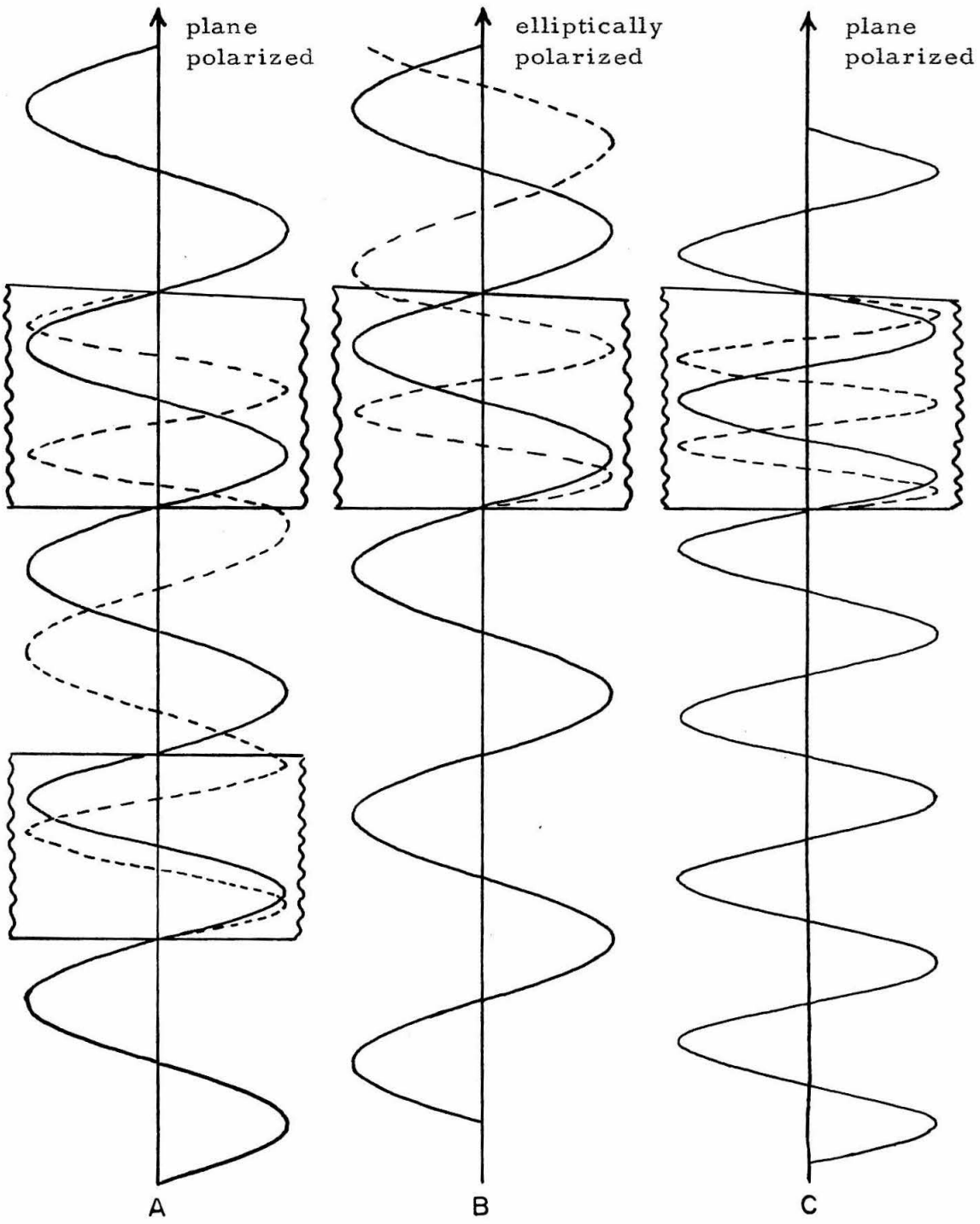

Figure 6. Two dimensional representation of retardation produced by quartz wedge and crystal.

For case C the crystal has been removed and the wavelength changed (the wedge was not moved) so that

$$\Delta n_q t_q = 393 \text{ m}\mu \qquad (2)$$

This method of measurement is somewhat simplified because Δn_q does not change with wavelength. From equation 2 we can determine $\Delta n_q t_q$, and then from equation 1, solve for the retardation of the crystal, $\Delta n_c t_c$. In this example, $\Delta n_c t_c = 196$ mμ. If the crystal has a birefringence of $\Delta n = 0.1$, then its physical thickness is $t = \frac{R}{\Delta n} = \frac{196 \text{ m}\mu}{0.1} = 1.96 \mu$. The birefringence of the crystal is measured independently; e.g., oil immersion determination of the refractive indices.

If the wedge has a thickness such that for 393 mμ light the slow ray is retarded two full wavelengths, then the total retardation is 786 mμ. In this case if the wavelength were fixed at 393 mμ, one could see that the dark fringe is a second order fringe by withdrawing the wedge and observing a second dark fringe when the thickness corresponding to the first order is in the field of view.

Orthoscopic observations with the microspectrophotometer were used to orient all crystals for retardation measurements and in spectrophotometry. A crystal could be oriented to within one degree between crossed polarizers. Retardations of the crystal were measured with a quartz wedge in the manner described above. A wavelength of

589 mμ was selected. The crystal was rotated 45° with respect to the extinction direction. A quartz wedge was inserted into the body tube at an angle of 45° with respect to the vibration direction of the analyzer. With the ocular removed so that the eye could focus on an interference fringe, the wedge was pushed in until an interference fringe bisected the image of the field. With the wedge fixed, the ocular was put in and the crystal was moved off the field of view. The reference aperture was brought into view and centered with the help of the ocular cross-hairs. The ocular was again removed and the wavelength was varied until the interference fringe bisected the field. Care was taken to know the order of the fringe; this was done by counting fringes as the wedge was slowly pulled out. Since the birefringence of quartz is constant over the visible region, the reading on the monochromator drum times the order is the retardation of the quartz wedge. Depending on the position of the slow and fast rays of the crystal, the retardation of the quartz plus or minus the retardation of the crystal is some integral multiple of 589 mμ. For most retardation measurements the first order was an adequate range. In some cases crystal retardations were larger than 100 mμ; it was then necessary to use the second or third order fringe of the quartz wedge. If the crystal retardation was larger than 589 mμ, its order was easily determined up to about fourth order. The crystal was oriented so that its fast component was coincident with the slow component of the quartz wedge. The quartz

wedge was pushed in until the zeroth order interference fringe appeared. One could recognize the zeroth order by noting that the fringe did not move when the wavelength drum was moved. When the zeroth order was found, the order of the wedge was measured. The order of the wedge is the order of the crystal. The wedge has four orders for 589 mμ. For first order work the retardation of the quartz was reproduced within 2 to 3 mμ. Ten measurements were usually made; five with added retardations and five with subtracted retardations. From an independent birefringence determination of the crystals at 589 mμ, and from the retardation measurements, the physical thickness was computed.

THE PREPARATION OF CRYSTALS

Crystal Growth. Three different crystals were studied in this work. 1-Methylthymine, Lot No. 1074, and 9-methyladenine, Lot No. 1075, were purchased from the Cyclo Chemical Corporation. The compounds were, separately, once recrystallized from water and dried at room temperature under vacuum. Monoclinic crystals of each compound were grown by evaporation of aqueous solutions at room temperature. 1-Methylthymine usually had {111} and {100} as the predominant forms and was prismatic in shape. A less predominant face is the (102). The well-developed edges were 0.4 mm to 0.7 mm. By spreading a hot solution, saturated in 1-methylthymine onto a quartz coverslip, very thin plates were obtained. The (102) face predominated. Some plates were as thin as 0.7 μ with a cross section of 0.2 mm X 0.1 mm. 9-Methyladenine crystals appeared as needles with the c-axis parallel to the needle axis and with forms {110} and {001} well developed. The {010} was a less prominent form. The crystals were 2 mm to 3 mm long and 0.2 mm to 0.4 mm along the edges of the {001} face.

In order to grow a hydrogen bonded pair of 1-methylthymine and 9-methyladenine, hereafter called the Hoogsteen dimer, equimolar quantities of the two compounds were dissolved in water. Upon

evaporation to dryness at room temperature well formed, monoclinic needles were obtained. The b-axis lies parallel to the needle axis. Forms {100}, {001} and {010} predominated. Typical dimensions were 1 cm X .4 mm X 0.2 mm.

The Technique for Preparing Thin Sections. The major problem in obtaining ultraviolet absorption spectra of single organic crystals lies in the preparation of thin sections. The compounds are typically 10 M in the crystalline state and have molar absorptivities of the order of 10^4 ℓ. mole^{-1} cm^{-1}. In order to obtain measurable absorbances, the crystals must have a thickness of the order of 10^{-5} cm. In the past investigators have had to sublime thin plates or to crystallize compounds between closely spaced, quartz plates. Up to the present, there seemed to be no satisfactory, general technique for making thin sections of single crystals with cross sections as large as 0.2 mm X 0.2 mm. However, a general technique for preparing thin sections of tractable crystals has been developed.

We first attempted to prepare a thin section by conventional slicing techniques using an ultramicrotome of the type used for preparing electron microscope specimens. This method, which is described in detail in the next paragraph, failed because the crystal, when cut, shattered into a mosaic of microcrystals.

The actual procedure was as follows. A uracil crystal, which is a layer structure (20), was coated with polyvinyl alcohol and then imbedded in a methacrylate block by polymerizing a mixture of methyl methacrylate and n-butylmethacrylate monomers around it. At this stage the crystal extinguished well under crossed polarizers. The block was oriented so that the (001) face (the plane of the molecular layers) was in the plane of the cutting edge. The block was waxed onto a rod which fits into a standard chuck for the Servall Porter-Blum microtome. With the microtome set at $\frac{1}{4}\mu$ increments the crystal was cut with a diamond knife. The sections were floated on a water-acetone solution saturated in uracil. The polyvinyl alcohol prevented the uracil from falling out of the methacrylate section. The sections were recovered by catching them on a quartz coverslip. Out of a thousand slices four were recovered. The sections often wrinkled as they were cut. Under orthoscopic observation the recovered sections extinguished, but not sharply, and appeared to have grainy surfaces. The retardation of one section was 26 mμ. From the birefringence (8), the calculated thickness was 0.15 μ. The absorbance at 290 mμ was 1.82 for $E \parallel b$ and 1.00 for $E \perp b$. From 290 mμ down to 240 mμ the apparent absorbance rose smoothly to 3 and 2, respectively. These results seemed suspicious for two reasons. In the first place the absorbance at all wavelengths is too high as compared with the solution

spectrum. In the second place the solution spectrum shows a maximum at 258 mμ and a minimum at 229 mμ. A conoscopic observation revealed that the Bxa figure was a superposition of many little Bxa figures; the isogyres were highly distorted. It was concluded that the crystal was shattered during the cutting and that a mosaic of microcrystalline regions remained. Therefore, the birefringence was low and the calculated thickness too small. The same experience was encountered for a 1-methylthymine crystal.

While repeating the same experiment with 1-methylthymine, it was observed that the crystal face remaining on the methacrylate block after sectioning seemed to be optically polished. It was reasoned that one could cut the crystal down to a very thin section on the methacrylate block by taking advantage of the microtome's small advance increments. The smallest setting on the microtome is .025 μ. After some practice and adaptations the following technique was found adequate for cutting crystals to sections as thin as 0.1 μ.

For a crystal with a thickness of 5×10^{-5} cm and cross-sectional dimensions of 10^{-2} cm, it is necessary that the two faces be parallel within 0.001 radians (4' of an arc) for the thickness to be constant within 20% across the crystal. The technique used was capable of satisfying these tolerances. It is described schematically by the following steps and accompanying figures.

Step I. Carve a small nipple out of a methacrylate block with a sharp razor blade. A nipple $\frac{1}{2}$ mm in diameter is adequate.

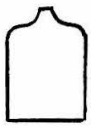

Step II. Mount the methacrylate block into an adjustable chuck (to be described below; see Figure 7) which fits the microtome. Shave off 10 to 20 μ of the plastic with a diamond knife to make an optically polished face parallel to the cutting plane.

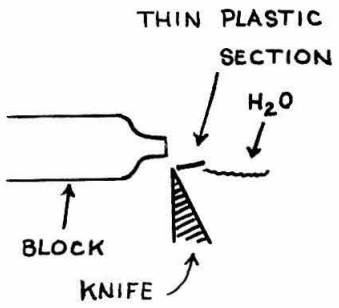

Step III. Remove the chuck from the microtome. Glue the desired, natural, developed face onto the optically polished nipple face by applying a few microliters of ethylene dichloride. It is possible to do this and maintain the crystal face parallel within 1° of the methacrylate face.

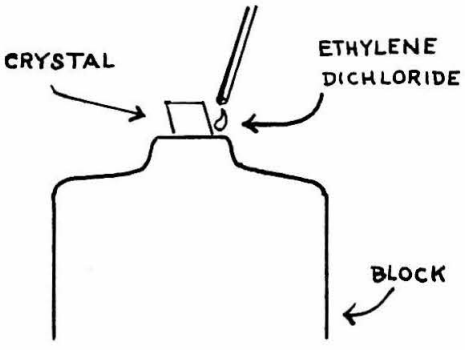

Step IV. Remount the chuck onto the microtome. The crystal face is now parallel to the cutting edge. Shave off 10 to 20 μ of the crystal; this leaves an optically polished face on the crystal.

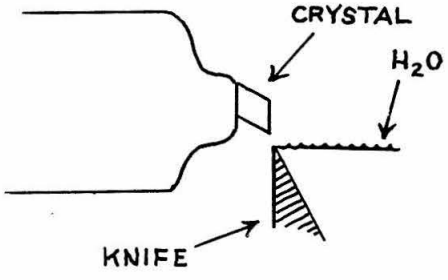

Step V. Remove the chuck and carefully cut the crystal loose from the methacrylate block with a sharp razor blade. Cover the crystal with the polished face up. The crystal should be ~ 75 μ thick at this stage in order to avoid straining the polished face while removing it from the methacrylate block.

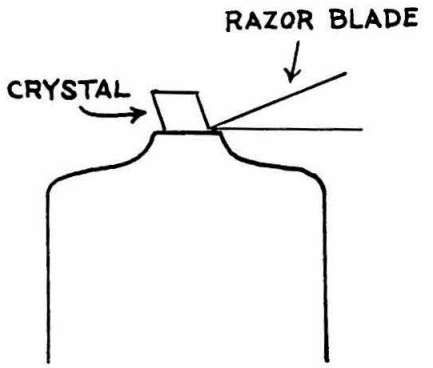

Step VI. Insert a stainless steel-methacrylate rod into the chuck, which has a quartz block mounted on it. The nipple end of the quartz block is covered with a 5 μ layer of ultraviolet "transparent" methacrylate by pipetting several microliters of a dilute solution of the polymethacrylate.

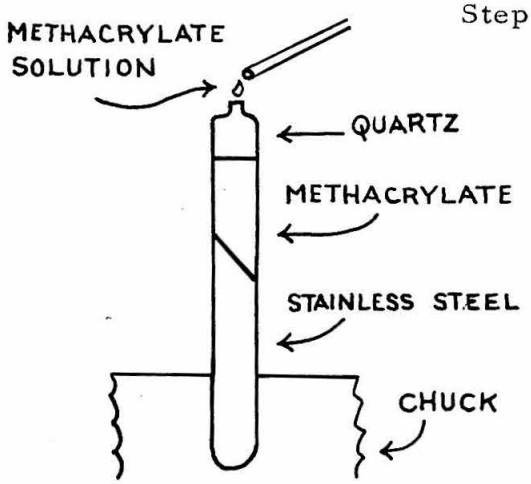

Step VII. Shave 1 to 2 μ off the 5 μ plastic film with the microtome in order to define a plane on the film which is parallel to the cutting plane. Care must be taken to align the quartz block in order to avoid grinding the quartz while polishing the thin methacrylate film.

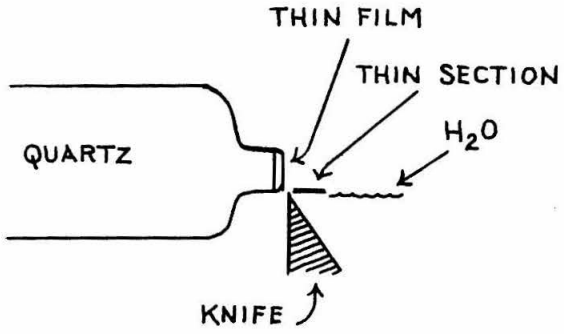

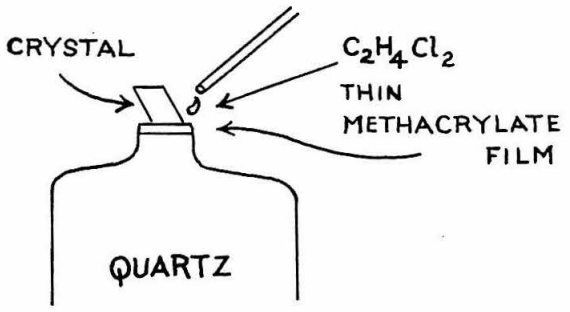

Step VIII. Mount the previously polished crystal face onto the polished thin film of methacrylate by applying a microliter of ethylene dichloride at the interface of the crystal and plastic.

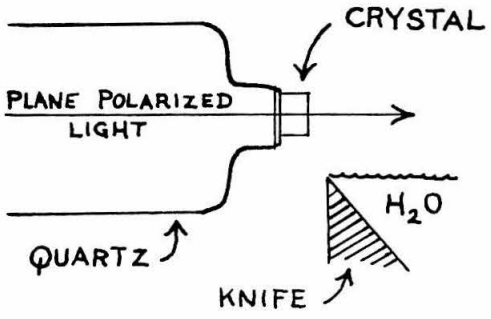

Step IX. Grind the crystal down to the desired thickness with the microtome. For the highly birefringent materials used in this work, interference colors appear when the crystal is 10 μ thick. Keep these colors uniform while grinding by adjusting the cutting angle with the chuck.

Plane polarized, white light is reflected off the face of the stainless steel-methacrylate rod which holds the quartz block. The light becomes elliptically polarized in passing through the crystal. The plane of polarization is perpendicular to the rod axis. With a crossed polaroid the interference colors of the crystal are observed. Figure 7 illustrates the optical system. These interference colors are observed during the process of grinding (Step IX) in situs with the apparatus depicted in Figure 8.

An adjustable chuck was built to move the block through small angles. Figure 7 is a sketch of the chuck. A collar attaches the main axis of the chuck to the ball joint of the microtome arm. A second collar cinches the cutting block into the chuck. Two, large-head screws fit 90° apart on the second collar. The outer perimeters of the screw heads are marked off every 3.6 degrees. The pitch of the screws is 32 turns/inch; the screws are set 1-7/32 inches out from the center of the chuck. These screws work against two other screws (springs were unsuccessful) to adjust the inclination of the cutting block with respect to the cutting edge of the knife. In principle, a displacement as small as 26" of an arc can be resolved, but due to backlash, a practical limit is about 1' of an arc.

The entire assembly of the grinding apparatus is shown in the photograph in Figure 8. The microtome advancement is controlled manually by the handle to the right of the gear box. The mounting plate

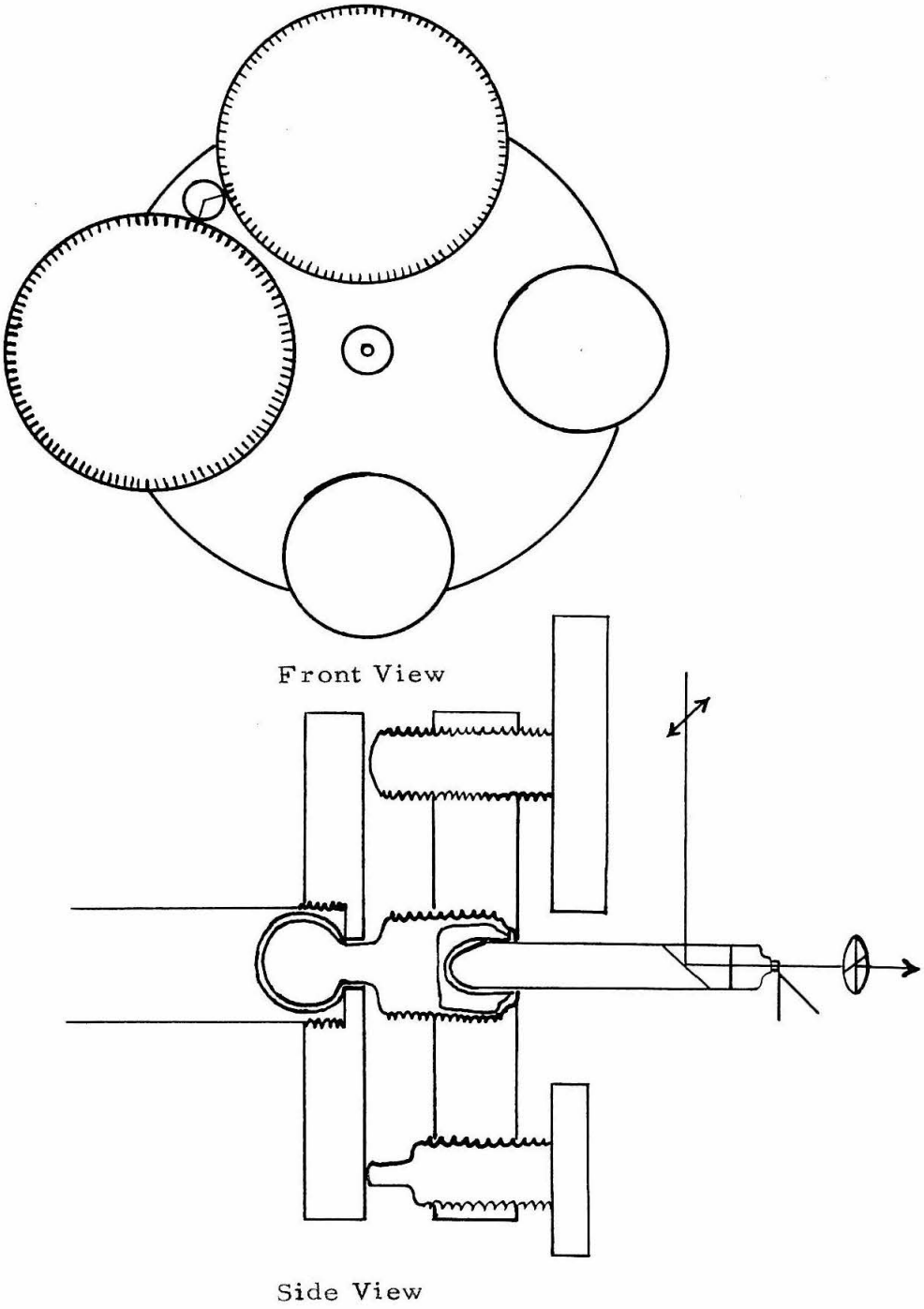

Figure 7. Chuck used for orienting crystals with respect to the cutting knife.

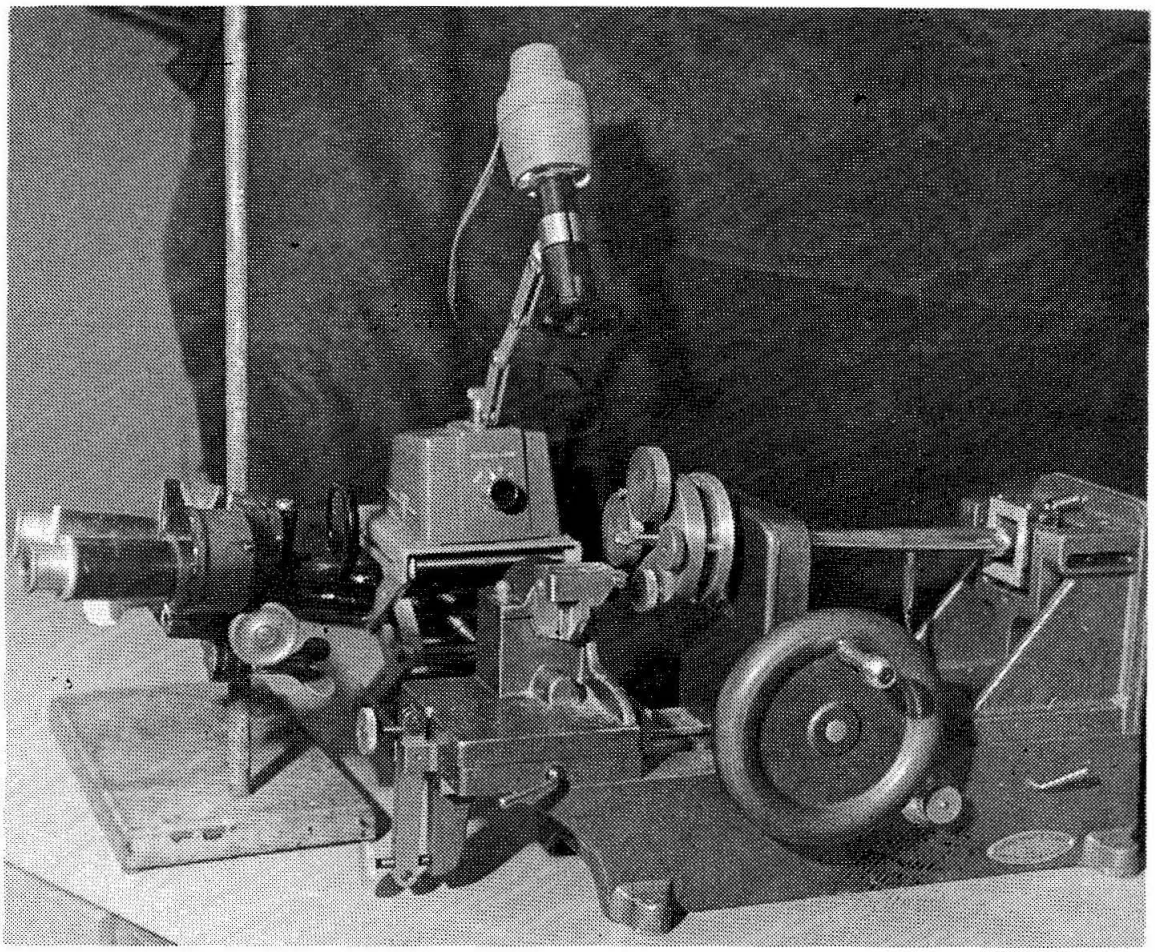

Figure 8. The total assembly of the apparatus used for grinding crystals. The diamond, not visible here, is mounted in the trough directly below the quartz block attached to the adjustable chuck. See text on pages 40 and 43 for general description.

for the knife holder is fixed while the microtome arm is advanced. The adjustable chuck is mounted on the microtome arm. The stainless steel-methacrylate-quartz cutting block is mounted in the chuck. The light source above the cutting rod is covered with a polaroid filter. A 2.5X power binocular was used to observe the crystal and the interference colors; the analyzer was usually held just in front of the binoculars.

A detailed discussion of the various steps carried out in the preparation of these thin crystal sections is found below. Following this discussion there appear some comments on the limitation of the procedure and a derivation of the absorption behavior for an optical wedge.

A methacrylate block is glued to a brass rod by wetting the block with 1,2-dichloroethane. With a sharp razor blade a small nipple of about 0.5 mm in diameter is carved at the end of the block. A face is developed on the nipple by cutting off 10 μ to 20 μ of the plastic with the microtome. A particular crystal face is then placed onto the polished face of the methacrylate. A few microliters of ethylene dichloride is added by touching the plastic edge with a small capillary. The solvent flows around the crystal and dries within a minute. In this manner the crystal is fixed to the plastic block with the crystal face parallel to the polished plastic face. About 10 μ to 20 μ of the crystal is cut off with $\frac{1}{1}$ μ to $\frac{1}{8}$ μ sections per slice in order to insure an optically polished face free of fractures or cleavages. A trough,

to which the diamond knife is attached, is filled with water up to the cutting edge of the knife. The sections which are taken off of the crystal float onto the water and dissolve. With each slice then, the crystal face is left clean. It is important, however, that the knife edge be cleaned with a soft, wooden stick about every twenty sections, for crystal grains will pile up on the knife edge and leave a scratched face on the crystal. The knife must also be free of small dirt particles which can mar the face with fine streaks. When an optical polish on one face has been achieved, the crystal is then carefully cut off the methacrylate block by stroking along the polished, plastic face with a sharp razor blade. In order to avoid strain or damage to the crystal's polished face, the crystal should be at least 75 μ thick. The crystal is transferred to a dirt free microscope slide with a tungsten pick. The polished face is placed upwards and the crystal is covered.

A stainless steel rod with its end cut 45° with respect to the rod axis is fixed to a methacrylate cylinder. One face of the methacrylate is ground to an angle of 45° with respect to its rod axis by a sander. The plastic is glued to the steel rod by wetting the plastic face with ethylene dichloride. The front face of the plastic is sanded to a flat surface near perpendicular to the rod axis. A cylindrical, brass block with a hole machined to clear the plastic by a few thousandths of an inch is used for grinding a flat surface on the front face of the plastic. The methacrylate-stainless steel rod is slipped into the

brass block to maintain a fixed orientation while grinding the plastic on an optically flat piece of glass with levigated alumina. The method insures a flat surface perpendicular to the rod axis.

A fused quartz block, with an optically polished face, is then mounted onto the flat surface of the methacrylate with a small amount of ethylene dichloride. Under crossed polarizers the quartz has no detectable strains. The cylindrical quartz block is 4 mm in diameter at the base. The front face, a small nipple 0.5 mm in diameter, is parallel to the base and has a grainy polish of several microns. The block is 3 mm thick. The total assembly is shown in the side view in Figure 7.

A thin film of methacrylate coats the front face of the quartz. This film is a specially prepared, ultraviolet transparent polymer. Methylmethacrylate and n-butylmethacrylate monomers were distilled at about 40°C under reduced pressure. A 7.2 molar ratio of methylmethacrylate to n-butylmethacrylate was heat polymerized for 24 hours at 65° after initiation with an H85 A 3 G.E. mercury arc. The absence of an aromatic catalyst such as benzoyl peroxide is necessary. Otherwise the plastic will have intolerable ultraviolet absorption. 30.4 mg of the polymer were dissolved in 10 ml of 1,2-dichloroethane, spectro grade Lot No. 34 from Eastman Organic Chemicals. A uniform layer of the solution was spread on a quartz coverslip to give a plastic film of about 10 μ. The solution evaporated and the film was pumped on with

a fore-pump for an hour. The absorption spectra of the film was recorded with a Cary Model 14 Spectrophotometer. An absorption maximum at 215 mμ with an absorbance 0.71 was obtained. Above 240 mμ the absorbance fell below .04 units. The spectrum agreed well with the literature value (29). A 5 μ layer contributes about 0.2 absorbance units at 230 mμ. 1.5 microliters of the methacrylate solution pipetted onto the nipple of the quartz block forms a 5 μ layer in good optical contact with the quartz. The refractive indices are close matching in the visible, but in the ultraviolet, undoubtedly, some reflections occur at the interface of the two materials. A reasonable estimate is a 1.5% loss in the intensity of a ray traveling from plastic into quartz.

When the methacrylate layer has dried, the assembly is mounted on the microtome and aligned by eye with respect to the knife edge. The diamond knife is set near the front face of the quartz. At 0.1 μ intervals the quartz assembly is slowly advanced until the first segment of plastic comes off the quartz nipple. Usually another 5 to 10 sections are taken. Sometimes the alignment is so poor that an edge of the quartz nipple is ground. With angular adjustments fixed, the chuck is removed from the microtome arm. The optically polished face of the crystal is placed on the polished methacrylate film. Care was taken to set an extinction direction of the crystal at approximately 45° with respect to a line colinear with the stainless steel face. The crystal

was fixed to the quartz block with a small drop of spectro quality 1,2—dichloroethane. After drying, the crystal was sectioned every 1/4 μ to 1/8 μ per slice. With polarized light optical wedge effects can be readily seen and progressively corrected with the adjustable chuck. As the crystal becomes thinner, the microtome intervals are reduced to 1/40 μ increments. The thickness can be followed down to a corresponding retardation of about 25 mμ. Below that, one must simply count the number of sections taken. When the crystal is about 1 μ thick, sectioning is very critical. By this time it is very important that the crystal is aligned and that the sectioning is done at a constant rate. If a rhythm is not established, back-lash in the gears of the microtome will cause the arm to advance too far, and this will destroy the crystal. One must learn to observe the interference colors while the crystal moves across the field of view.

When the crystal has been ground to a desirable thickness, the quartz block is removed from the methacrylate rod with a razor blade. It is often helpful to soften the methacrylate block with ethylene dichloride. The softening must be done with caution; ethylene dichloride vapors can soften the thin methacrylate film on the nipple and thus shatter the crystal. The thick quartz base provides absorption for any shock or strain which the crystal would otherwise suffer in its removal from the cutting block. A tight-fitting, brass sleeve provides support for the quartz block when placed over an aperture.

The larger the birefringence of the crystal, the more accurately one can cut the crystal to a desired thickness. If the birefringence is less than .02 the technique is of marginal use for thicknesses less than 0.7 u. One would probably have to set up an elaborate optical system and follow reflected interference fringes in order to take the crystal to thinner sections with confidence. Ultraviolet absorbing crystals which have interesting dichroism, however, usually have a birefringence larger than .02. A low birefringence poses another problem. Optical wedges can then only be observed for relatively large angles. For a typical cross-section of 0.15 mm the smallest angle which can be observed for a birefringence of .02 is .007 radians.

The problem of absorption for an optical wedge over a circular aperture is treated in the following way. The crystal is oriented so that the plane of polarization is coincident with a principal direction. The angle of the wedge is α and the thickness $t = t_o + \alpha r \cos\theta$ where t_o is the crystal thickness at the center of the aperture.

$$I/I_o = \frac{\int_0^a \int_0^{2\pi} e^{-K(t_o + \alpha r \cos\theta)} \, r \, d\theta \, dr}{\pi a^2}$$

where a is the radius of the aperture.

$$\text{Then } I/I_o = e^{-Kt_o} \frac{2I_1(K\alpha a)}{K\alpha a}$$

$$\text{or } A_{CBS} = A_{real} - \log_{10} \frac{2I_1(K\alpha a)}{K\alpha a}$$

I_1 is an imaginary Bessel function of the first kind. $K(\lambda)$ is an absorptivity constant in cm^{-1}. One can approximate K from the absorbance measurement and then calculate the correction term. The angle α may be determined by measuring retardations at two different places on the crystal. Figure 9 is a plot of $\log_{10} \frac{2I_1(K\alpha a)}{K\alpha a}$ as a function of $K\alpha a$. For $K\alpha a$ less than unity, the correction is less than .05 absorbance units. K is usually no more than 5×10^5 and a typical aperture radius is 2.5×10^{-3} cm. Thus an angle less than 0.001 radians is tolerable. For strong absorption, therefore, the crystal faces should be parallel to within 4' of arc.

All three crystals studied in this work are layer structures. The cleavage planes are always well-defined and cutting along the cleavage face poses no problem. 1-Methylthymine has no natural face perpendicular to the cleavage plane. Since the diamond knife in its present mounting is stationary, it was not possible to cut 1-methylthymine perpendicular to the (102) plane. The 9-methyladenine molecules are coplanar with (001), but the {010} form was so poorly developed that the crystal could not be mounted on the (010) face. The Hoogsteen dimer, however, does have well developed {001} and {100} forms, both of which are perpendicular to the plane of molecular layers. The crystal could be cut along the (100) to a section as thin

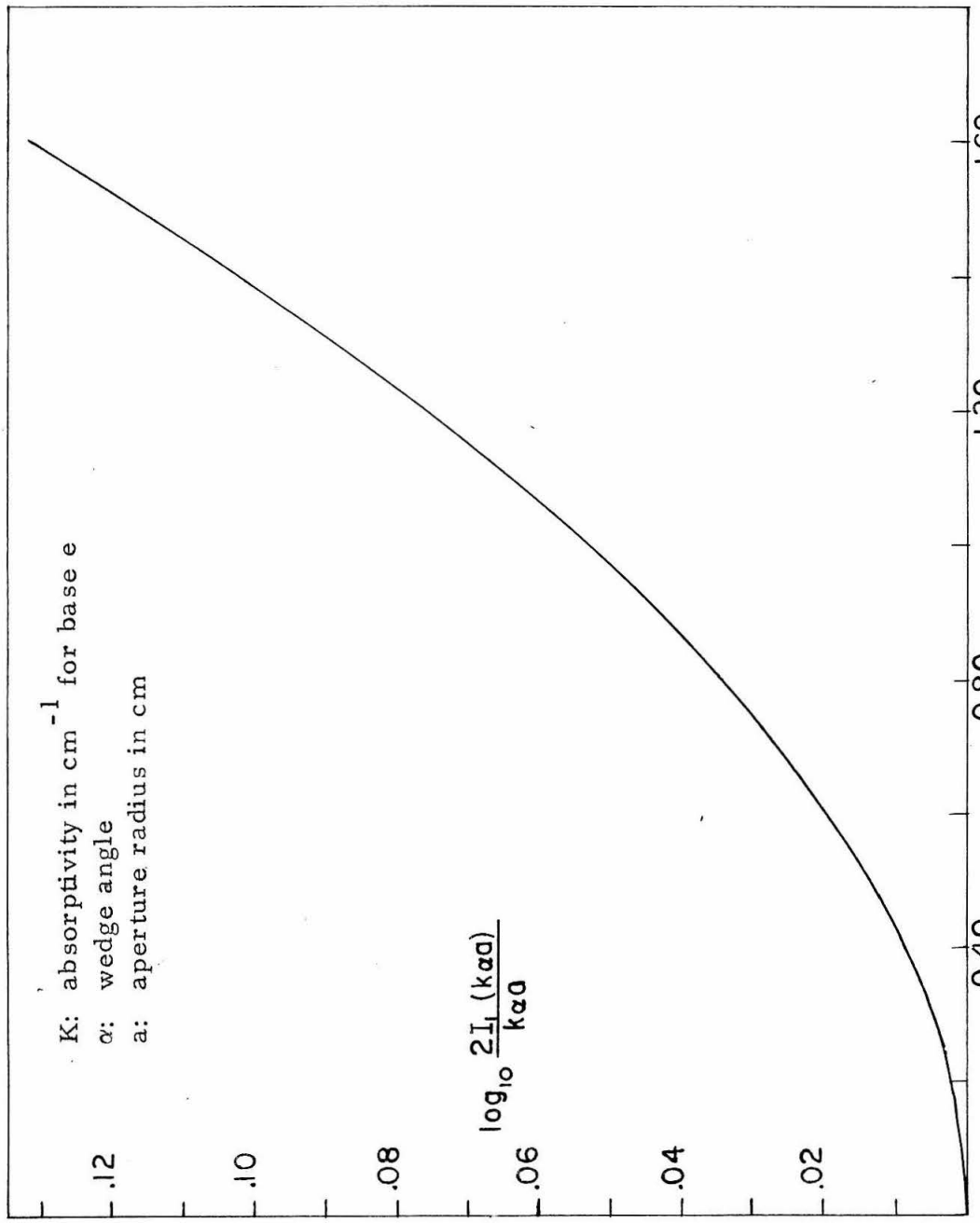

Figure 9. Absorbance error due to an optical wedge over a circular aperture.

as 1 μ without cleaving. This thickness was sufficient for the spectra reported here.

The crystal sectioning technique described above takes full advantage of the high birefringence which these purines and pyrimidines have. For the general problem of sectioning soft organic crystals, the optical system would have to be improved. Reflected light from the diamond knife and from the crystal face can provide for long, optical lever arms which are needed for accurate cutting orientations. A rotatable knife would eliminate the present necessity of having to polish a natural crystal face. I do feel, however, that with a sharp diamond knife and a microtome which has a small advance increment, one can cut soft organic crystals to thicknesses of the order of 0.1 μ.

OPTICAL PROPERTIES OF CRYSTALS AND CRYSTALLOGRAPHIC DATA

The refractive indices of the crystals were determined by oil immersion. A student model Leitz polarizing microscope was used for the measurements. A sodium D line source was simulated with a 589 mμ interference filter and a Corning glass filter, No. 3480, placed together in front of a tungsten light source. The immersion oils were calibrated with an Abbe refractometer. The indices for high refractive index oils were determined by the method of minimum deviation. 2V measurements were made with a Leitz universal stage. In the case of 9-methyladenine the 2V angle was estimated from conoscopic observation of a Bxa figure.

For the Hoogsteen dimer, assignment of the indicatrix to the crystallographic axes was made with a Weissenberg photograph. For 1-methylthymine the b-axis assignment was verified with a Weissenberg photograph. The b-axis of 9-methyladenine was assigned from morphology and from the pronounced horizontal dispersion.

The optical properties of the three crystals are listed below.

A. 1-methylthymine

NY = 1.660 ± .002 Y = b Opt(-)

NZ = 1.762 ± .002 Dispersion r < v, inclined

2V = 59.0° ± 0.2°

NX = 1.428 (calculated)

B. 9-methyladenine

NZ = 1.880 ± .002 Z = b Opt(-)

NY = 1.783 ± .002 Dispersion r < v, strong, horizontal

2V ≈ 55°

NX ≈ 1.53 (calculated)

C. Hoogsteen Dimer

NX = 1.448 ± .001 X = b Opt(-)

NY = 1.746 ± .001 Dispersion r < v, crossed

NZ = 1.783 ± .001 Z∧a = 25.4 ± 0.4

2V = 34.0° ± 0.6° β = 106° ± 1°

The crystal structures of 1-methylthymine and the Hoogsteen dimer have been determined (10). The space group and unit-cell dimensions for 9-methyladenine have been reported (11), but the crystal structure has not been determined. Crystallographic data of the three crystals are tabulated below.

1-methylthymine (10)

a = 7.351 ± .004

b = 12.091 ± .006

c = 7.602 ± .004

β = 89° 58' ± 3'

Space group: $P2_1/c$

$\rho = 1.381$ g/cm^3

z = 4

9-methyladenine (11)

a = 7.67 ± .03

b = 12.24 ± .04

c = 8.47 ± .03

β = 123° 26' ± 10'

Space group: $P2_1/c$

$\rho = 1.471$ g/cm^3

z = 4

Hoogsteen dimer (10)

$a = 8.304 \pm .002$

$b = 6.552 \pm .002$

$c = 12.837 \pm .003$

$\beta = 106° 50' \pm 3'$

Space group: $P2_1$ or $P2_1/m$

$\rho = 1.433$ g/cm^3

SOLUTION SPECTRA AND OSCILLATOR STRENGTHS

The solution spectra of 1-methylthymine and 9-methyladenine were recorded on a Cary Model 14 spectrophotometer. Both compounds, once recrystallized from water and dried under vacuum, were assumed to be pure and dry. The molar absorptivities were calculated; the results are shown in Figure 10. An equimolar mixture of the purine and pyrimidine were also recorded. This spectrum, also shown in Figure 10, is the sum of the corresponding absorptivities of 1-methylthymine and 9-methyladenine. For all solutions the pH was about 6.

For both 1-methylthymine and 9-methyladenine the respective spectra appear to consist of two bands. For 1-methylthymine the first band has λ_{max} = 273 mμ, the second band has λ_{max} = 207 mμ and the minimum occurs at λ_{min} = 238 mμ. For 9-methyladenine the first band has λ_{max} = 261 mμ, the second band has λ_{max} = 205 mμ and the minimu occurs at λ_{min} = 228 mμ.

The oscillator strengths for the several absorption bands were determined by the formula $f = 4.33 \times 10^{-9} \int a\,d\upsilon$ (22)

where a is in $l \cdot mole^{-1} \cdot cm^{-1}$ for base 10 units

and υ is in cm^{-1}.

For the second absorption bands, the area under the red side was determined and then doubled. The oscillator strengths are listed below.

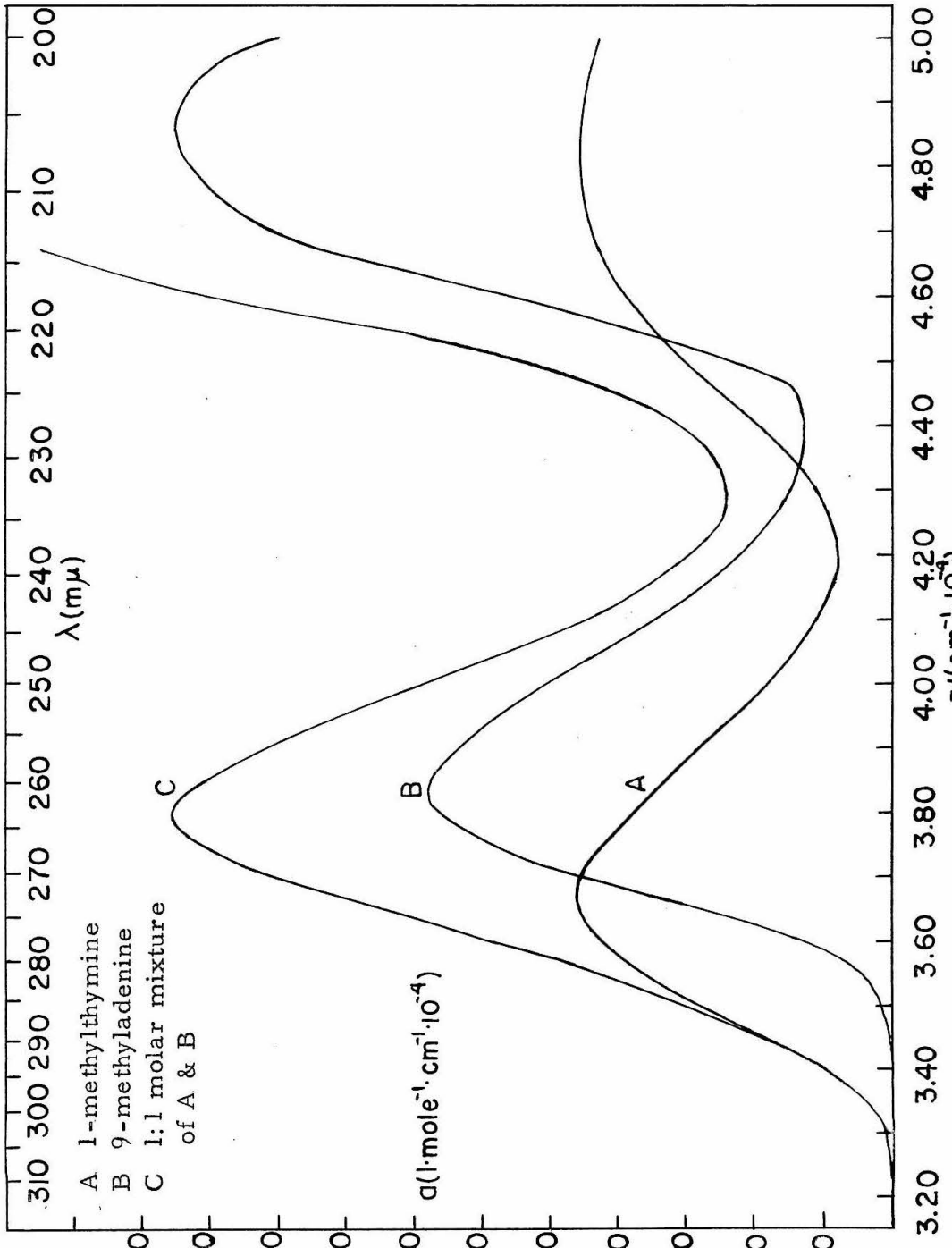

Figure 10. Solution spectra.

1-methylthymine			9-methyladenine	
λ_{max}	273 mμ	207 mμ	261 mμ	205 mμ
f	0.19	0.28	0.28	0.52

POLARIZED ABSORPTION SPECTRA OF THE SINGLE CRYSTALS

The crystal absorption spectra are presented in this section. For each substance the final results were obtained by averaging of data from several specimens of different thicknesses. It is important to record the details of the experiments so that the critical reader can evaluate their reliability and overall consistency. Corrections for reflections, eccentricity of the polarized light, convergence of the light beam, and photodamage to the crystal must be considered.

In the interest of clarity, for each substance below, our final conclusions as to the absorption spectra of the crystal are first presented. This is followed by a discussion of the experimental details and the corrections.

1-Methylthymine. The crystal absorption spectra in the (102) plane of 1-methylthymine are shown in Figure 11; the molar absorptivities are listed in Table II. One recalls that (102) is the plane of the molecular layers.

The first transmission data for 1-methylthymine were obtained from a naturally grown, thin plate. The prominent face was the (102) as determined from a conoscopic observation. The molecules lie coplanar to one another in the (102) plane. The cross-sectional

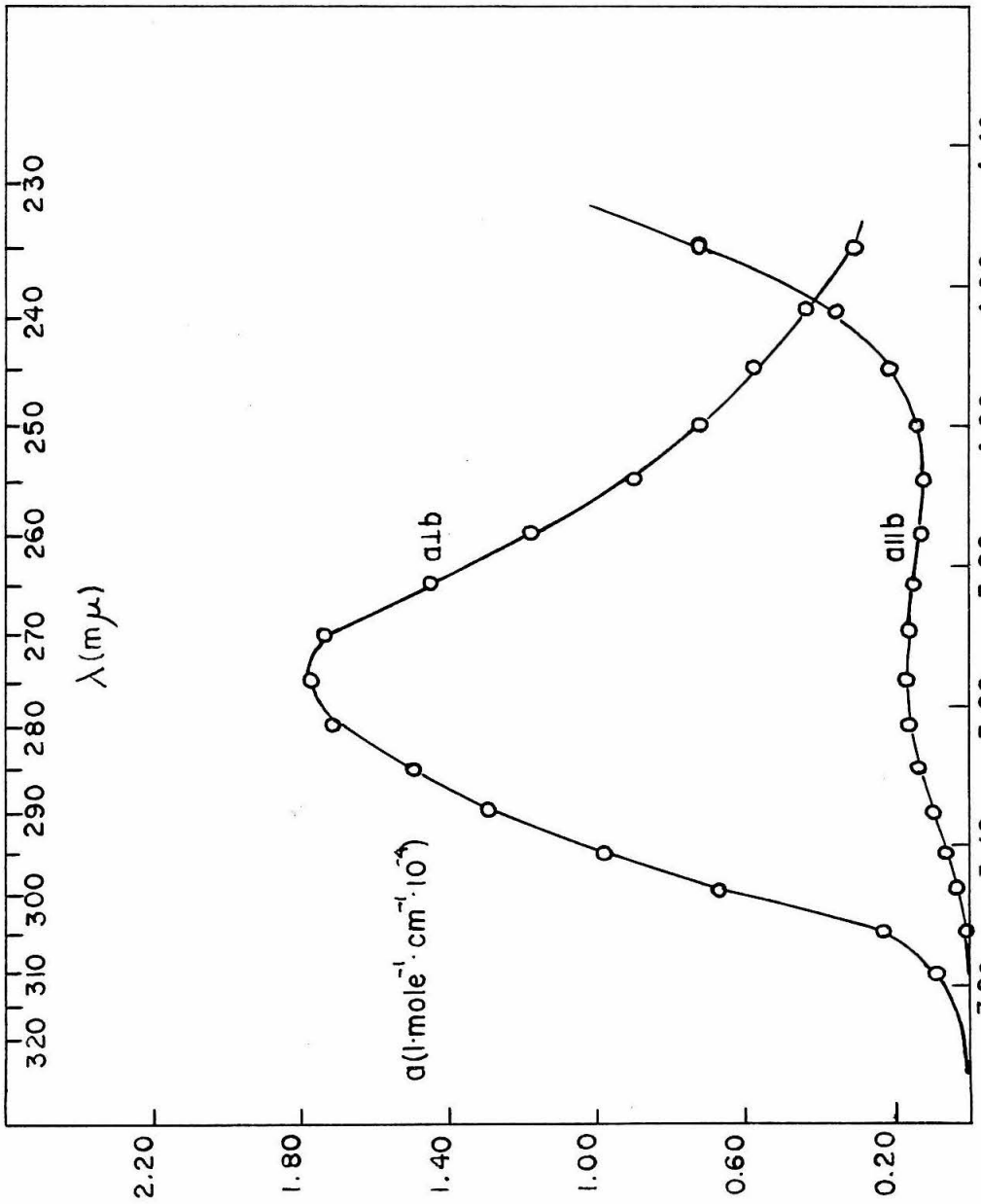

Figure 11. Absorption spectra in (102) of 1-methylthymine.

TABLE II. Molar Absorptivities of 1-Methylthymine in the (102) Plane

λ(mμ)	a ⊥ b ($l \cdot mole^{-1} \cdot cm^{-1} \cdot 10^{-3}$)	a ∥ b ($l \cdot mole^{-1} \cdot cm^{-1} \cdot 10^{-3}$)	Dichroic Ratio
305	2.2 ± 0.8	0.1 ± .09	22 ± 28
300	6.7 ± 1.7	0.27 ± .10	25 ± 16
295	9.8 ± 2.4	0.62 ± .12	15.8 ± 6.9
290	12.9 ± 3.0	1.05 ± .16	12.3 ± 4.7
285	14.9 ± 3.4	1.3 ± .2	11.5 ± 4.4
280	17.1 ± 3.8	1.6 ± .2	10.7 ± 3.7
275	17.7 ± 4.0	1.7 ± .2	10.4 ± 3.6
270	17.4 ± 3.9	1.6 ± .2	10.9 ± 4.1
265	14.8 ± 3.4	1.4 ± .2	10.6 ± 3.9
260	11.8 ± 2.8	1.3 ± .2	
255	9.0 ± 2.2	1.3 ± .2	
250	7.2 ± 1.8	1.4 ± .2	Dav. =
245	5.8 ± 1.6	2.1 ± .2	11.2 ± 1.0
240	4.4 ± 1.3	3.4 ± .3	
235	3.0 ± 1.6	7.3 ± 2.0	

dimensions of the crystal were 0.2 mm X 0.2 mm. Unfortunately, the retardation was not measured until after the transmission measurements were made. During the course of the measurements considerable photodamage of the crystal took place. The damage was detected when the crystal was observed under crossed polarizers with white light. A dark region, the size of the aperture, of much lower retardation than the rest of the crystal was evident. The retardation measurements, therefore, were not characteristic for a crystal of 1-methylthymine. The physical thickness of the crystal was regarded as too uncertain for molar absorptivity calculations.

The nature of the photodamage is probably the formation of 1-methylthymine dimers (30). It has been suggested that the 5,6 double bond opens and forms a cyclobutane ring with a near neighbor 5,6 double bond (31). The molecular orientations are favorable for the dimerization reaction. (See Fig. 18, molecules Nos. 1 and 3.) The effect of saturating the 5,6 double bond is to remove the first ultraviolet absorption band from thymine. Hence, photodamage will cause an increase in transmission of the crystal over the first ultraviolet band. To the extent that there is photodimerization taking place during a measurement, calculated molar absorptivities will be low.

The general features of the spectra were useful. The weak absorption is along the b-axis and it reached a maximum at 275 mμ to 270 mμ. Perpendicular to the b-axis the absorption rose very rapidly

from 305 mμ down to 295 mμ. From 295 mμ to 255 mμ the absorbance flattened out to a plateau of about 5 absorbance units. At 240 mμ the two directions crossed. The dichroic ratio at 295 mμ was about ten. The section was evidently too thick for absorption in the strong direction.

More quantitative spectra were obtained from ground sections of 1-methylthymine. For the absorption perpendicular to the b-axis in the (102) plane, a crystal was cut to 0.1 μ. The retardation was measured before transmission measurements were made. The calculated thickness was 0.10 ± 0.02 μ. The maximum at 275 mμ was 1.72 absorbance units. Along the b-axis the absorbance was too weak for reliable measurements (0.15 at 270 mμ). At 241 mμ the absorbances of the two directions cross. After transmissions were made the retardation had fallen about 30%. Although care was taken to make the transmission measurement as rapidly as possible, some photodamage had evidently occurred. Thus some uncertainty is introduced into the absorption spectrum; the magnitude of the error is hard to assess.

Another 1-methylthymine crystal was cut in the (102) plane to a thickness of 0.5 μ. From the retardation measurement, the thickness was calculated to be 0.49 ± .03 μ. The transmission was measured along the b-axis, but not in the direction perpendicular to the b-axis. The maximum of the first absorption band was at 275 mμ; the absorption started rising strongly into a second band at 240 mμ.

At the conclusion of the experiment there was no measurable decrease in retardation. The raw absorbances for the two different sections are listed in Table III. These data are uncorrected for reflections off the crystal face, but a base correction from the edge of the absorption curve was made. The reported errors are based on the accuracy of the intensity measurements.

The reflection coefficients for 1-methylthymine in the region of the measured absorption were calculated by an IBM 7090 computer. The Drude theory for an optical electron was assumed. The full dispersion formula was approximated with two terms. For the first term the measured absorption band was used; the oscillator strength and position of the second ultraviolet absorption band were taken from solution. By fitting the calculated refractive index to the measured value at 589 mμ, a reiterative procedure was used until a consistent set of refractive indices was computed. The general theory and details of the calculation are found in Appendix A. The calculated reflection spectra along the b-axis and perpendicular to the b-axis off the (102) face are shown in Figure 12. The computed refractive indices and reflection coefficients are found in Appendix A. The input data are also listed in Appendix A.

For reflection corrections of the raw absorbance data, it was assumed that the back crystal face was in good optical contact with the methacrylate film. Reflections off the film are small compared

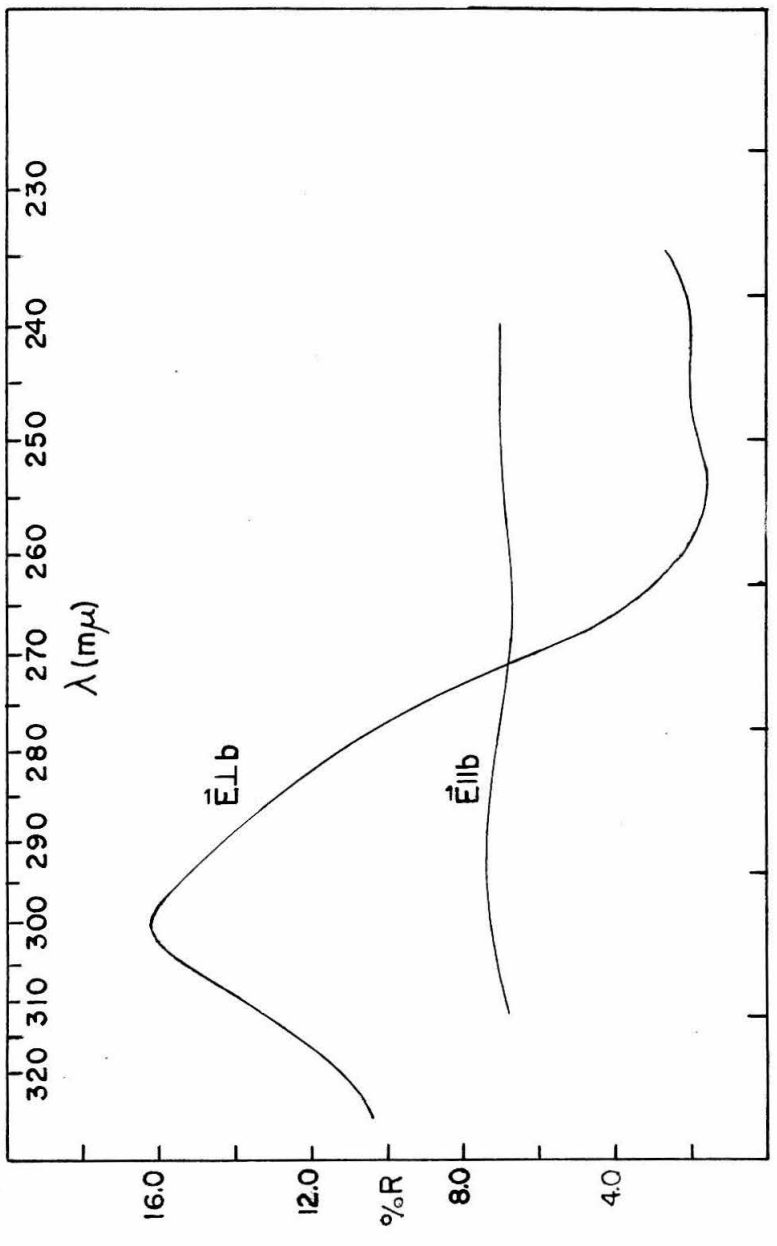

Figure 12. Calculated reflection spectra off the (102) of 1-methylthymine.

TABLE III. Raw Absorbance Data for 1-Methylthymine

λ(mμ)	t = 0.10 ± .02 μ		t = 0.49 ± .03 μ
	A ⊥ b	A ∥ b	A ∥ b
320	0	0	0
315	0		0
310	0.05 ± .04	0	0
305	0.23 ± .04		0.05 ± .04
300	0.68 ± .04	0.08 ± .04	0.13 ± .04
295	0.98 ± .04		0.30 ± .04
290	1.28 ± .04	0.12 ± .04	0.51 ± .04
285	1.47 ± .04		0.65 ± .04
280	1.68 ± .04	0.13 ± .04	0.77 ± .04
275	1.72 ± .04		0.84 ± .04
270	1.68 ± .04	0.15 ± .04	0.77 ± .04
265	1.41 ± .04	0.13 ± .04	0.73 ± .04
260	1.11 ± .04	0.09 ± .04	0.64 ± .04
255	0.84 ± .04	0.08 ± .04	0.64 ± .04
250	0.66 ± .04	0.07 ± .04	0.68 ± .04
245	0.52 ± .04	0.15 ± .04	1.02 ± .04
240	0.38 ± .04	0.51 ± .04	1.66 ± .05
235	0.24 ± .06	0.72 ± .06	>2.5
230	~0.7	>1.6	

to the established error of .04 absorbance units. Thus only reflections off the front face of the crystal were considered. Along the b-axis the correction was negligible; perpendicular to the b-axis the correction amounted to .05 absorbance units at the most.

With the raw absorbance corrected for reflections, molar absorptivities were calculated. The density of 1-methylthymine is reported with the crystal structure determination (10). Table II is a tabulation of the calculated values with errors based on the accuracy of intensity measurements, on the birefringence uncertainty, and on the reproducibility of retardation measurements. The weak absorption values were calculated from the thicker of the two sections. Figure 11 is a plot of the absorptivities as a function of wavelength and wave number. The errors are not shown. The slightly saw-toothed shape of the strong absorption curve may reflect the photodamage which took place during the measurements.

9-Methyladenine. The crystal absorption spectra of 9-methyladenine in the (001) plane are shown in Figure 13 and Table IV. Although the crystal structure of 9-methyladenine has not been determined, its unit cell dimensions have been reported (11). The x-ray diffraction data also suggest that the crystal is a layer structure with the molecules lying in the (001) plane (12). The crystals do have a pronounced cleavage plane (001).

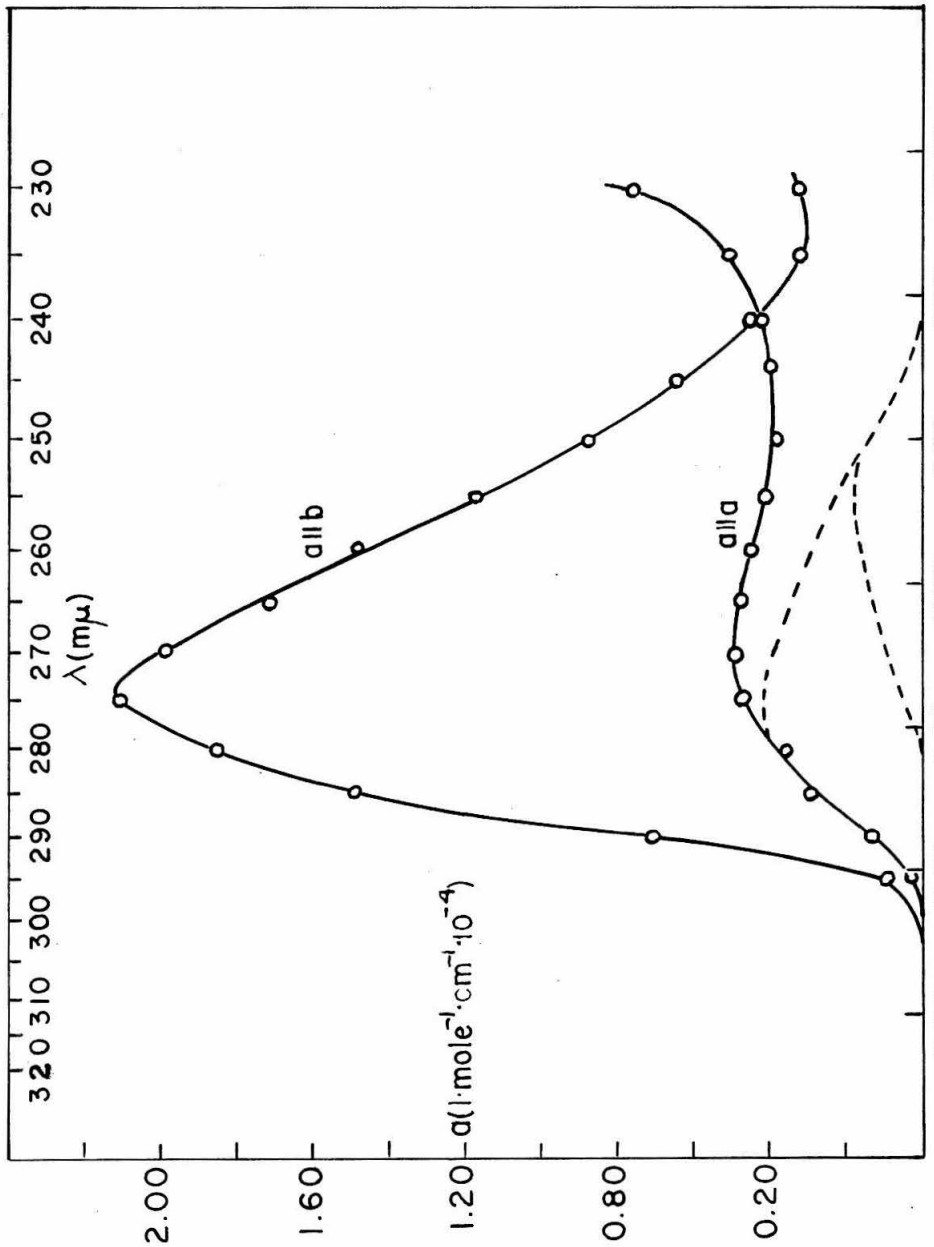

Figure 13. Absorption spectra in (001) of 9-methyladenine.

TABLE IV. Molar Absorptivities for 9-Methyladenine in the (001) Plane

λ(mμ)	a ∥ b ($l \cdot mole^{-1} \cdot cm^{-1} \cdot 10^{-3}$)	a ⊥ b ($l \cdot mole^{-1} \cdot cm^{-1} \cdot 10^{-3}$)	Dichroic Ratio
300	0	0	
295	0.9 ± .4	0.20 ± .08	4.9 ± 3.9
290	7.0 ± 1.3	1.2 ± 0.2	5.7 ± 1.3
285	14.9 ± 2.5	2.9 ± 0.3	5.0 ± 0.5
280	18.5 ± 3.1	3.6 ± 0.4	5.1 ± 0.4
275	21.0 ± 3.4	4.7 ± 0.5	4.5 ± 0.3
270	19.8 ± 3.3	4.9 ± 0.6	
265	17.1 ± 2.8	4.7 ± 0.5	
260	14.8 ± 2.4	4.5 ± 0.5	
255	11.7 ± 2.1	4.1 ± 0.6	
250	8.8 ± 1.6	3.8 ± 0.5	
245	6.5 ± 1.3	3.9 ± 0.5	
240	4.5 ± 1.3	4.2 ± 0.9	
235	3.2 ± 0.7	5.0 ± 1.0	
230	3.2 ± 0.7	7.6 ± 1.4	
	Dav. = 5.1 ± 0.5		

A 9-methyladenine crystal was ground to a thin section in the (001) plane. The thickness, determined from the retardation measurements, was 0.16 ± .03 μ. There was no evidence of photodamage during the transmission measurements. The direction of strong absorption was along the b-axis with a maximum at 275 mμ. Along the a-axis the absorption reached a maximum at about 270 mμ and remained relatively flat to 240 mμ. Below 240 mμ the a-axis becomes the direction

of strong absorption. At 240 mμ the two absorption curves cross. In order to measure the absorption along the a-axis with greater accuracy, a thicker section of the (001) plane was prepared. The second sample had a thickness of 0.61 ± .05 μ. The agreement with the thinner section was reasonable. Table V is a tabulation of the raw absorbance data uncorrected for reflections.

TABLE V. Raw Absorbance Data for 9-Methyladenine

λ	t = 0.16 ± .03 μ		t = 0.61 ± .05 μ	
	$A_{\parallel} b$	$A_{\perp} b$	$A_{\parallel} b$	$A_{\perp} b$
320	0			
315	0			
310	0			0
305	0			0
300	.03 ± .04			0
295	.18 ± .04		0.82 ± .04	.12 ± .04
290	1.17 ± .04	.20 ± .04	2.68 ± .04	.67 ± .04
285	2.45 ± .04	.48 ± .04		1.90 ± .04
280	3.03 ± .04	.59 ± .04		2.15 ± .04
275	3.41 ± .04	.76 ± .04		2.85 ± .04
270	3.21 ± .04	.74 ± .04		2.97 ± .04
265	2.76 ± .04	.73 ± .04		2.90 ± .04
260	2.37 ± .04	.71 ± .04		2.78 ± .04
255	1.85 ± .04	.59 ± .04		2.61 ± .04
250	1.39 ± 0.4	.50 ± .04		2.50 ± .04
245	1.01 ± .04	.54 ± .04		2.63 ± .04
240	0.69 ± .04	.68 ± .04		~3.0
235	0.47 ± .04	.80 ± .04		
230	0.48 ± .04	1.22 ± .04		

Reflection spectra off the {001} face were calculated in the same manner for 9-methyladenine as for 1-methylthymine. The input data and computed refractive indices and reflection coefficients are listed in Appendix A. The calculated reflection spectra are shown in Figure 14.

The appropriate reflection corrections were made in the same manner as for 1-methylthymine. Molar absorptivities were then computed. The density of the crystal is reported with the unit cell dimensions (11). Table IV is a tabulation of the results. The errors are based on the thickness uncertainty and on the limited accuracy of intensity measurements. The absorbances near the maximum of the strong absorption band may have been low due to the small out of plane component of the polarized light. At the worst they are low by 0.2 absorbance units. (See section on the microspectrophotometer.) The weak absorption band was averaged from the absorption measurements of the two different thicknesses. Figure 13 is a plot of the molar absorptivities as a function of wavelength and of wavenumber.

Hoogsteen Dimer. The hydrogen bonded complex of 1-methylthymine and 9-methyladenine lies in the (010) plane. Therefore, the symmetry (b) axis of the monoclinic crystal is perpendicular to the molecular planes.

The absorption spectrum for the light polarized along the b-axis is recorded on page 80a.

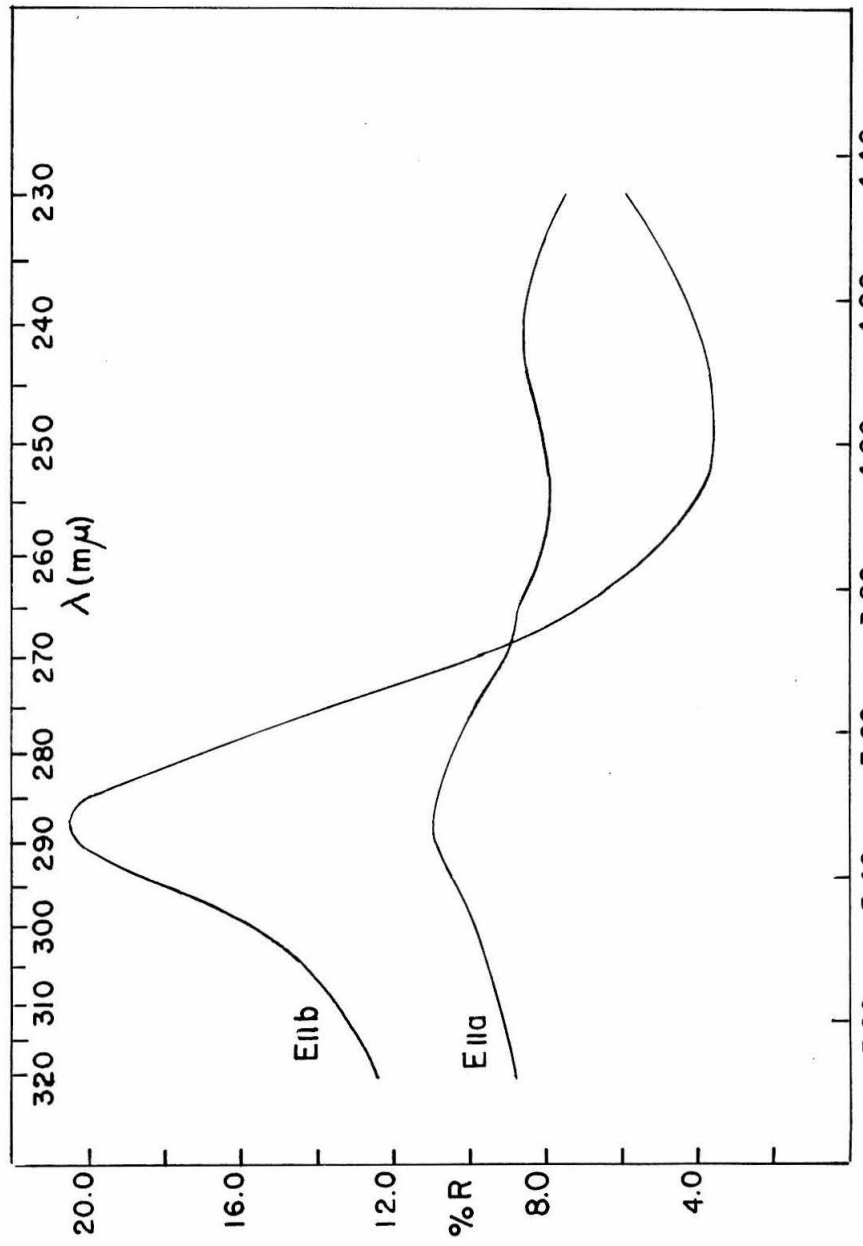

Figure 14. Calculated reflection spectra off the (001) of 9-methyladenine.

The spectral data for light polarized in the molecular plane are necessarily more complicated than was the case for 1-methylthymine or 9-methyladenine crystals. Both 1-methylthymine and 9-methyladenine are monoclinic, but in each case the b-axis lies in the plane of the molecules. Therefore, for 1-methylthymine and 9-methyladenine, for light polarized in the plane of the molecules, the b-axis is a principal direction and the absorptivity ellipsoid has its principal directions parallel and perpendicular to b. However, for the Hoogsteen dimer the orientation of the absorptivity ellipsoid is not fixed by crystallographic symmetry and in fact can and does vary with wavelength. The experimenter must determine both the orientation of the principal axes with respect to a crystal face and the magnitudes of the absorbances along the principal axes.

If φ is the angle between a crystal face and the electric vector of the incident light and θ is the angle between the same crystal face and a principal axis, then the transmission is

$$I/I_o = \cos^2(\varphi - \theta)\ 10^{-A_2} + \sin^2(\varphi - \theta)\ 10^{-A_1}$$

where A_1 and A_2 are the absorbances along the two respective principal axes. From measurements of I/I_o as a function of φ, the quantities A_1, A_2, and θ as a function of wavelength have been determined by a least squares analysis. (See Appendix B.) The results are presented in Table VI.

TABLE VI. Molar Absorptivities of Principal Directions and Position Angles for the Hoogsteen Dimer

λ (mμ)	$a_{max} \cdot 10^{-3}$ ($l \cdot mole^{-1} \cdot cm^{-1}$)	$a_{min} \cdot 10^{-3}$ ($l \cdot mole^{-1} \cdot cm^{-1}$)	θ (degrees)	Dichroic Ratios
		$t = 0.22 \pm .07$ μ		
230	11.6 ± 4.5	3.6 ± 1.5	91.9 ± 1.1	3.2
235	9.3 ± 5.2	3.9 ± 2.5	92.2 ± 5.2	2.4
240	7.6 ± 3.0	4.8 ± 2.0	83.4 ± 2.9	1.6
245	7.4 ± 2.6	5.9 ± 2.2	28.8 ± 4.0	1.2_5
250	9.4 ± 3.2	5.5 ± 1.8	14.2 ± 0.6	1.7
255	12.0 ± 4.3	5.7 ± 2.2	10.4 ± 1.1	2.1
260	13.4 ± 4.6	6.1 ± 2.2	12.2 ± 1.1	2.2
265	14.6 ± 4.9	7.2 ± 2.5	11.0 ± 0.6	2.0
270	15.9 ± 5.8	8.8 ± 3.3	9.1 ± 1.7	1.8
275	15.4 ± 5.1	9.9 ± 3.2	7.3 ± 0.6	1.5_5
280	14.2 ± 4.8	9.6 ± 3.2	6.0 ± 1.1	1.4_8
285	11.6 ± 4.0	8.4 ± 2.9	6.2 ± 1.7	1.3_7
290	10.0 ± 3.5	7.5 ± 2.8	4.4 ± 2.9	1.3_3
295	8.1 ± 2.8	5.9 ± 2.0	7.8 ± 1.1	1.3_7
300	4.0 ± 1.6	3.2 ± 1.4	-29.4 ± 9.4	1.2_5
305	2.1 ± 0.8	1.2 ± 0.5	-12.6 ± 2.3	1.7
		$t = 0.49 \pm .05$ μ		
240	11.9 ± 1.6	10.8 ± 1.4	96.9 ± 5.0	1.1
295	7.9 ± 0.8	7.6 ± 0.8	16.6 ± 6.0	1.0_5
300	3.0 ± 0.6	2.2 ± 0.4	-54.7 ± 5.2	1.3_5

NOTA BENE: The data for 240 mμ was in very poor agreement for the two sections analyzed. It is hard to understand why the dichroism for the thick section is much smaller than for the thin section. The transmission near the direction for strong absorption may have been too high for the thick section, although this seems unlikely. These data represent the largest discrepancy encountered in all the crystal measurements presented in this work.

TABLE VI (continued)

NOTA BENE (continued):

The data for 240 mμ from the 0.49 μ section were scaled down to fit smoothly into the three dimensional model. Values chosen were:

$a_{max} = 7.6 \times 10^3$, $a_{min} = 6.9 \times 10^3$, $\theta = 96 \pm 5$.

Compared to 1-methylthymine and 9-methyladenine, the Hoogsteen dimer is not very dichroic in the molecular plane. It should be realized that the more isotropic the absorption (that is, the closer A_2/A_1 is to unity), the less accurate is the determination of the angle θ. A sketch of a three dimensional model representing the absorption surface is shown in Figure 15. The structure was built around a cylindrical coordinate system. Each plate, perpendicular to the cylindrical axis, corresponds to a different wavelength. The wavelength, in 5 mμ increments, runs from 300 mμ to 230 mμ down the cylindrical axis. The radial coordinate represents absorption and the angular coordinate is defined in the manner described below. The struts, running down the sides of the model, follow the principal directions; one pair corresponds to the larger axis and the other pair to the smaller axis.

The preparation of a thin crystal in the (010) plane was a difficult task because the birefringence is only .037. When the crystal

Figure 15.

Three dimensional model of polarized absorption in the (010) of the Hoogsteen dimer.

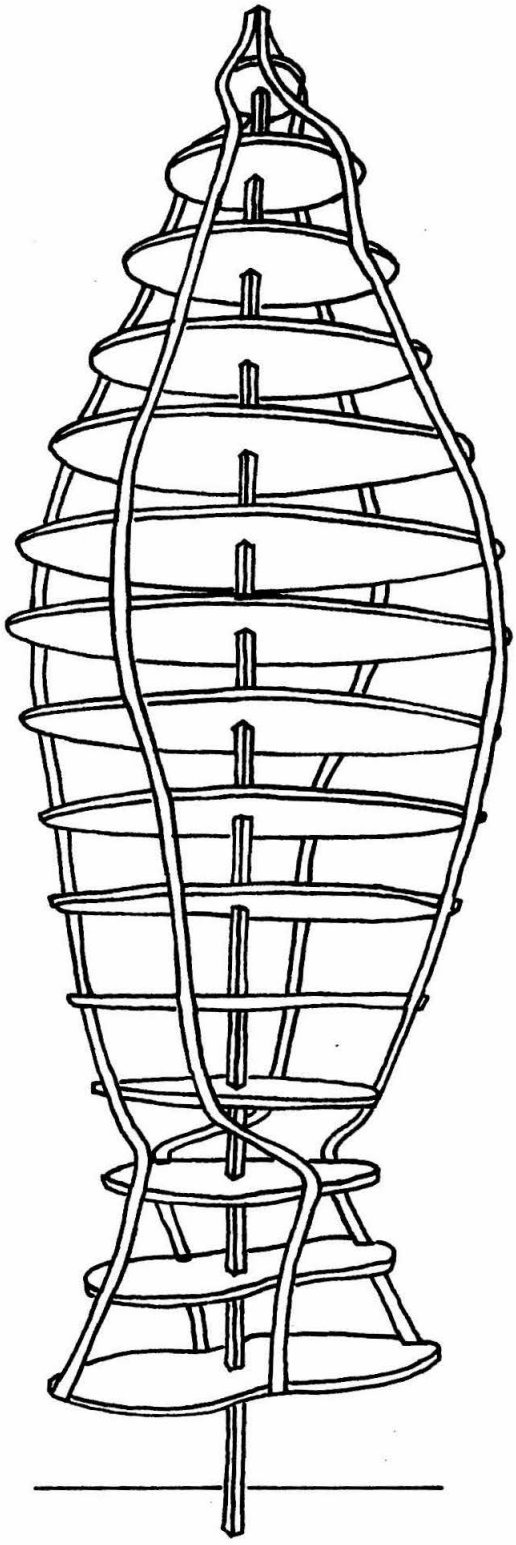

was less than 1 μ, the interference colors could no longer be detected. Of several sections prepared only one was thin enough (0.22 μ) for a complete determination of the absorption. Two other sections of thicknesses 0.49 μ and 0.55 μ were useful in confirming the toe-absorption near 300 mμ and the absorption near 240 mμ. There was no evidence of photodamage during the course of the transmission measurements. The (010) plane, perpendicular to the b-axis, has no principal directions fixed by crystallographic symmetry. Hence, the transmissions were measured by rotating the crystal at increments of 30° with respect to the electric vector of the polarized light. The crystal was rotated through a total angle of 240° for each wavelength. The angular dependence of the transmission is understood if one considers the absorption of light arising from two independent rays polarized along the two principal directions. The electric vector projects its amplitude along the two principal directions, which have characteristic cross-sections. The amplitude components are then attenuated exponentially as the rays proceed through the crystal. If φ is the angle between an arbitrary line on the crystal and the electric vector, then the angular dependence of the absorption is

$$A = -\log_{10} (\beta \cos 2\varphi + \gamma \sin 2\varphi + \delta)$$

for which the three parameters, β, γ and δ, determine the respective cross-sections of the two principal directions and the position of the principal directions in the crystal.

$\gamma/\beta = \tan 2\theta$ where θ is the angle between a line on the crystal and one of the principal directions. The absorbance A_1 along the principal direction P_1 is $A_1 = -\log_{10} \left(\frac{\delta \cos 2\theta - \beta}{\cos 2\theta} \right)$ and for the other principal direction, P_2, $A_2 = -\log_{10} \left(\frac{\delta \cos 2\theta + \beta}{\cos 2\theta} \right)$. (See Appendix B.)

The dichroism for the first absorption band was never more than two. The reflections off the {010} face, therefore, are isotropic within the accuracy of a transmission measurement. To the extent that reflections are the same for all directions, the above angular dependence of absorbance is independent of reflections. The raw absorbance data were fitted to the above equation by a least squares analysis. An IBM 7090 computer was used for the computations. The general theory and derivations for the analysis are in Appendix B.

The isotropic absorption of the (010) face was determined by removing the polarizer. Rotation of the crystal did not change the transmitted signal. From the isotropic absorption a set of "mean" reflection coefficients for the (010) face were computed. Since the dichroism is small, such a treatment is justified. Nevertheless, there is a slight weighting towards the smaller absorption of the two principal directions. For the refractive index at 589 mμ, the value $1.764 = \sqrt{N_x N_y}$ was used. The input data, computed refractive indices, and reflection coefficients are listed in Appendix A.

A plot of the isotropic absorption in the (010) plane is shown in Figure 16. The absorbances at 240 mμ and 245 mμ are weighted

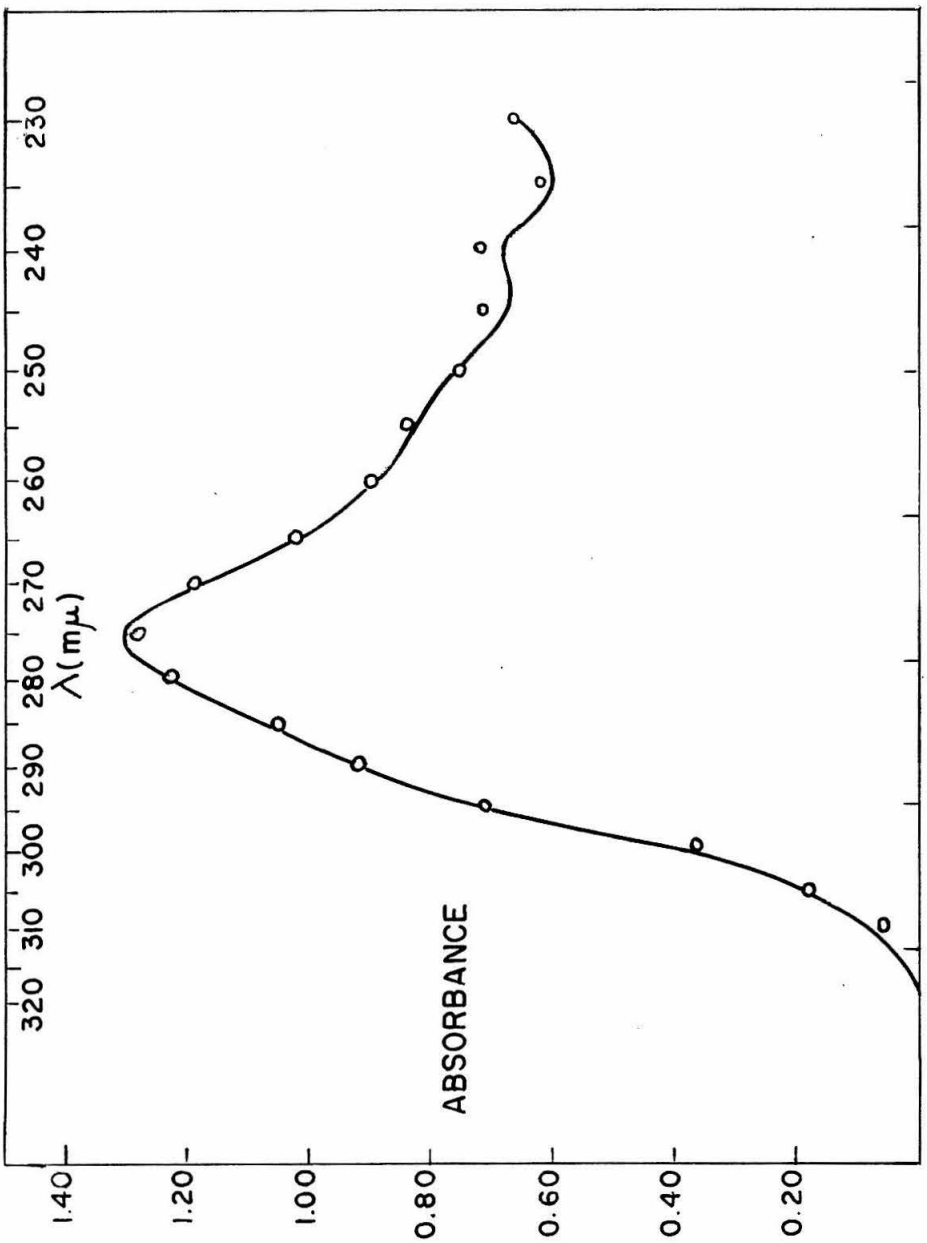

Figure 16. Isotropic absorption in (010) of Hoogsteen dimer. Smooth curve is measured absorption. Circles are calculated from principal axes in least squares analysis.

with the data from a section 0.49 μ thick. The points on the curve are calculated from corrected absorbances of the principal directions, which were obtained from the least squares analysis. The agreement for all wavelengths is within the standard absorbance error of .04. The small peak at 240 mμ, evident in the isotropic absorption spectrum, may be symptomatic of a new band. It is by no means conclusive, however. The contour of the isotropic absorption curve is very sensitive to the polarization properties of the various transitions. The polarized spectra must be analyzed in order to understand the isotropic absorption. The isotropic absorption curve does provide a useful confirmation of the absorbance values calculated for the principal axes.

The raw absorbance data for the polarization studies were corrected for reflections in the usual way. The corrections amounted at most to .03 absorbance units. Molar absorptivities for the principal directions were computed. The calculated least square curves were plotted on polar coordinates in molar absorptivity units. The angular variable is defined as zero along the c-axis of the crystal and increases in a right handed sense towards the acute angle of the (010) plane. The curves for 300 mμ and 240 mμ are based on measurements from a thicker section (0.49 μ). These curves, with the experimental points, are found in Appendix B. The a-c plane is drawn on a polar coordinate graph for convenience. The molar absorptivities of the principal directions with corresponding errors and the position angles, ρ, with

their calculated standard deviations are tabulated in Table VI. The angle θ is from the c-axis to the smaller of the two principal axes.

The absorption spectrum along the b-axis (perpendicular to the molecular planes) of the Hoogsteen dimer is shown in Figure 17. The molar absorptivities are found in Table VII.

TABLE VII. Molar Absorptivities along the b-Axis of the Hoogsteen Dimer

λ	$t = 6.10 \pm .05\ \mu$ $a(l \cdot mole^{-1} \cdot cm^{-1} \cdot 10^{-2})$	$t = 1.97 \pm .02\ \mu$ $a(l \cdot mole^{-1} \cdot cm^{-1} \cdot 10^{-2})$
230		10.3 ± 0.6
235		10.0 ± 0.7
240	~ 10	9.0 ± 0.6
245	9.1 ± 0.4	8.3 ± 0.5
250	7.7 ± 0.2	7.7 ± 0.5
255	6.7 ± 0.2	7.5 ± 0.5
260	6.0 ± 0.2	6.9 ± 0.5
265	5.6 ± 0.2	6.2 ± 0.5
270	5.4 ± 0.2	5.5 ± 0.5
275	5.0 ± 0.2	4.6 ± 0.5
280	4.1 ± 0.2	4.0 ± 0.4
285	3.4 ± 0.2	3.3 ± 0.4
290	3.0 ± 0.1	2.7 ± 0.4
295	1.6 ± 0.2	1.8 ± 0.4
300	0.5 ± 0.1	0.7 ± 0.5
305		~ 0

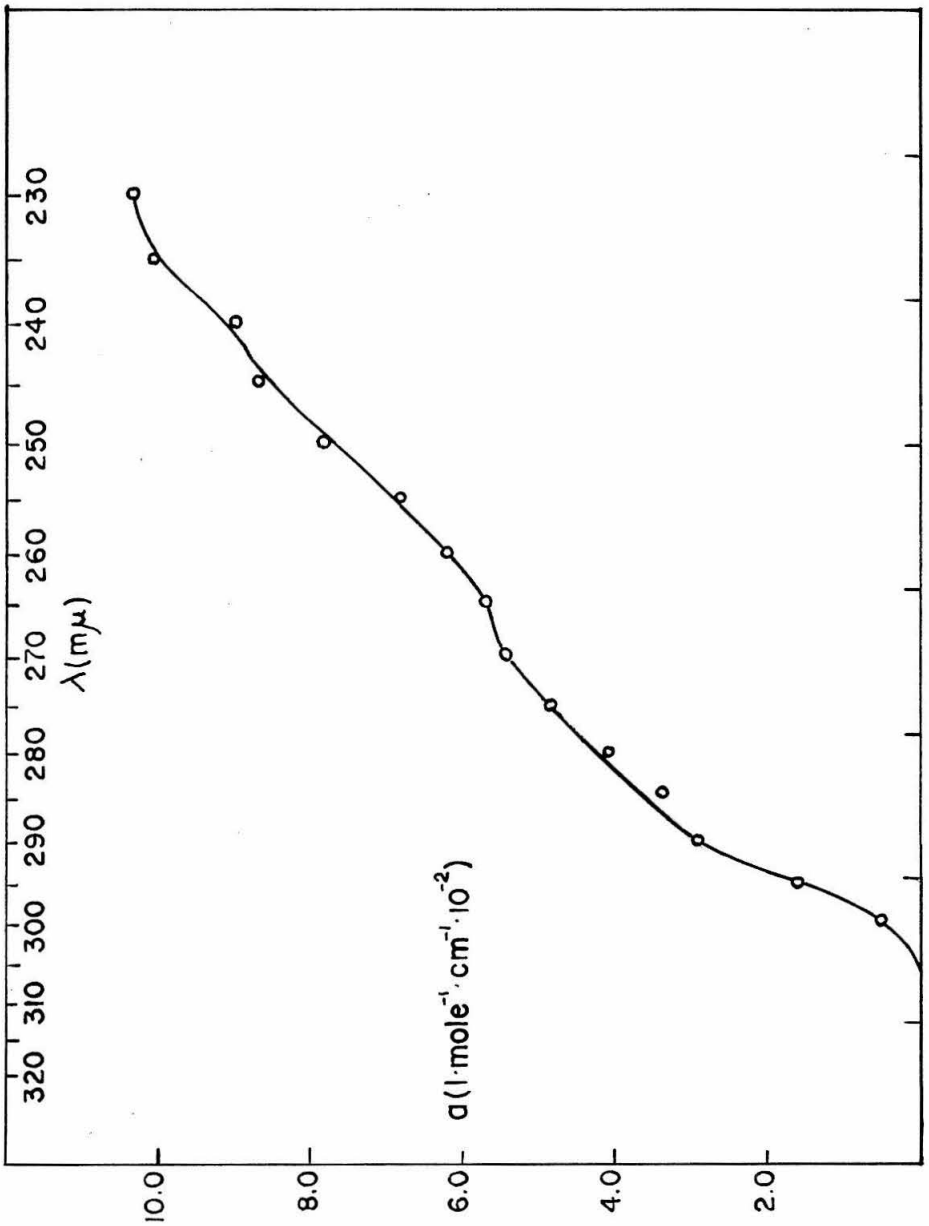

Figure 17. Spectrum parallel to the b-axis in the Hoogsteen dimer.

For transmission measurements along the b-axis, that is, perpendicular to the molecular planes, a variety of different thicknesses were used. A natural crystal of the Hoogsteen dimer with a thickness of 96 $\pm$ 2 μ was placed over a 100 μ aperture with the {100} face incident to the light beam. A residual absorbance of .05 at 400 mμ increased linearly to 0.11 at 310 mμ. The values are a little high for the expected reflections and probably indicate a small amount of impurity in the crystal. The thick crystal measurements, however, did establish an upper limit of 1 to 2 molar absorptivity units for absorption between the molecular layers from 400 mμ to 310 mμ. At 310 mμ the absorbance perpendicular to the b-axis was 0.76 and rose to ~3.5 at 305 mμ. The absorption parallel to the b-axis did not rise sharply until the exciting light reached 300 mμ. It is clear from these studies that any n-π^* transition which is polarized perpendicular to the purine ring is well inside the π-π^* absorption bands.

Another Hoogsteen dimer was ground to a section ~ 11 μ thick in the (100) plane. The dichroism is extremely large ($a\perp b/a\parallel b$ = 60 to 40) in the wavelength region 300 mμ to 280 mμ. In determining the absorption spectrum for light polarized perpendicular to the molecular plane ((010)), the possibility of an absorption contribution from components in the molecular planes must be considered. One such contribution occurs because the incident light is converging and not perfectly parallel.

For the wavelengths from 295 mμ to 280 mμ the aperture on the

1:1 imaging lens was varied. The absorbance values were independent of the solid angle, which varied from 6.29×10^{-3} steradians down to 1.1×10^{-3} steradians. The theory for the interaction of plane polarized light with an anisotropic absorbing plane is found in Appendix C. The transmission dependence on the angle of convergence, where this angle is small, so that $\tan \eta = \sin \eta = \eta$, is expressed as a series. It is

$$I/I_o = e^{-Ay} \sum_{n=o}^{\infty} \frac{(-1)^n (2n)!}{2^n (n+1)! (n!)^2} (Az\, \eta^2)^n$$

where Ay and Az are the weak and strong absorbances, respectively, and η is the angle of convergence. The series converges absolutely, and independently of the argument. To my knowledge the series is not a tabulated function. In order to have a measurable solid angle dependence, however, $Az\eta^2$ must be about unity. In base 10 units Az would have to be about 100, which is far too large for the thickness studied. From this argument it is concluded that the observed absorbance perpendicular to the molecular layers is bonafide absorption and not some artifact due to the geometry of the system.

The absorption spectrum perpendicular to the molecular planes was satisfactorily determined from two sections ground in the (100) plane. One section was $6.10 \pm .05$ μ and the other was $1.97 \pm .02$ μ. The thicker section had a wedge angle of .0036 radians, but for the 50 μ aperture used, the absorbance error was not measurable. (See

the section on crystal preparation.) Reflections off the {100} face along the b-axis are negligible. The calculated absorptivities for the two samples are listed in Table VII. Figure 17 is a plot of the absorbtivities as a function of wavenumber and wavelength. The absorption curve is a weighted average of the two samples.

DISCUSSION

Transition Moment Directions and Wavelength Shifts.

1-Methylthymine. The crystal structure in the (102) plane is shown in Figure 18. For convenience the absorption spectra from page 59 are repeated here in Figure 19.

There appears to be a single band from 305 mμ to 265 mμ polarized mainly along the pseudo-axis p (perpendicular to b in the (102)) with a dichroic ratio of 11.2 ± 1.0 which is constant within the rather large experimental error. A second band with the opposite polarization behavior begins at perhaps 265 mμ and is dominant below 240 mμ.

Suppose that at any one wavelength there is a unique direction of absorption (the direction of the transition moment) for a given 1-methylthymine molecule. We also assume there is zero absorption in the perpendicular direction. Information about this direction can be obtained from the polarized, crystal absorption spectra. Molecules (1) and (2) (see Fig. 18) are a hydrogen bonded pair which are related to each other by a center of symmetry. Therefore, the transition moment directions of these molecules are the same. The orientation of the hydrogen bonded pair, molecules (3) and (4), is obtained from (1) and (2) by a reflection in a plane perpendicular to the b-axis. Let

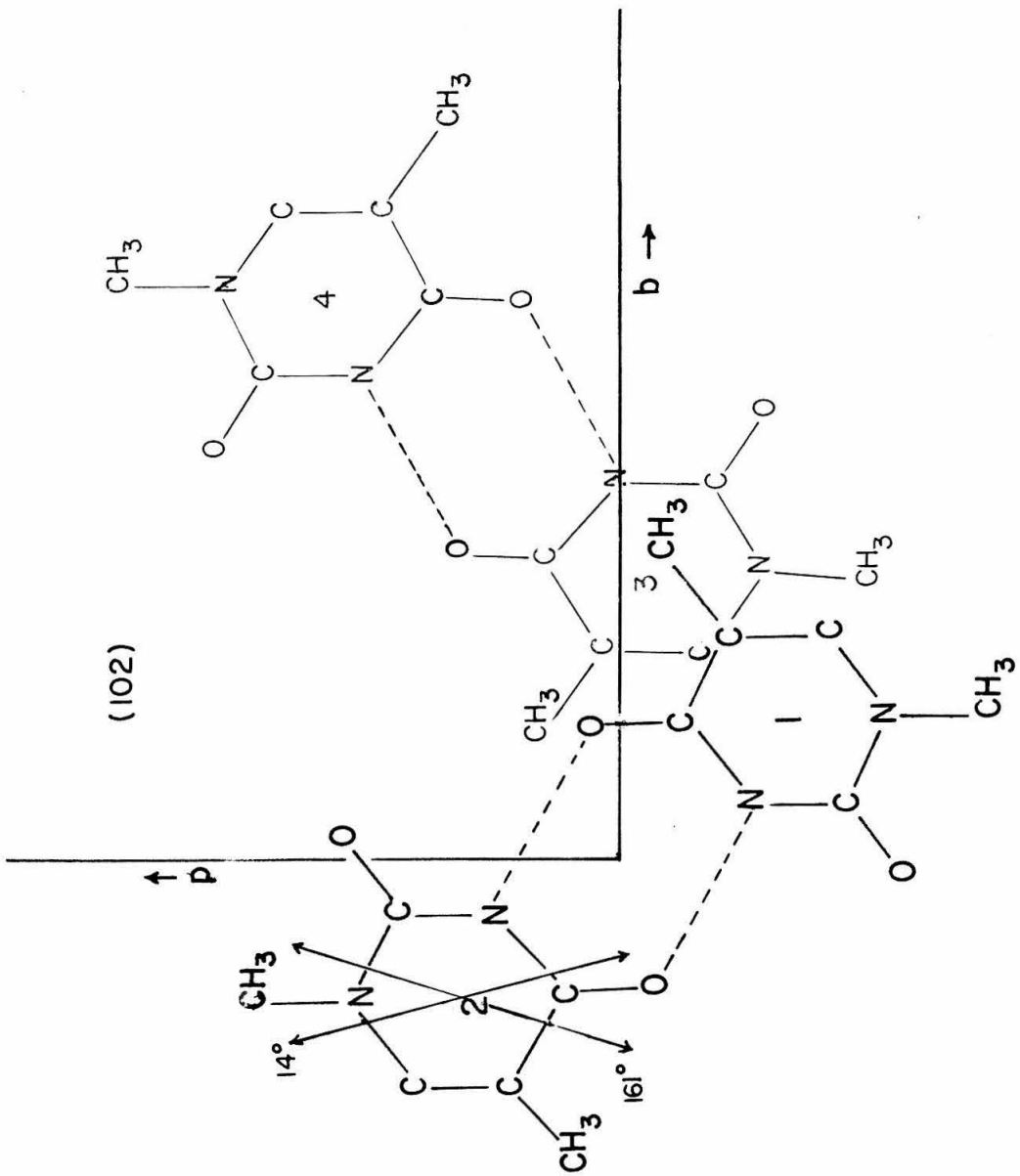

Figure 18. The (102) plane of 1-methylthymine showing the four molecules per unit cell. Molecules 3 and 4 (in light type) are in a layer below the plane of the paper. The significance of the arrows is described in the text.

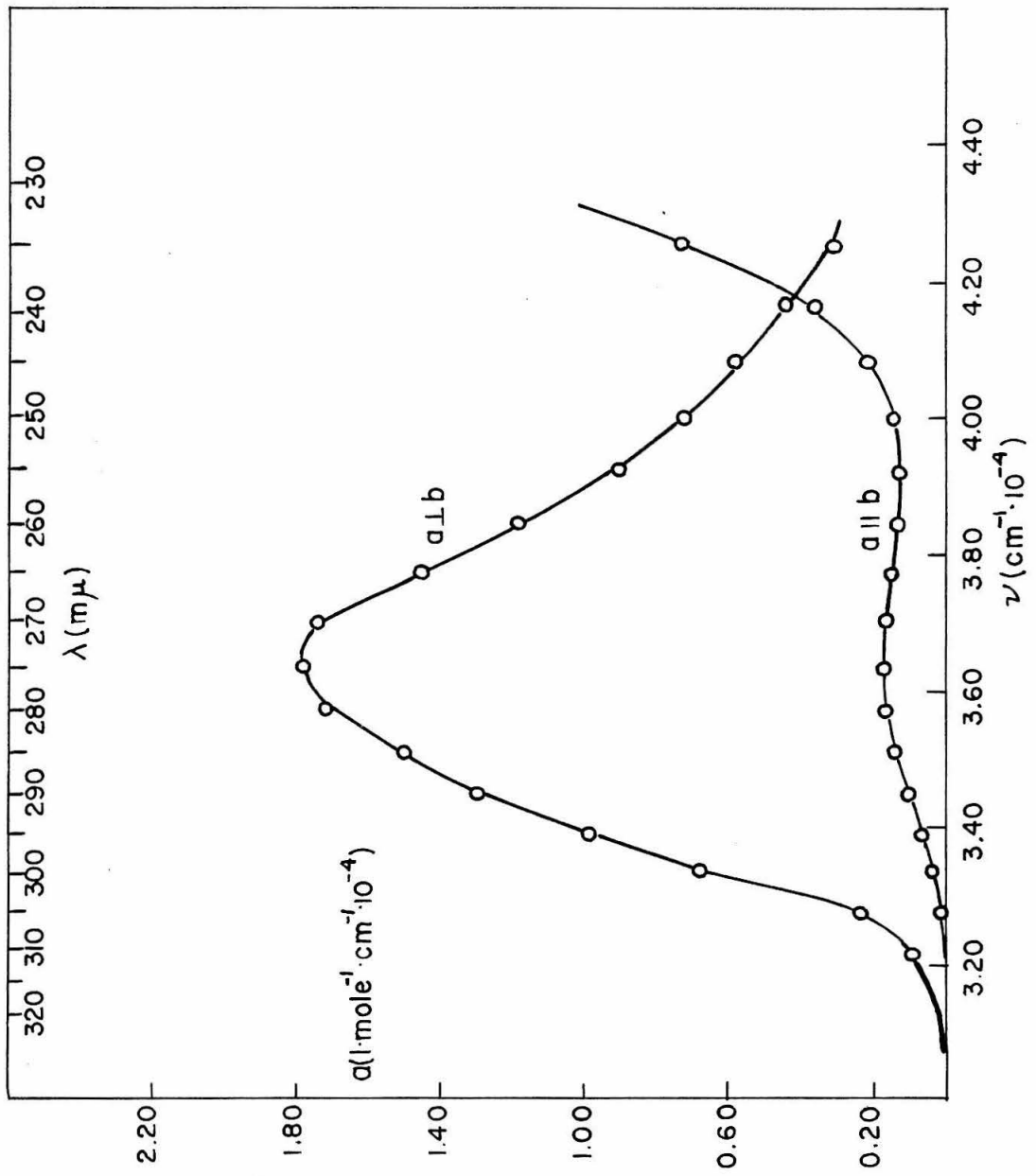

Figure 19. Absorption spectra in (102) of 1-methylthymine.

φ be the angle which the transition moments of the 1-2 pair make with the pseudo axis p; then $-\varphi$ is the angle made by the transition moment of the 3-4 pair. The dichroic ratio, $(a\perp b/a\parallel b)$, would then be $D = \cot^2\varphi$.

The absolute angle, calculated from the weighted average of the dichroic ratios over the first band is $\varphi = 16.5° \pm 0.8°$. The dichroic ratios from 305 mμ to 265 mμ are listed in Table II. The full error implied from the tabulated dichroic ratios places the transition dipole moment from 21° to 12° on either side of the p-axis. By Tinoco's convention (5') the transition dipole moment direction is assigned to either an angle of $14° \pm 2°$ or an angle of $161° \pm 2°$. The corresponding directions are shown on molecule 2 in Figure 18.

The above calculation assumes that for any one molecule there is a unique direction of absorption with an infinite dichroic ratio. This is expected theoretically for a single allowed electronic transition in the absence of vibronic or other perturbations.

The oscillator strength of the first absorption band is 0.19, corresponding to a transition dipole moment of 3.3 Debyes. This is intermediate between an allowed electronic dipole transition and a forbidden transition (3). In the latter case the intensity would mainly be "borrowed" by vibronic interactions with higher, allowed electronic states. The constancy of the dichroic ratio from 295 mμ to 265 mμ suggests that the band is allowed.

We now consider the "resonance-force" (26) or "exciton" (4) interaction between molecules. The dipole-dipole interaction energy of two transition dipoles is

$$\Delta E = \frac{\vec{\mu}_1 \cdot \vec{\mu}_2}{R^3} - \frac{3(\vec{\mu}_1 \cdot \vec{R})(\vec{\mu}_2 \cdot \vec{R})}{R^5}$$

The important near neighbors are molecules 1 and 3 in Figure 18. The center to center distance is 4.38 Å . The calculated interaction energy is $\pm$ 200 cm^{-1}. For the large number of stacked molecules (several hundred) the interaction is doubled to $\pm$ 400 cm^{-1}. The vibrational half-band width for the solution spectrum is 3720 cm^{-1}. According to the Simpson criterion (26), the system may be considered "weak-coupled." Therefore, assuming 800 cm^{-1} spacing for each vibrational level, the interaction of the vibrational levels should be about $\frac{1}{4}$ of the calculated strong coupled system. This is about a 50 cm^{-1} interaction or 100 cm^{-1} total splitting for each vibrational level.

The crystal spectrum is red-shifted about 800 cm^{-1} compared to solution. (See Fig. 24, p. 110 .) The calculated exciton interaction cannot account for the overall red shift. The difference in solvation by water as compared to other 1-methylthymine molecules probably accounts for the relative red shift.

9-Methyladenine and the Hoogsteen Dimer. Since the crystal structure of 9-methyladenine is not yet known, it is not possible to draw conclusions

about the directions of transition moments with respect to molecular axes. A plausible assignment can be made, however, by consideration of this crystal and the Hoogsteen Dimer; this consideration leads to a suggested molecular orientation for the 9-methyladenine crystal. (See Proposition I .)

The polarized absorption spectra of 9-methyladenine (Fig. 13 repeated here for the reader's convenience as Figure 20) shows a strong band with a peak at 275 mμ which is strongly polarized along the b-axis. Down to 280 mμ the dichroic ratio of ($a \parallel b$)/($a \perp b$) is constant with a weighted average ratio equal to 5.1 ± 0.5. The absorption from 280 mμ to 255 mμ perpendicular to the b-axis can be plausibly decomposed into a component of the $\parallel b$ band with a dichroic ratio of 1/5 and a second weak band with a maximum near 255 mμ. The weak band so constructed has an estimated oscillator strength of .008.

There is a very marked red shift of the crystal spectrum with a maximum at 275 mμ compared to the solution spectrum with a maximum at 263 mμ.

The hydrogen bonded complex of 1-methylthymine and 9-methyladenine lies in the (010) plane. There are two dimers per unit cell which are related by a two-fold screw axis. Therefore, all thymines and adenines have their respective transition dipole moments aligned in the same direction. Figure 21 is a drawing of the two dimers per unit cell. The molecular layers are separated by a vertical distance of 3.276 Å.

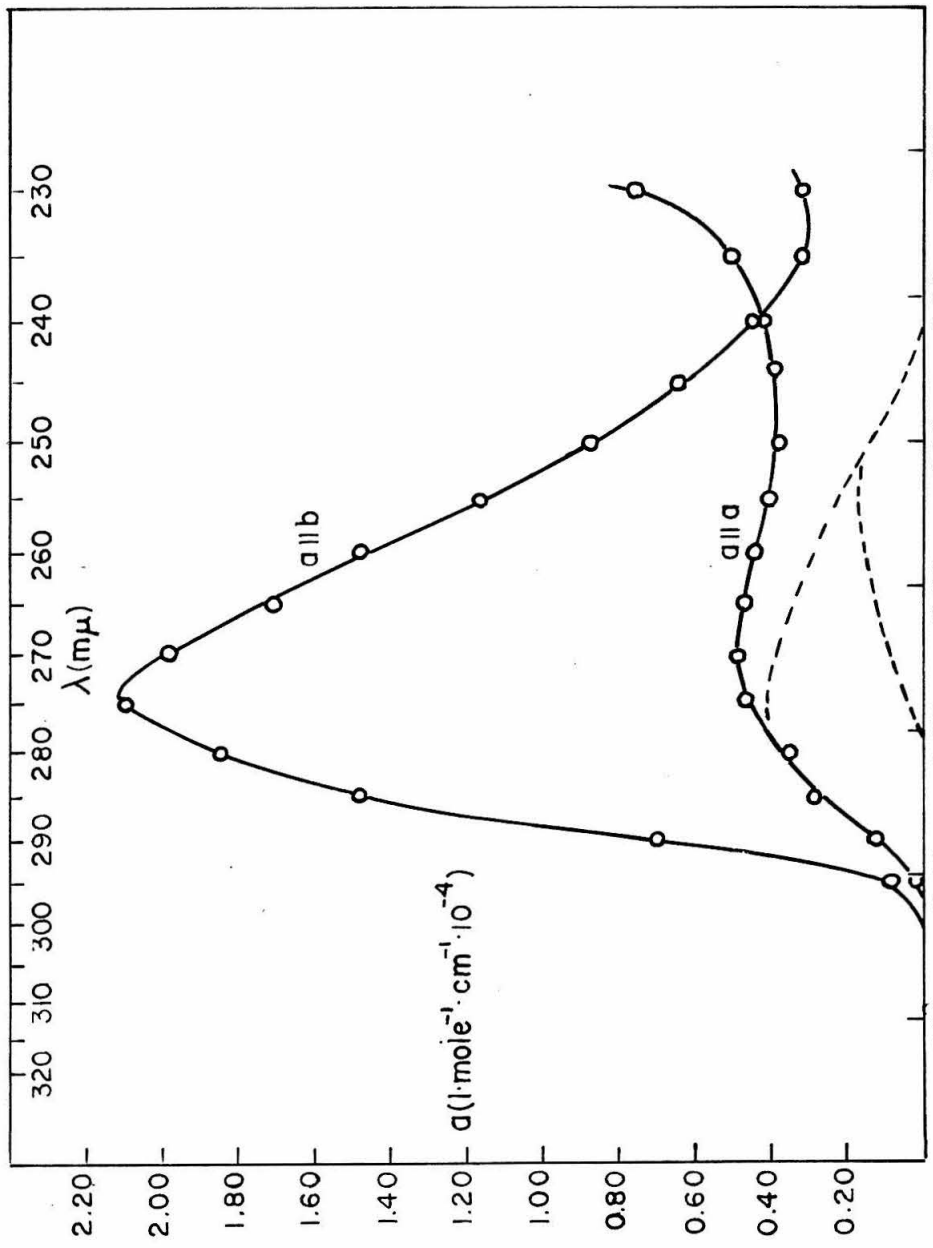

Figure 20. Absorption spectra in (001) of 9-methyladenine.

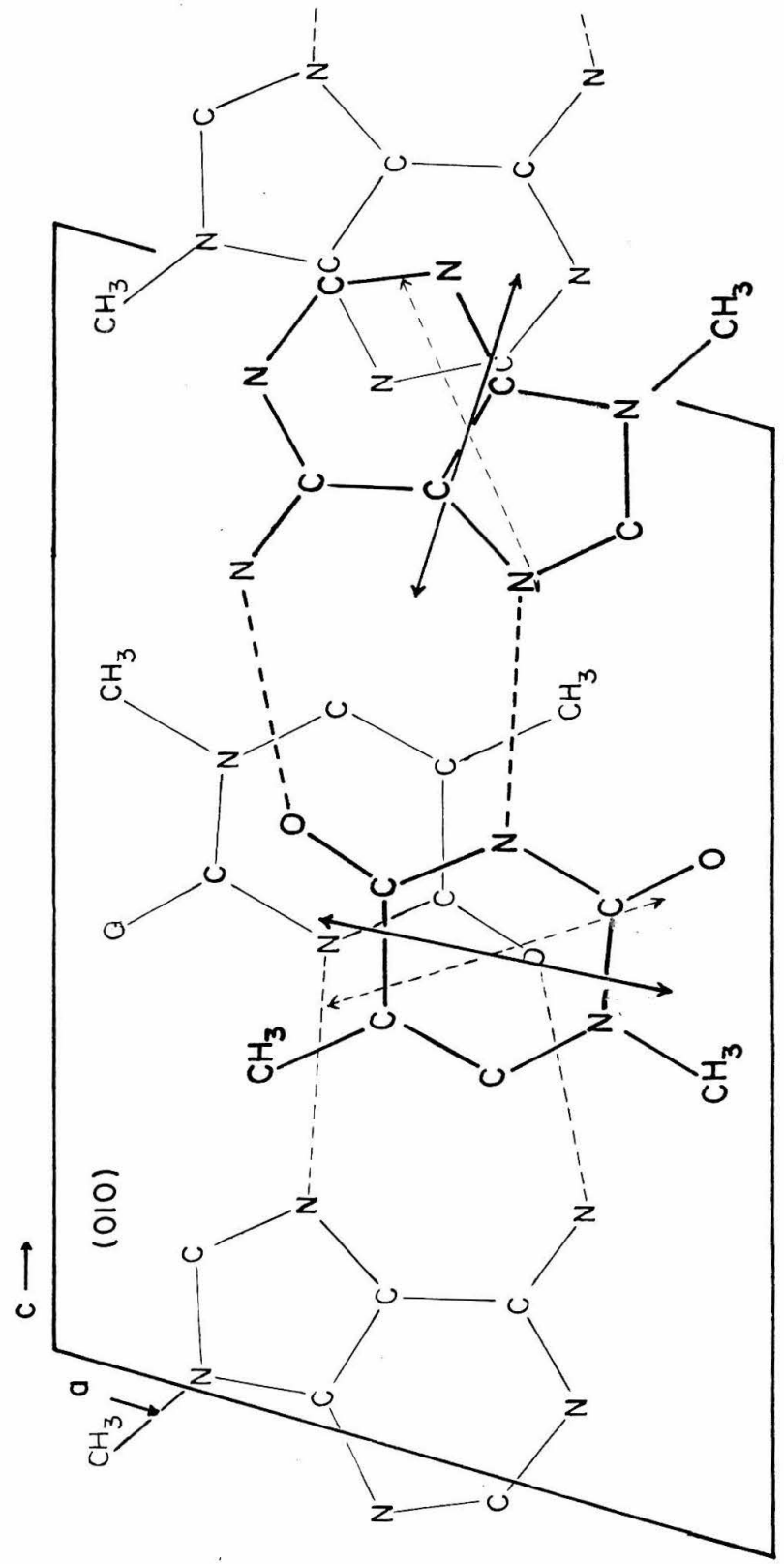

Figure 21. The (010) of the hydrogen bonded complex of 9-methyladenine and 1-methylthymine, showing the two dimers per unit cell. Molecules drawn in light type are below the plane of the paper.

The general features of the polarized absorption in the (010) are as follows. The tabulated values for the absorptivity ellipsoids are repeated here for convenience in Table VIII. The minor axis of the principal directions has a maximum absorption at about 277 mμ, while the major axis has a maximum at 273 mμ. The dichroic ratio increases from 1.3 at 295 mμ to 2.1 at 255 mμ. Over the first absorption band the angular orientation is relatively constant with the exception of wavelengths at 300 mμ and 305 mμ. Between 245 mμ and 240 mμ the directions of the major and minor axes reverse about 90° and the dichroism at 230 mμ becomes large (~3). At 240 mμ the dichroic ratio is about 1.5, but for this wavelength the two different sections are in poor agreement.

The relatively small dichroism in the (010) plane from 305 mμ to 290 mμ is surprising. From the solution spectra (Fig. 10), one would expect only thymine absorption from 310 mμ to 290 mμ. If this were the case, the dichroism would be very large with essentially all the absorption in the direction of the transition moment for 1-methylthymine. The very small dichroism on the red side of the absorption curve suggests several alternate hypotheses.

Suppose that the crystal is disordered. The N_3-C_6 axis in 1-methylthymine is almost a two-fold symmetry axis. In the hydrogen bonded complex crystal structure the N_3-C_6 axis is essentially parallel to the c-axis (see Fig. 21). If the 1-methylthymine molecules went into

TABLE VIII. Molar Absorptivities of Principal Directions and Position Angles for the Hoogsteen Dimer

λ (mμ)	$a_{max} \cdot 10^{-3}$ ($l \cdot mole^{-1} \cdot cm^{-1}$)	$a_{min} \cdot 10^{-3}$ ($l \cdot mole^{-1} \cdot cm^{-1}$)	ϕ (degrees)	Dichroic Ratios
		$t = 0.22 \pm .07$ μ		
230	11.6 ± 4.5	3.6 ± 1.5	91.9 ± 1.1	3.2
235	9.3 ± 5.2	3.9 ± 2.5	92.2 ± 5.2	2.4
240	7.6 ± 3.0	4.8 ± 2.0	83.4 ± 2.9	1.6
245	7.4 ± 2.6	5.9 ± 2.2	28.8 ± 4.0	1.2_5
250	9.4 ± 3.2	5.5 ± 1.8	14.2 ± 0.6	1.7
255	12.0 ± 4.3	5.7 ± 2.2	10.4 ± 1.1	2.1
260	13.4 ± 4.6	6.1 ± 2.2	12.2 ± 1.1	2.2
265	14.6 ± 4.9	7.2 ± 2.5	11.0 ± 0.6	2.0
270	15.9 ± 5.8	8.8 ± 3.3	9.1 ± 1.7	1.8
275	15.4 ± 5.1	9.9 ± 3.2	7.3 ± 0.6	1.5_5
280	14.2 ± 4.8	9.6 ± 3.2	6.0 ± 1.1	1.4_8
285	11.6 ± 4.0	8.4 ± 2.9	6.2 ± 1.7	1.3_7
290	10.0 ± 3.5	7.5 ± 2.8	4.4 ± 2.9	1.3_3
295	8.1 ± 2.8	5.9 ± 2.0	7.8 ± 1.1	1.3_7
300	4.0 ± 1.6	3.2 ± 1.4	-29.4 ± 9.4	1.2_5
305	2.1 ± 0.8	1.2 ± 0.5	-12.6 ± 2.3	1.7
		$t = 0.49 \pm .05$ μ		
240	11.9 ± 1.6	10.8 ± 1.4	96.9 ± 5.0	1.1
295	7.9 ± 0.8	7.6 ± 0.8	16.6 ± 6.0	1.0_5
300	3.0 ± 0.6	2.2 ± 0.4	-54.7 ± 5.2	1.3_5

the crystal with equally probable orientations about the N_3-C_6 axis and if the transition moment were at an angle of ~ 45° with respect to the c-axis for the orientation shown in Figure 21, then the other orientation would have a moment at ~135°. Hence the moments of the respective 1-methylthymine molecules would be nearly right angles and the absorption on the red side of the band would be almost isotropic. From the dichroic ratio analysis of single 1-methylthymine crystals, one of the two possible transition moment directions is at an angle of 45° $\pm$ 2° with respect to the c-axis. However, Dr. Hoogsteen has pointed out that the molecule has sufficient asymmetry to remove any ambiguity as to its atomic positions; the C_5-C_6 double bond is considerably shorter than the C_6-N_1 bond. The refined structure of the crystal, moreover, indicates that any disorder must be less than 20% of the structure. If 20% is the upper limit for the type of disorder mentioned above, then the smallest dichroic ratio should be about 4:1. Therefore, the x-ray crystallographic data rules out the disorder hypothesis.

A second hypothesis is to assume that 9-methyladenine has shifted to the red compared to solution (or even compared to the single crystal spectra) and that the transition moment for 9-methyladenine is at nearly right angles to the transition moment direction for 1-methylthymine. The purine and pyrimidine moieties are sufficiently separated

(6 A) that one would expect only weak coupling of the respective transition moments. To test the feasibility of this second hypothesis, the polarized absorption in the (010) must be interpreted.

In order to analyze the polarized absorption data, the relationship between the principal directions and the directions of molecular absorption must be understood. The two different molecules in the Hoogsteen dimer are viewed as two oscillators which are perhaps weakly coupled. Regardless of the coupling strength, the crystal can be approximated as two independent oscillators (the eigen oscillators) whose directions of vibrations (at any one wavelength) are at a fixed angle χ with respect to each other. The oscillators have respective cross-sections a_1 and a_2 for photon absorption. Let α be the angle from principal direction P_2 to the oscillator with cross-section a_2.

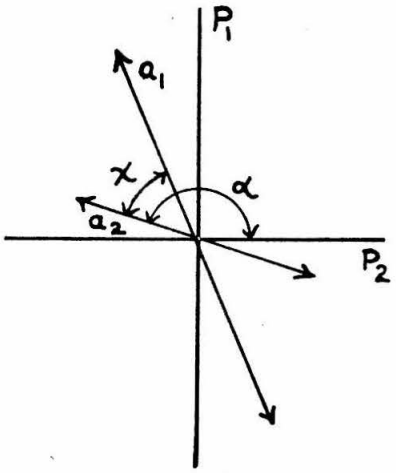

Then
$$P_2 = a_2 \cos^2\alpha + a_1 \cos^2(\alpha - \chi)$$
$$P_1 = a_2 \sin^2\alpha + a_1 \sin^2(\alpha - \chi) \qquad (1)$$
$$P_2 + P_1 = a_2 + a_1$$

Since a principal direction is an extremum for the projections of a_1 and a_2,

$$\frac{\partial P_2}{\partial \alpha} = 0$$

or

$$\cot 2\nu = \frac{a_2 + a_1 \cos 2\chi}{a_1 \sin 2\chi} \qquad (2)$$

$$= \frac{R + \cos 2\chi}{\sin 2\chi} \qquad \text{where } R = a_2/a_1$$

If α is constant throughout an absorption band characteristic to the two oscillators, that is, over a region in which χ is constant, then either R is constant or χ is 90°. A constant ratio for the oscillator cross-sections over an absorption band would determine a constant ratio P_2/P_1. This was not observed for the Hoogsteen dimer. The angular position of the principal directions, however, was nearly constant over the first absorption band. Figure 22 is a plot of θ, the angular position of the principal directions, as a function of wavelength. The calculated standard deviations of θ are also shown. The small variation of θ indicates that the oscillators are almost at right angles to one another. Any change in α is the same change for θ. Equation 2 may be solved simultaneously for two different wavelengths. The final result is:

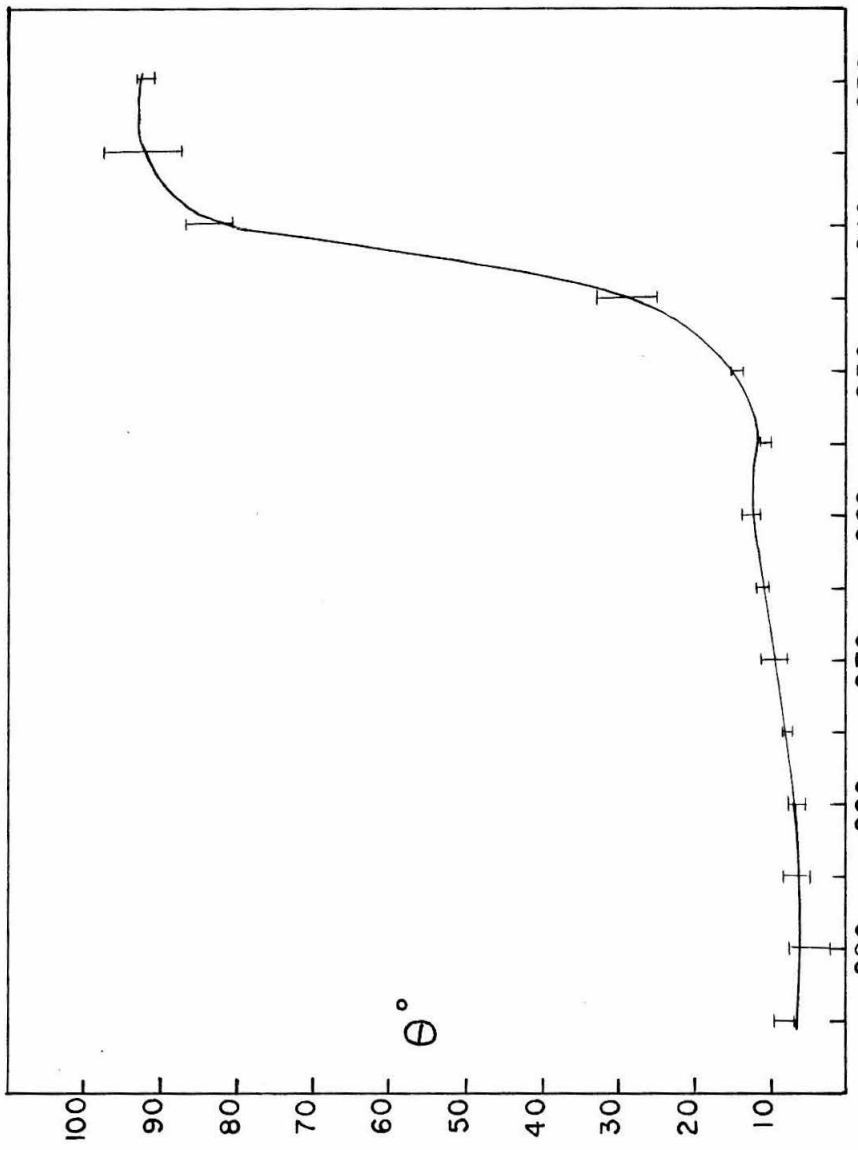

Figure 22. Variation of angular orientation of the absorptivity ellipsoids in the (010) of Hoogsteen dimer with wavelength.

$$[(R_1 + R_2)^2 + (R_2 - R_1)^2 \cot^2 2\Delta\theta] \cos^2 2\chi + 2(R_2 + R_1)(1 + R_2R_1) \cos 2\chi +$$
$$(1+R_1R_2)^2 - (R_2-R_1)^2 \cot^2 2\Delta\theta = 0$$

where R_1 and R_2 are respective ratios of the oscillator cross-sections at wavelengths λ_1 and λ_2 and $2\Delta\theta = 2(\alpha_1 - \alpha_2)$. To the extent that χ is near 90°, the ratios of the principal axes serve as approximations to R_2 and R_1. The angle χ can then be determined. The quadratic equation in cos 2χ will yield a solution of four possible angles, two supplementary pairs. The equation was solved for the three wavelengths of 290 mμ, 275 mμ and 260 mμ. One supplementary pair of angles varied considerably for the three different solutions. The other pair χ = 85° or 95° was constant within one degree. By eliminating α from equations 1 and 2, the cross-section ratios over the absorption band can be solved in terms of the principal axes and the angle χ. The equation for the solution is:

$$R = -B \pm \sqrt{B^2 - 1}$$

where

$$B = \frac{\cos 2\chi - \left(\frac{P_2/P_1 - 1}{P_2/P_1 + 1}\right)^2}{1 - \left(\frac{P_2/P_1 - 1}{P_2/P_1 + 1}\right)^2}$$

For the Hoogsteen dimer, the first approximation of the ratios was adequate for determining χ within the errors of the principal axes.

With R and χ determined in a self-consistent manner, α may now be determined from equation 2. There are two sets of values for α since χ, from the treatment above, cannot be resolved from a pair of supplementary angles. The sum of α and θ for the wavelengths of interest locates one of the oscillators with respect to a crystal axis. One of the supplementary angles, χ, should give a constant value for the angular position of the oscillator. The calculated values with the estimated errors are listed below. A one degree uncertainty in χ is a three degree uncertainty in α. The columns labelled $< c \wedge a_1$ and $< c \wedge a_2$ are values for the angle from the c-axis to the vibration direction of the oscillators with respective cross-sections a_1 and a_2.

λ (mμ)	θ	$\alpha_{\chi=95°}$	$<c \wedge a_1$	$<c \wedge a_2$	$\alpha_{\chi=85°}$	$<c \wedge a_1$	$<c \wedge a_2$
300	55±5°	168°±4	28±9	113±9	221±4	166±9	81±9
295	7.8±1.1	18±4	26±6	111±6	162±4	170±6	85±6
290	4.4±2.9	19±4	23±8	108±8	161±4	165±8	80±8
285	6.2±1.7	18±4	24±7	109±7	162±4	168±7	83±7
280	6.0±1.1	17±4	23±6	108±6	163±4	169±6	84±6
275	7.3±0.6	16±4	23±6	108±6	164±4	171±6	86±6
270	9.1±1.7	13±4	22±7	107±7	167±4	176±7	91±7
265	11.0±0.6	12±4	23±6	108±6	168±4	179±6	94±6
260	12.2±1.1	11±4	23±6	108±6	169±4	181±6	96±6
255	10.4±1.1	12±4	22±6	107±6	168±4	178±6	93±6

The angle $\chi = 95° \pm 1°$ gives fixed angles for the directions of the two oscillators. The corresponding directions are shown with broken lines in Figure 21; one line is over 1-methylthymine and the other is over 9-methyladenine. From the dichroism studies of 1-methylthymine crystals, the transition dipole moment assignment places the dipole vector at either $78° \pm 2°$ or $45° \pm 2°$ with respect to the c-axis in the Hoogsteen dimer. Both of these values are in gross disagreement with the oscillator directions determined from the assignment for $\chi = 95°$.

For the assignment $\chi = 85°$, one of the hypothetical oscillators is in agreement with one of the two possible dipole moment directions of 1-methylthymine. From 300 mμ to about 275 mμ the oscillator direction is constant to within the error ($83° \pm 7°$). Below 295 mμ the oscillator of larger magnitude corresponds to one of the transition moment directions for 1-methylthymine. At 300 mμ the magnitudes of the two oscillators are reversed. For this wavelength the "phase" angle θ was determined from a thicker section ($t = 0.49\ \mu$) since the absorbances are more reliable than for the thin section. The reversal in the oscillator magnitudes at 300 mμ means that the toe absorption of 9-methyladenine is to the red of 1-methylthymine.

Below 275 mμ the calculated direction of the proposed oscillator changes from ~86° to ~96°. But for 9-methyladenine the dichroic ratio was no longer constant below 280 mμ and a second, weak band was evident. This second, weak band is perhaps polarized in a direction

more or less at right angles to the major absorption band. The constructed, weak band had a molar absorptivity of about 1000 to 2000 from 270 mμ down to 255 mμ. This absorptivity value is about 15% of the molar absorptivity for the major, principal axis, which lies nearest the transition dipole moment direction for 1-methylthymine. If the weak band were polarized at an angle of about 120° or 130° with respect to the c-axis, then the change in the principal direction from 280 mμ to 255 mμ can be accounted for. Unfortunately, the full analysis of the principal directions in terms of three oscillators is an indeterminate problem. The independent evidence of a weak absorption band for 9-methyladenine, however, is qualitatively consistent with the directional change of the principal axes.

On the basis of the above argument and on the basis of dichroism studies of 1-methylthymine, the transition dipole moment direction for 1-methylthymine is assigned to the angle 161° $\pm$ 2°, where the angle is defined by the Tinoco convention (5'). The transition dipole moment for the strong absorption band of 9-methyladenine is assigned to the angle 168° $\pm$ 3°. The corresponding assignments are shown in Figure 21 with solid arrows over the respective molecules.

On the basis of a two oscillator model, χ and R were determined in the self-consistent manner outlined above. We now calculate a_1 and a_2, the molar absorptivities of the two eigen oscillators responsible for the absorption of the crystal. This calculation is easy because

$a_1 + a_2 = P_1 + P_2$ and $a_2/a_1 = R$. (Actually, a_1 and a_2 are almost exactly equal to P_1 and P_2, respectively.) The results are shown in Figure 23. As discussed above, we believe that oscillator a_2 is mainly due to 1-methylthymine down to about 240 mμ, although the weak perpendicular band of 9-methyladenine makes some contribution from 270 mμ to 250 mμ. The maximum for 1-methylthymine in the pure crystal, in the Hoogsteen diner, and in the solution all occur at about 273 mμ. We believe that oscillator a_2 is mainly due to 9-methyladenine down to about 250 mμ, where the strong second band of 1-methylthymine begins to contribute. The maximum for 9-methyladenine is about 277 mμ in the single crystal and in the Hoogsteen dimer. In solution 9-methyladenine has a maximum at 261 mμ.

From the assignments of the transition dipole moments, the resonance force, electrostatic interaction between nearest neighbors was calculated. For 1-methylthymine the center to center distance is 3.88_3 Å. The transition dipole moment is 3.3_2 Debyes as determined from solution. The calculated energy of interaction is 316 cm^{-1}, or a total of 632 cm^{-1} for the number of molecules stacked above one another. The transition dipole moment, calculated from solution, for 9-methyladenine is 3.9_4 Debyes. The center of gravity of the electrons for 9-methyladenine was calculated from Pullman's electronic charges of adenine (23) and from an estimate of 2 for the formal charge for the methyl group in the 9 position. The center of gravity for the π electrons

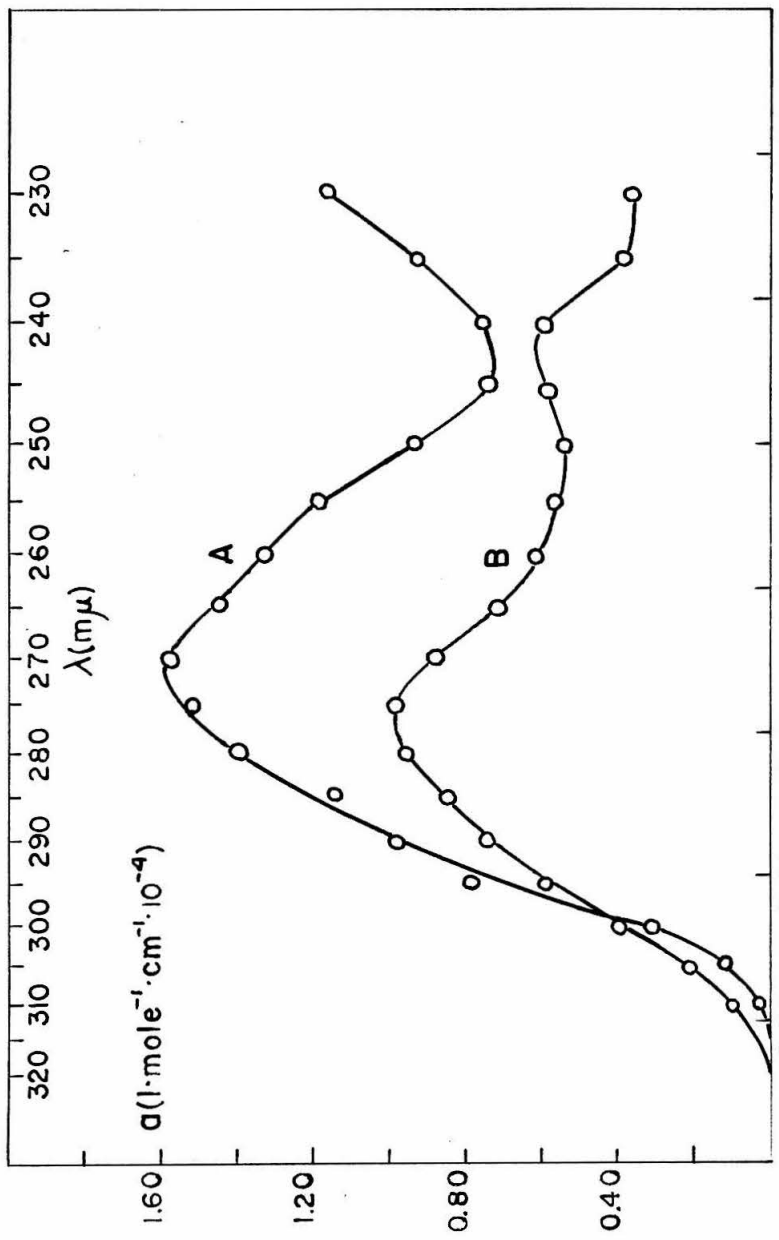

Figure 23. Partially resolved molecular spectra from polarized absorption in (010) of the Hoogsteen dimer.

A 1-methylthymine spectrum down to ~265 mμ Below these wavelengths
B 9-methyladenine spectrum down to ~ 260 mμ spectra are unresolved.

See text for detailed discussion.

lies essentially at the midpoint of the C_4-C_5 bond. This point was taken as the center of the molecule. The center to center distance of nearest neighbors is 4.19$_1$ Å. The calculated energy of interaction is 233 cm^{-1}, or a total of 466 cm^{-1} for molecules above and below. These calculations show that the purine and pyrimidine moieties are weak coupled to themselves by the Simpson criterion (26), because the solution band widths are 3000 to 4000 cm^{-1}. Thus the 2000 cm^{-1} red shift for the maximum of 9-methyladenine compared to solution cannot be explained by this simple exciton calculation.

A more detailed discussion of the various molecular spectra in the several crystal systems and in solution is presented immediately below. Intensities as well as spectral shapes are compared.

Intensities and Comparison of Molecular Spectra

The various crystal spectra, when compared to solution and to each other, have interesting features. Unfortunately, the intensities for the crystal spectra have uncertainties varying from 10% to 40%. Thus any intensity differences between solution and the crystal which are outside of the error must be relatively large to be observed.

Tinoco has presented a dispersion theory to account for the loss of or gain in intensity for a particular absorption band when molecules are condensed from the free state into a polymer (27).

His treatment is based on a first order perturbation theory and on the assumption that no exchange for optical electrons takes place between the individual molecules. Hence, only coulombic interactions account for intensity changes. A comparison of the intensity of the polymer to the intensity of the monomer in solution is justified within the first order approximation if the solvent molecules are in a spherical array about the monomer. Thus to first order, the intensity of the free molecule is the same as for the molecule in solution. When a molecule is placed in a non-spherical environment of other species that have absorption bands near the band of the molecule of interest, then the dispersive interaction of the optical electron with bands of the other species will have a non-zero effect on the intensity for absorption of that optical electron. The optical electron will also be perturbed by permanent dipoles of the ground and excited states of neighboring species. But Tinoco has shown that for purine and pyrimidine derivatives the latter interaction is small compared to the former (5). If F_A is the area under band A for the polymer and f_a is the area under band a for the monomer, then the hypochromism or hyperchromism is given by

$$H = 1 - F_A/f_a = \frac{2.015 \times 10^{-3}}{\sum_i \mu_{ia}^2/\lambda_{ia}} \sum_{j \neq i} \sum_{a \neq b} \frac{\lambda_{ia}\lambda_{jb}}{\lambda_{ia}^2 - \lambda_{jb}^2} V_{ia;jb} \vec{\mu}_{ia} \cdot \vec{\mu}_{jb}$$

where

$$V_{ia;jb} = \frac{1}{R_{ij}^3} \left[\frac{\vec{\mu}_{ia} \cdot \vec{\mu}_{jb} - 3(\vec{\mu}_{ia} \cdot \vec{R}_{ij})(\vec{\mu}_{jb} \cdot \vec{R}_{ij})}{R_{ij}^2} \right]$$

For correct dimensions, λ is in $m\mu$, R is in angstroms, and μ, the transition dipole moment, is in Debyes. The index b refers to all other absorption bands which are not the same as a. Only the term for the dynamic electric field is in the above expression. For H positive, there is a decrease in intensity for the polymer compared to solution, and for H negative there is an increase in intensity.

In his intensity analysis of various polynucleotides Tinoco calculated the transition dipole moment directions for the first two ultraviolet bands of the several nucleotides from molecular orbital theory. The magnitudes of the moments were calculated from solution oscillator strengths. The second bands of the nucleotides were considered to make the major contributions to the hypochromism of the first absorption band in DNA and in other polynucleotides. Vacuum ultraviolet bands of the nucleotides and of the phosphate-sugar groups were considered negligible in this detailed calculation.

The crystals studied in this work are rough approximations to nucleotide polymers. The molecules are stacked, hydrogen-bonded pairs. The separation between pairs in the same plane is larger than the vertical separation. The calculated vertical interaction of nearest neighbors is larger than planar interactions by a factor of about two. For an approximate answer to H, it is sufficient to calculate the interaction of the two molecules nearest the molecule in excited state a.

These nearest neighbors are just above and below the molecule. Therefore,

$$H = 2(2.015 \times 10^{-3})\lambda_a^2 \sum \frac{\lambda_b}{\lambda_a^2 - \lambda_b^2} \mu_b^2 \frac{\vec{e}_a \cdot \vec{e}_b}{R^3} \left[\vec{e}_a \cdot \vec{e}_b - \frac{3(\vec{e}_a \cdot \vec{R})(\vec{e}_b \cdot \vec{R})}{R^2} \right]$$

where $\vec{e}$ is the unit vector for the respective transition dipole moments.

Unfortunately, we have no knowledge of the absorption bands in the vacuum ultraviolet; only very qualitative information on the transition moment directions for the second absorption bands of adenine and thymine was obtained in this research. The absorption of these bands, however, can be approximated by polarizabilities (28). The component of the polarizability of molecules j along the principal direction l at frequency ν is

$$\alpha_{jl} = 2/h \sum_b \frac{\nu_{jb} \mu_{jbl}^2}{\nu_{jb}^2 - \nu^2}$$

The fractional change in intensity may now be written

$$H = 2 \sum_{j \neq i} \alpha_{jl} \frac{1 - 3\cos^2 \theta_{ij}}{R^3} \qquad \text{(See reference (5).)}$$

where α_{jl} is the polarizability of the j molecules at frequency ν_a along direction l, which is parallel to $\vec{\mu}_a$. θ_{ij} is the angle between $\vec{\mu}_a$ and $\vec{R}_{ij}$. For nearest neighbor interaction the fractional change in intensity is

$$H = 4\alpha_{\ell} \left(\frac{1 - 3\cos^2\theta}{R^3}\right) . \qquad (1)$$

The polarizability, α_{ℓ}, can be approximately determined from the refractive index of a material.

By using the computed refractive indices in the absorption band region and the Clausis-Mosotti expression, the fractional change in intensity can be estimated. The refractive index at the absorption maximum is due to the absorption of all other bands and the contribution from the band of interest is eliminated. For both 1-methylthymine and 9-methyladenine the computed refractive indices along the principal directions at the respective maxima have small differences. These differences are reasonable since one would expect the polarizability to be approximately isotropic due to all other electrons in the system. The polarizabilities of 1-methylthymine and 9-methyladenine were calculated from the single crystal, refractive index computations in Appendix A. The polarizabilities at the first absorption maximum are 1.6×10^{-23} cm^3 and 1.9×10^{-23} cm^3 for the thymine and adenine derivatives, respectively. These polarizabilities are due to all the optical electrons of each molecule with the exception of the first band. It should be emphasized that in the calculations made here, the contribution of the second band is not calculated separately. The total contribution to the hypochromism (or hyperchromism) from all the bands below the first ultraviolet band is calculated by equation 1 .

Figure 24 is a plot of the solution spectrum and the crystal spectrum for 1-methylthymine where both spectra are assumed to come from a fixed one dimensional oscillator. That is, for the solution spectrum we plot three times the molar absorptivity from the isotropic absorption of 1-methylthymine in water and for the crystal we plot the sum of the in-plane absorptivities and assume the absorption perpendicular to the molecular plane is negligible. We call the latter construction the "single crystal sum spectrum." The intensity of the crystal spectrum has about a 25% error; near the relatively flat maximum the error is probably larger due to photodamage from the transmission measurements. The experimental hypochromism is $0.2_5 \pm .07$. The hypochromism calculated from equation 1 above is 0.40.

The spectrum for 1-methylthymine, rather poorly resolved from the polarization studies of the Hoogsteen dimer, is shown in Figure 24. (See the section above on the Hoogsteen dimer for details of the resolution.) The shoulder at 255 mμ is probably due to a major contribution from the weak band in 9-methyladenine. The intensity uncertainty is 40%. The integrated absorption for the solution spectrum is about twice that for 1-methylthymine in the Hoogsteen dimer. The experimental hypochromism is thus 0.5 ± 0.2. The calculated hypochromism from the dispersion theory outlined above is 0.36.

A spectrum which we call the single crystal sum spectrum of 9-methyladenine is shown in Figure 25. It is the sum of the molar

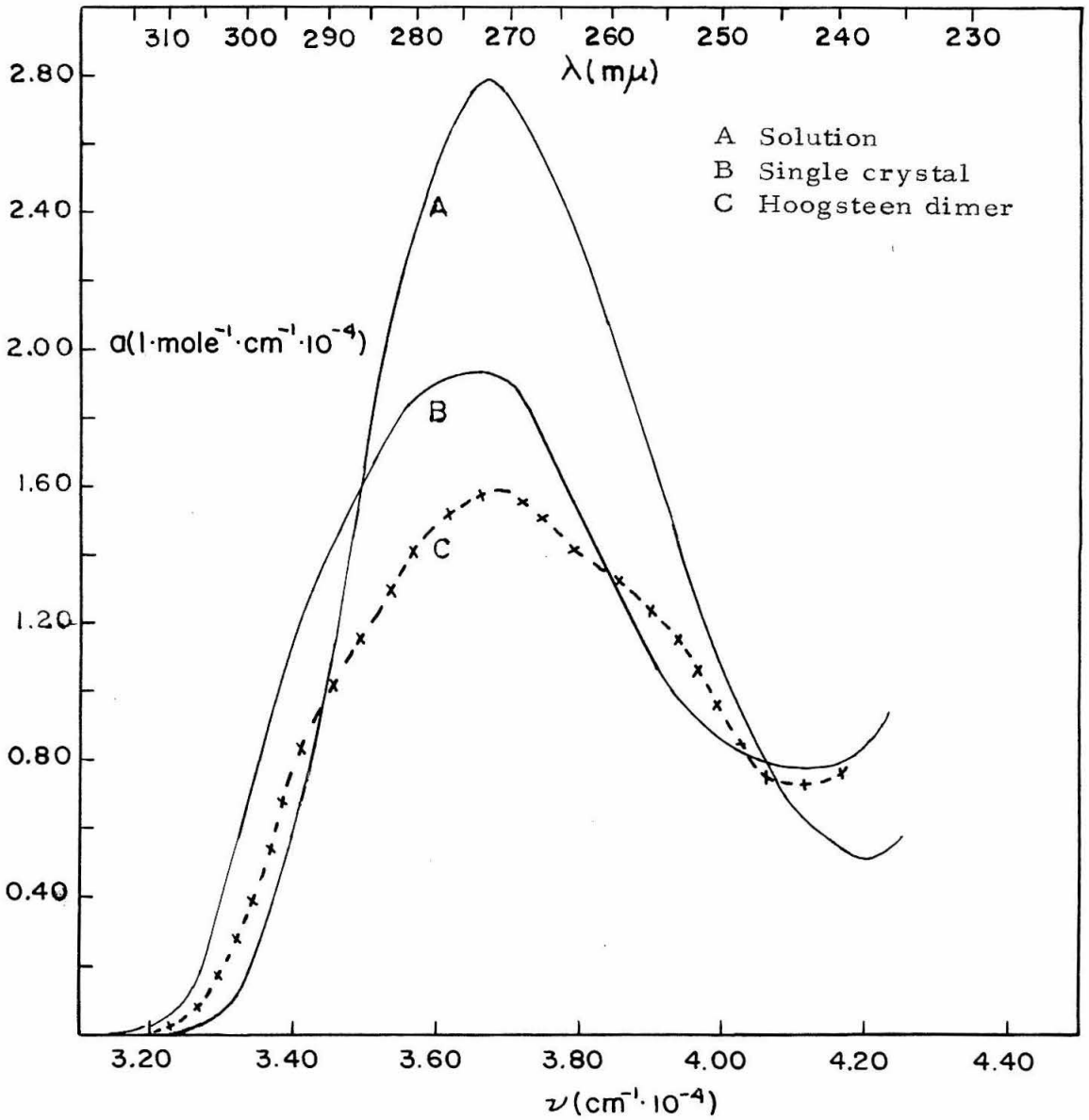

Figure 24. Absorption spectra of 1-methylthymine in different environments.

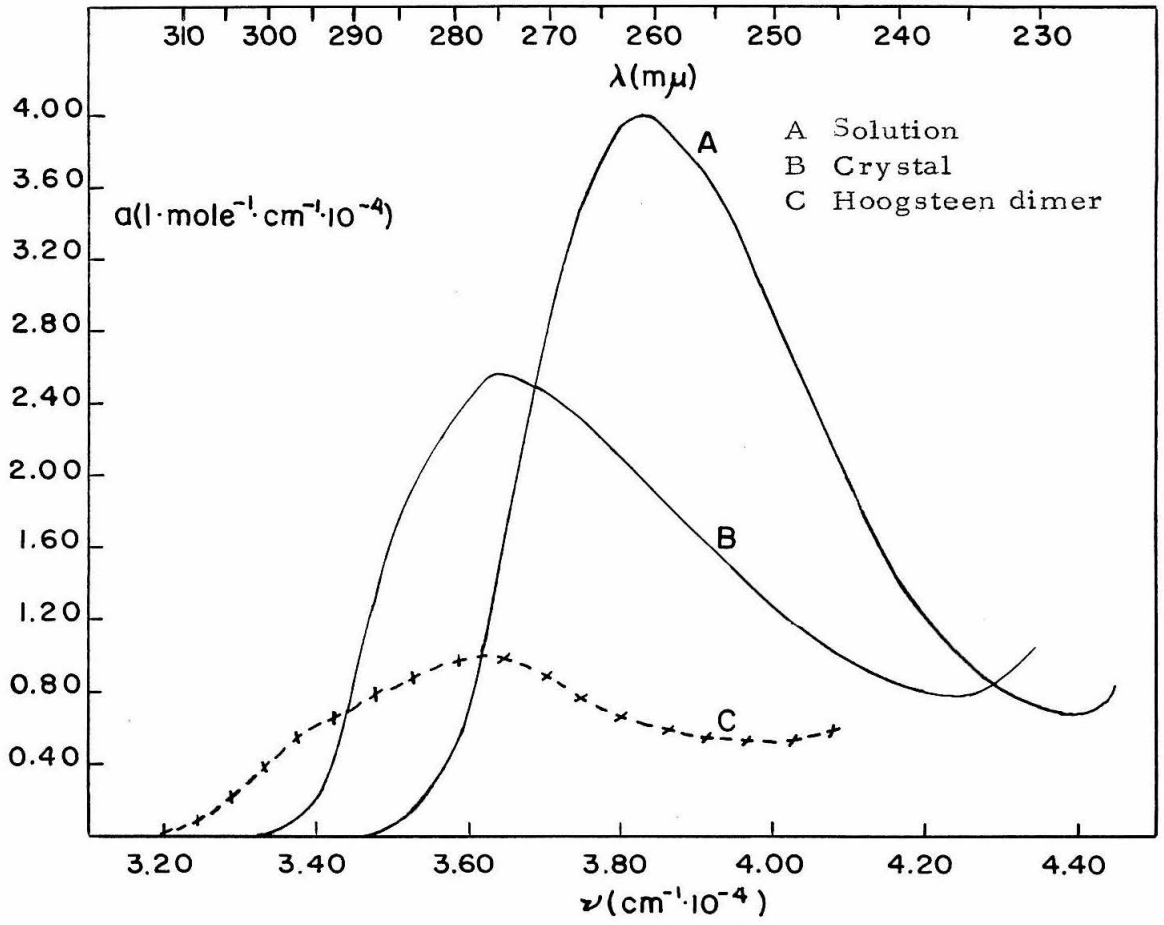

Figure 25. Absorption spectra of 9-methyladenine in different environments.

absorptivities for the two principal directions in the plane of the molecular layers (001). The solution spectrum is also shown and was constructed similarly to the solution spectrum for 1-methylthymine. (See above discussion and Fig. 24.) The isotropic spectrum of 9-methyladenine, however, probably has a component perpendicular to the molecular plane. The component was assumed to be comparable to the absorptivity along the b-axis of the Hoogsteen dimer and has been subtracted from the solution spectrum shown in Figure 25. The single crystal sum spectrum of 9-methyladenine is shifted to the red by 2000 cm^{-1} compared to solution. Moreover, the shapes of the two spectra are grossly different. The weak and strong components were not observed under the main band of the solution spectrum. Crystallization seems to have shifted the strong component to the red and perhaps the weak component to the blue.

The intensity of the single crystal absorption has an uncertainty of about 15%. The integrated absorption under the first absorption band has a hypochromism of 0.2 ± 0.1 compared to solution. A calculation of the hypochromism cannot be made because the crystal structure is not known.

The resolved spectrum of 9-methyladenine from the Hoogsteen dimer is also shown in Figure 25. (See the section above on the Hoogsteen dimer for details.) The integrated absorption is drastically smaller than that for the single crystal (a factor of about 0.4 of the area

under the single crystal band). The observed hypochromism compared to solution is 0.75 $\pm$.10. The calculated hypochromism for adenine in the Hoogsteen dimer is 0.29, from equation 1 above.

The spectrum, moreover, is red shifted on the toe absorption side of the curve relative to the single crystal of 9-methyladenine. The adenine derivative evidently suffers a major perturbation when taken from a single crystal of itself and placed in the Hoogsteen dimer. The molecular packing for 9-methyladenine in the Hoogsteen dimer is very close. The nearest atoms, C_4 and C_2, of the molecule below, are separated by only 3.28_6 Å. The electrostatic interaction of the formal charges on these cores is large at this distance and can grossly change the wavefunction of the molecule. Permanent dipole interactions can also change the electron density of the molecule. Regardless of the nature of the interaction, the perturbation is sufficiently strong to make identification of the strong band uncertain. The Hoogsteen dimer absorption assigned to 9-methyladenine, however, is very much larger (a factor of about 20) than the weak component observed in the single crystal. The maximum of 9-methyladenine in the Hoogsteen dimer agrees with the maximum for the strong component of the single crystal. It seems unlikely that the perturbation on 9-methyladenine would shift the weak component about 3000 cm^{-1} to the red and also increase the intensity by a factor of 20. If this were the case, then the strong component, observed in the single crystal, would have to be either

shifted to the blue about 10,000 cm^{-1} or lose its intensity by a factor of about 50.

With reservation then, the transition dipole moment direction, calculated from the polarization analysis of the Hoogsteen dimer, is regarded as the same for the strong band observed in the single crystal. Furthermore, the strong component of the single crystal is considered to be the major contribution to the first absorption band observed in solution. The polarization for the major absorption component in adenine, therefore, is along the short axis of the molecule (168° in the Tinoco convention). This result is inconsistent with Mason's assignment (18) based on substituent effects on purine. 6-Aminopurine (adenine) in solution has a main, first absorption band peaked at 260 mμ with a small shoulder at 267 mμ . The spectrum of purine is essentially identical to adenine. 8-Aminopurine has a maximum at 283 mμ and a second maximum at 241 mμ with the former band 4½ times more intense. 2-Aminopurine has a first maximum at 305 mμ , a second at 236 mμ , and both bands have comparable intensity. Mason argues that the amino group in the 8 position adds further conjugation to the purine ring and shifts the main component of the purine absorption band to the red. Hence, the major component is long-axis polarized. The amino group in the 2 position, which is 30° to the long axis, shifts the spectrum further to the red and decreases the intensity. For both cases the minor component is peaked around 240 mμ . The main

assumption here is that the red-shifted band, with intensities comparable to the adenine band, is the same as the major absorption band for adenine. Substitution of the amino groups, which have two π electrons, onto the purine ring causes large perturbations as compared to crystallization effects. It is hard to know with certainty which purine component is being enhanced by the substitution.

The assignment of the polarization can be resolved when the crystal structure of 9-methyladenine is determined. It is interesting to note that Rhodes could account for the hypochromicity of polyadenine if he assumed the first absorption band for adenine to be short-axis polarized (24). Tinoco's calculation for the hypchromism of poly AT is closer to the experimental value if short-axis polarization is assumed (5). The last two points, however, are not particularly weighty, because the dispersion theory for polynucleotides is highly approximate.

From molecular orbital theory, Tinoco has calculated the transition dipole moment directions for the near ultraviolet absorption bands of the several nucleotides (5). For adenine the first absorption band consists of two components, one polarized at 52° and the other at 147°. The assignment from our polarization experiments is 168° for the major component. This is 21° from the 147° direction and 64° from the 52° direction. Tinoco's calculated transition direction for thymine is 3°. The polarization experiments indicate that the direction is 161°, which is a discrepancy of 22°.

The absorption perpendicular to the (010) for the Hoogsteen dimer is probably due to n - π^* transitions in the purine moiety. Both the polarization and rather low intensities (100 to 1000 ℓ. mole^{-1} cm^{-1}) of the spectra suggest this assignment. It is interesting that the absorption perpendicular to the (010) is about 1000 cm^{-1} to the blue of the in-plane adenine absorption resolved from (010) polarization studies of the Hoogsteen dimer. For a variety of heteromolecules it has been observed that the longest wavelength transition (singlet-singlet) is an n - π^* transition (13). When the weak, out of plane absorption from the Hoogsteen dimer is compared to 9-methyladenine in solution, the former is about 1000 cm^{-1} to the red; when it is compared to the single crystal sum spectrum for 9-methyladenine, it is near the edge of the in-plane absorption. Figure 26 is a plot of the four spectra of 9-methyladenine in different environments.

Pyrimidine in cyclohexane has an n - π^* transition at 300 mμ (19). The transition is well resolved from the first π - π^* transition with a maximum at 245 mμ. The addition of an imidazole ring to the pyrimidine red shifts the π - π^* transition to 260 mμ, but the n - π^* seems to remain peaked at 295-300 mμ. The only purine which can be dissolved in cyclohexane is 9-methylpurine; the n - π^* transition appears as a shoulder, but is distinctly evident at 300 mμ (18). No n - π^* transitions of adenine or its derivatives have been observed in solution because the compounds are only soluble in water. The n - π^*

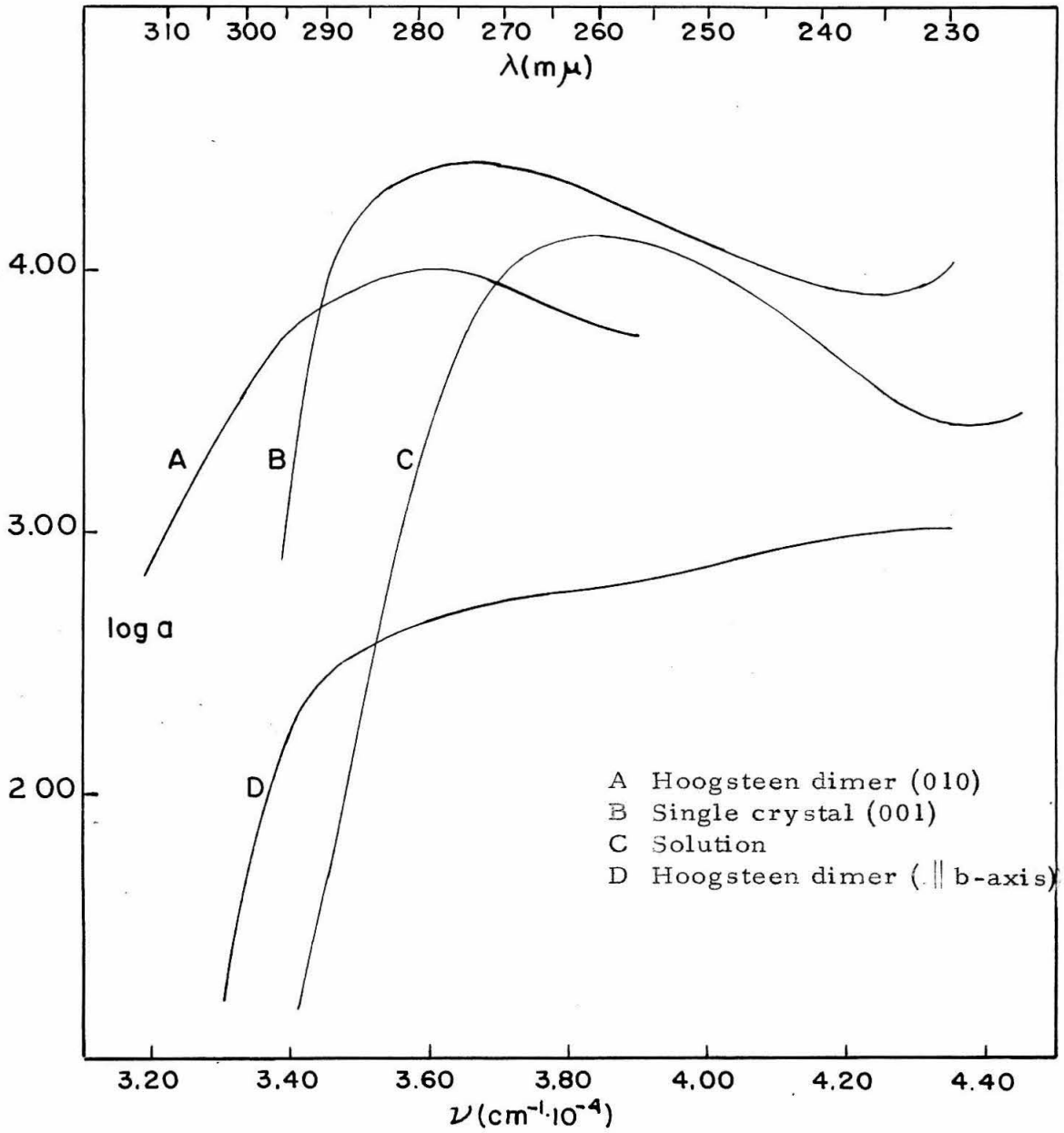

Figure 26. 9-Methyladenine absorption spectra in several systems.

transition energy is relatively insensitive to substituent effects, but is strongly blue shifted in the presence of hydrogen bonding solvents (16). The transition is relatively localized on the nitrogen and may be thought of as an n to p transition, where absorption by the optical electron involves a transition from an sp^2 orbital of the nitrogen to a 2p orbital on the nitrogen. The success of the "independent system" view has been demonstrated by Robinson in his diazine studies (7). In the absence of a hydrogen bonding solvent, then, one would expect the lowest $n - \pi^*$ transition energy of adenine to be similar to purine, just as pyrimidine and 9-methylpurine have their lowest $n - \pi^*$ transitions near the same energy. The (0,0) band for the allowed $n - \pi^*$ transition of crystalline pyrazine is -200 cm^{-1} to the red of the vapour spectrum (7). Crystallization of the diazine does not strongly shift the $n - \pi^*$ transition, but it does spread the band out. On these grounds one would not expect a large energy shift of the $n - \pi^*$ transition for adenine in the crystalline state.

Therefore, perpendicular absorption is viewed as a normal $n - \pi^*$ transition for adenine and has shifted about 1000 cm^{-1} to the red in going from water into the crystalline environment of the Hoogsteen dimer (similar to a hydrocarbon solvent). The grossly red-shifted $\pi - \pi^*$ transition for adenine in the Hoogsteen dimer is the feature which is difficult to understand.

The continually rising absorption perpendicular to the molecular planes is thought to be due to overlap of other $n-\pi^*$ transitions. The hydrogen bonded N_7 provides a site for the transition which is expected to be to the blue of the other $n-\pi^*$ transitions. Contributions from $n-\pi^*$ transition of the carbonyls in 1-methylthymine should be relatively small due to the pure p character of the non-bonding orbitals on the oxygens. As mentioned earlier, the adenines are packed closely with a nearest atom distance of 3.28_6 Å for two carbons. (See Fig. 21.) The calculated overlap, using Slater atomic orbitals, is .03. It may be that the absorption near 230 mμ is a charge transfer type between the rings, with some degree of delocalization of the excited state provided by the rest of the π-electron system. An absorption spectrum perpendicular to the (001) of a 9-methyladenine, single crystal would shed some light on this conjecture. The spacing of molecular layers is 3.6 Å. It was pointed out in the crystal preparation section, however, that the {010} was too poorly developed to mount the crystal for slicing in this direction.

APPENDIX A

Optical Dispersion Theory. The Drude theory for optical dispersion is based on the assumption that an optical electron is bound by Hooke's law forces and subject to a damping force proportional to the displacement velocity (6). Under the influence of an external electric field the equation of motion for the electron is

$$m \frac{\partial^2 \xi}{\partial t^2} = eX - \frac{4\pi e^2}{\theta} \xi - re^2 \frac{\partial \xi}{\partial t}$$

where X is the component of the external electric field,

$\frac{4\pi e^2}{\theta} \xi$ is the restoring force,

and $re^2 \frac{\partial \xi}{\partial t}$ is the damping force.

r and θ are positive constants.

Under stationary state conditions the displacement variable may be expressed as a periodic function of time. The solution to the equation of motion is then

$$e\xi = \frac{1}{4\pi} X \frac{\theta}{1 + i/\tau \; a - b/\tau^2}$$

where $\tau = T/2\pi$ is the angular period of the external electric field,

$a = \frac{r\theta}{4T}$ and $b = \frac{m\theta}{4\pi e^2}$.

The current in the x-direction is

$$j_x = \frac{1}{4\pi} \frac{\partial x}{\partial t} + \sum_j e N \frac{\partial \xi_j}{\partial t}$$

$$\therefore \quad j_x = \frac{1}{4\pi} \frac{\partial x}{\partial t} \left(1 + \sum_j \frac{\theta_j N}{1 - i/\tau \; a_j - b_j/\tau^2}\right)$$

From Maxwell's equations we identify

$$\epsilon' = 1 + \sum_j \frac{\theta_j N}{1 + i/\tau \; a_j - b_j/\tau^2} = n^2 (1 - ik)^2 .$$

ϵ' is the complex diolectric constant, n is the refractive index and k is the absorptivity per λ in the medium.

For the general linear differential equation,

$$\sum_{j=o}^{N} C_j \left(\frac{d}{dt}\right)^j \chi = e^{i\omega t}, \quad Q_N = \left[\sum_{j=o}^{N} C_j (i\omega)^j\right]^{-1}$$

is a solution

$$= J_N(\omega) - i H_N(\omega)$$

Then

$$J_N(\omega) = \frac{2}{\pi} \int_o^\infty \frac{H(y) y dy}{y^2 - \omega^2} \quad \text{and} \quad H_N(\omega) = \frac{2\omega}{\pi} \int_o^\infty \frac{J(y) dy}{\omega^2 - y^2}$$

The transformation relationships between $J_N(\omega)$ and $H_N(\omega)$ are called the Kramers-Kronig transformations (17).

But $Q_N(\omega) = \sum_j \frac{\theta_j N}{1 + i/\tau \; a_j - b_j/\tau^2}$

is the solution to Drude's equation.

$$\therefore \epsilon' = n^2 (1 - ik)^2 = 1 + \Omega(\omega) = 1 + J(\omega) - iH(\omega)$$

$$n^2 - (nk)^2 = 1 + J(\omega)$$

$$2n(nk) = H(\omega)$$

$$J(\omega) = \frac{2}{\pi} \int_0^\infty \frac{H(y)y\,dy}{y^2 - \omega^2}$$

$\int_0^\infty \frac{H(y)y\,dy}{y^2 - \omega^2}$ is approximated with the measured absorption band, a dispersion term for the second absorption band near 2000 Å and a constant term.

$$\therefore n^2(\omega) - (nk)^2(\omega) = n_o^2(\omega) + \frac{2}{\pi} \int_{\omega_1}^{\omega_2} \frac{2n(y)nk(y)dy}{y^2 - \omega^2}$$

where ω_1 to ω_2 covers the angular frequency over the measured absorption band. In terms of λ, the vacuum wavelength, and $a(\lambda)$, an absorptivity term in cm^{-1}, the expression rearranges to

$$n^2(\lambda_o) = n_o^2(\lambda_o) + 0.226102\,\lambda_o^2 \left[0.143911\, a^2(\lambda_o) + \int_{\lambda_1}^{\lambda_2} \frac{n(\lambda)a(\lambda)d\lambda}{\lambda_o^2 - \lambda^2} \right]$$

with $n_o(\lambda) = n_o + \frac{fe^2 N \lambda_s^2}{mc^2 \pi (1 - \lambda_s^2/\lambda^2)}$

where n_o is a constant,

λ_s is the maximum for the second absorption band,

f is the oscillator strength,

and N is the density of optical electrons.

The procedure for calculation is as follows:

1. Compute $A(589\ m\mu) = (0.226102)(589)^2 \int_{\lambda_1}^{\lambda_2} \frac{n_o(\lambda)_I\, a(\lambda)\, d\lambda}{(589)^2 - \lambda^2}$

where λ_1 to λ_2 is over the measured absorption band and $n_o(\lambda)_I$ has been first approximated from the oscillator strengths of the first two ultraviolet absorption bands in solution.

Then $\sqrt{N^2(589)\text{measured} - A} = n_o(\lambda)_{II} = n_{oII} + \frac{f^2 e\, n\lambda_s^2}{mc^2 \pi (1-\lambda_s^2/(589)^2)}$

2. With $n_o(\lambda)_{II}$, refractive indices for all wavelengths of interest are calculated:

$$n = \left[n_o^2(\lambda)_{II} + 0.226102\lambda^2 \left(0.143911\, a^2(\lambda) + \int_{\lambda_1}^{\lambda-1} \frac{n_o(\lambda')_{II}\, a(\lambda')\, d\lambda'}{\lambda^2 - \lambda'^2} + \frac{n_o(\lambda)_{II}\, a(\lambda)}{2\lambda} \log_e \left(\frac{2\lambda+1}{2\lambda-1}\right) + \int_{\lambda+1}^{\lambda_2} \frac{n_o(\lambda')_{II}\, a(\lambda')\, d\lambda'}{\lambda^2 - \lambda'^2}\right)\right]^{\frac{1}{2}}$$

where $a(\lambda) = a(\lambda - 1) = a(\lambda + 1)$ for λ in $m\mu$ and $a(\lambda) = 0$ for $\lambda > \lambda_2$.

3. Reflection coefficients for wavelengths of interest are computed:

$$R(\lambda) = \frac{(n(\lambda)-1)^2 + \left[\frac{\lambda a(\lambda)}{4\pi}\right]^2}{(n(\lambda)+1)^2 + \left[\frac{\lambda a(\lambda)}{4\pi}\right]^2}$$

4. The computation is repeated by returning to 1 and fitting to the measured refractive index at 589 $m\mu$ to get $n(\lambda)_{III}$. The number of iterations is taken on a trial and error basis.

The calculations were done on an IBM 7090 computer with a Fortran code. Ten iterations were more than adequate to give a consistent set of refractive indices to three decimal places.

The input data and calculated refractive indices for the several crystals are tabulated below. The raw absorbance data is omitted.

b-Axis Dispersion in (102) of 1-Methylthymine

$f_{207\ m\mu} = 0.17$

$f_{270\ m\mu} = .0105$

$$n_I(\lambda) = 1.61_0 + \frac{.0391}{1-(207)^2/\lambda^2} \qquad n_Y\ (589) = 1.660$$

λ (mμ)	Cycle Number 7 N	R
240	1.715	.070
245	1.721	.070
250	1.720	.070
255	1.710	.069
260	1.701	.068
265	1.700	.067
270	1.703	.068
275	1.715	.070
280	1.729	.072
285	1.739	.073
290	1.748	.074
295	1.749	.074
300	1.741	.073
305	1.730	.071
310	1.716	.069
320	1.705	
340	1.692	
360	1.684	
380	1.678	
400	1.674	

p-Axis Dispersion in (102) of 1-Methylthymine

$f_{207} = .015_6$

$f_{270} = .116$

$$n_I(\lambda) = 1.700 + \frac{.0036}{1 - (207)^2/\lambda^2} \qquad n_z(589) = 1.762$$

λ(mμ)	Cycle N	Number 7 R
235	1.360	.025
240	1.319	.020
245	1.299	.019
250	1.301	.020
255	1.244	.016
260	1.250	.023
265	1.306	.034
270	1.503	.063
275	1.728	.091
280	1.912	.113
285	2.042	.128
290	2.169	.144
295	2.257	.153
300	2.330	.162
305	2.281	.153
310	2.176	.137
315	2.085	.124
320	2.007	.112
340	1.913	
360	1.864	
380	1.836	
400	1.817	

b-Axis Dispersion in (001) of 9-Methyladenine

$f_{207} = 0.16$

$f_{270} = .15_5$

$$n_I(\lambda) = 1.762 + \frac{.0366}{1 - (207)^2/\lambda^2} \qquad n_z(589) = 1.880$$

λ(mμ)	Cycle N	Number 7 R
230	1.640	.059
235	1.562	.049
240	1.500	.041
245	1.454	.037
250	1.428	.036
255	1.433	.040
260	1.502	.054
265	1.597	.070
270	1.775	.098
275	2.059	.139
280	2.306	.169
285	2.563	.200
290	2.631	.203
295	2.484	.182
300	2.327	.159
305	2.220	.144
310	2.170	.136
320	2.096	
340	2.040	
360	1.977	
380	1.954	
400	1.936	

a-Axis Dispersion in (001) of 9-Methyladenine

$f_{207} = 0.16$

$f_{270} = 0.031$

$$n_I(\lambda) = 1.628 + \frac{.0366}{1 - (207)^2/\lambda^2} \qquad n_y(589) = 1.783$$

λ (mμ)	Cycle N	Number 7 R
230	1.741	.075
235	1.796	.082
240	1.822	.086
245	1.818	.085
250	1.794	.081
255	1.780	.079
260	1.799	.082
265	1.827	.087
270	1.854	.091
275	1.909	.099
280	1.945	.104
285	1.984	.109
290	1.989	.110
295	1.949	.104
300	1.919	.099
305	1.889	
310	1.875	
320	1.856	
340	1.833	
360	1.820	
400	1.805	

"Mean" Dispersion in (010) of Hoogsteen Dimer

$f_{200} = 0.5$

$f_{270} = 0.2$

$$n_I(\lambda) = 1.65_0 + \frac{.0539}{1 - (200)^2/\lambda^2} \qquad \sqrt{n_y n_z} = 1.764$$

Cycle Number 4

λ(mμ)	N	R
230	1.712	.069
235	1.730	.072
240	1.735	.073
245	1.727	.072
250	1.723	.071
255	1.723	.071
260	1.723	.071
265	1.727	.072
270	1.752	.076
275	1.809	.085
280	1.869	.093
285	1.908	.099
290	1.942	.103
295	1.984	.109
300	1.987	.109
305	1.961	.105
310	1.933	.101
315	1.908	.098
320	1.886	.094
340	1.839	
360	1.818	
380	1.804	
400	1.795	

APPENDIX B

Least squares analysis of polarized absorption. One may think of crystal absorption as involving a projection of the electric vector from the incident light onto a set of orthogonal axes (principal axes). the amplitudes of these electric vector components are then attenuated in the usual Beer's law form along the principal directions as the ray passes through the crystal (21).

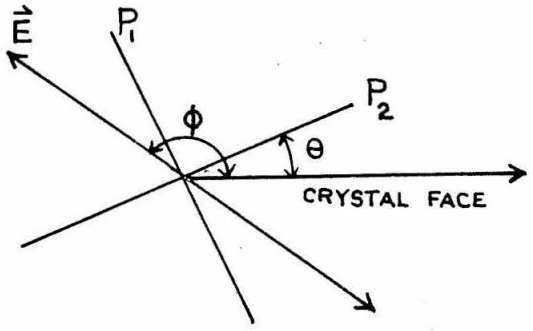

If φ is the angle between a crystal face and the electric vector of the incident light, and θ is the angle from the same crystal face to a principal axis, then the transmission

$$I/I_o = \cos^2(\varphi - \theta)10^{-A_2} + \sin^2(\varphi - \theta)10^{-A_1}$$

where A_2 and A_1 are the absorbances along the corresponding principal directions P_2 and P_1. With rearrangements the expression can be linearized to give

$$T(\varphi) = I/I_o = \tfrac{1}{2}(T_2-T_1)\cos 2\theta \cos 2\varphi + \tfrac{1}{2}(T_2-T_1)\sin 2\theta \sin 2\varphi + \tfrac{1}{2}(T_2+T_1)$$

where $T_2 = 10^{-A_2}$ and $T_1 = 10^{-A_1}$.

Thus the measured transmission as a function of the polarized angle φ is

$$T(\varphi) = \beta\xi + \gamma\eta + \delta \qquad \text{where } \xi = \cos 2\varphi \text{ and } \eta = \sin 2\varphi$$

$$\theta = \tfrac{1}{2}\tan^{-1}\gamma/\beta$$

$$T_2 = \frac{\delta\cos 2\theta + \beta}{\cos 2\theta} \quad \text{and} \quad T_1 = \frac{\delta\cos 2\theta - \beta}{\cos 2\theta}$$

For a least squares analysis the linear form for $T(\varphi)$ is convenient. ξ and η are errorless and the error in T is proportional to T. The parameters β, γ, and δ are determined from the least squares condition,

$$\frac{\partial f}{\partial\beta} = \frac{\partial f}{\partial\gamma} = \frac{\partial f}{\partial\delta} = 0$$

where $$f(\beta,\gamma,\delta) = \Sigma w_i\,(T_i - \beta\xi_i - \gamma\eta_i - \delta)^2$$

and $$w_i = 1/T_i^2$$

Hence, Det $= \begin{vmatrix} \Sigma\xi_i^2/T_i^2 & \Sigma\xi_i\eta_i/T_i^2 & \Sigma\xi_i/T_i^2 \\ \Sigma\xi_i\eta_i/T_i^2 & \Sigma\eta_i^2/T_i^2 & \Sigma\eta_i/T_i^2 \\ \Sigma\xi_i/T_i^2 & \Sigma\eta_i/T_i^2 & \Sigma 1/T_i^2 \end{vmatrix}$

and

$$\beta = \begin{vmatrix} \Sigma T_i\xi_i/T_i^2 & \Sigma\xi_i\eta_i/T_i^2 & \Sigma\xi_i/T_i^2 \\ \Sigma T_i\eta_i/T_i^2 & \Sigma\eta_i^2/T_i^2 & \Sigma\eta_i/T_i^2 \\ \Sigma T_i/T_i^2 & \Sigma\eta_i/T_i^2 & \Sigma 1/T_i^2 \end{vmatrix} \Big/ \text{Det}$$

$$\gamma = \begin{vmatrix} \Sigma\xi_i^2/T_i^2 & \Sigma T_i\xi_i/T_i^2 & \Sigma\xi_i/T_i^2 \\ \Sigma\xi_i\eta_i/T_i^2 & \Sigma T_i\eta_i/T_i^2 & \Sigma\eta_i/T_i^2 \\ \Sigma\xi_i/T_i^2 & \Sigma T_i/T_i^2 & \Sigma 1/T_i^2 \end{vmatrix} \Big/ \text{Det}$$

$$\delta = \begin{vmatrix} \Sigma \xi_i / T_i^2 & \Sigma \xi_i \eta_i / T_i^2 & \Sigma T_i \xi_i / T_i^2 \\ \Sigma \xi_i \eta_i / T_i^2 & \Sigma \eta_i^2 / T_i^2 & \Sigma T_i \eta_i / T_i^2 \\ \Sigma \xi_i / T_i^2 & \Sigma \eta_i / T_i^2 & \Sigma T_i / T_i^2 \end{vmatrix} \Big/ \text{Det}$$

From the general theory of statistical analysis the inverse matrix elements from the matrix whose determinant is Det can be used to calculate the errors of the parameters β, γ, δ. With the standard deviations of the parameters, the standard deviations of θ, A_1, and A_2 were computed. The algebraic expressions are:

$$\sigma_\theta^2 = \left[\left(\frac{\partial h}{\partial \beta}\right)^2 \overleftrightarrow{H}^{-1}_{1,1} + 2 \frac{\partial h}{\partial \beta} \frac{\partial h}{\partial \gamma} \overleftrightarrow{H}^{-1}_{1,2} + \left(\frac{\partial h}{\partial \gamma}\right)^2 \overleftrightarrow{H}^{-1}_{2,2} \right] (2.303)^2 \sigma_A^2$$

$\overleftrightarrow{H}^{-1}_{i,j}$ are the inverse matrix elements of the matrix whose determinant is Det. And $h = \frac{1}{\delta} \tan^{-1} \gamma/\beta$

$$\sigma_{A_{max}}^2 = \left[\left(\frac{\partial g}{\partial \beta}\right)^2 \overleftrightarrow{H}^{-1}_{1,1} + \left(\frac{\partial g}{\partial \gamma}\right)^2 \overleftrightarrow{H}^{-1}_{2,2} + \left(\frac{\partial g}{\partial \delta}\right)^2 \overleftrightarrow{H}^{-1}_{3,3} + 2\left(\frac{\partial g}{\partial \beta}\right)\left(\frac{\partial g}{\partial \gamma}\right) \overleftrightarrow{H}^{-1}_{1,2} \right.$$

$$\left. + 2\left(\frac{\partial g}{\partial \beta}\right)\left(\frac{\partial g}{\partial \delta}\right) \overleftrightarrow{H}^{-1}_{1,3} + 2\left(\frac{\partial g}{\partial \gamma}\right)\left(\frac{\partial g}{\partial \delta}\right) \overleftrightarrow{H}^{-1}_{2,3} \right] (2.303)^2 \sigma_A^2$$

$$g = -\log_{10} (\delta - \sqrt{\beta^2 + \gamma^2})$$

$\sigma_{A_{min}}^2$ = above for $\sigma_{A_{max}}^2$ except use f

where $f = -\log_{10}(\delta + \sqrt{\beta^2 + \gamma^2})$

$$\sigma_A^2 = \sum \frac{(\text{error})_i^2}{(n - 3)}$$ from the curve fitted to

$$A(\varphi) = -\log_{10}(\beta\xi + \gamma\eta + \delta).$$

All computations were carried out with an IBM 7090. The program was written in Fortran.

With the appropriate reflection correction, assumed to be isotropic, $A(\varphi)$ was converted to molar absorptivity units. The computed curves are shown below on polar coordinates with the experimental points. The ac plane with the refractive indices N_z and N_y is shown on a polar coordinate graph for convenience.

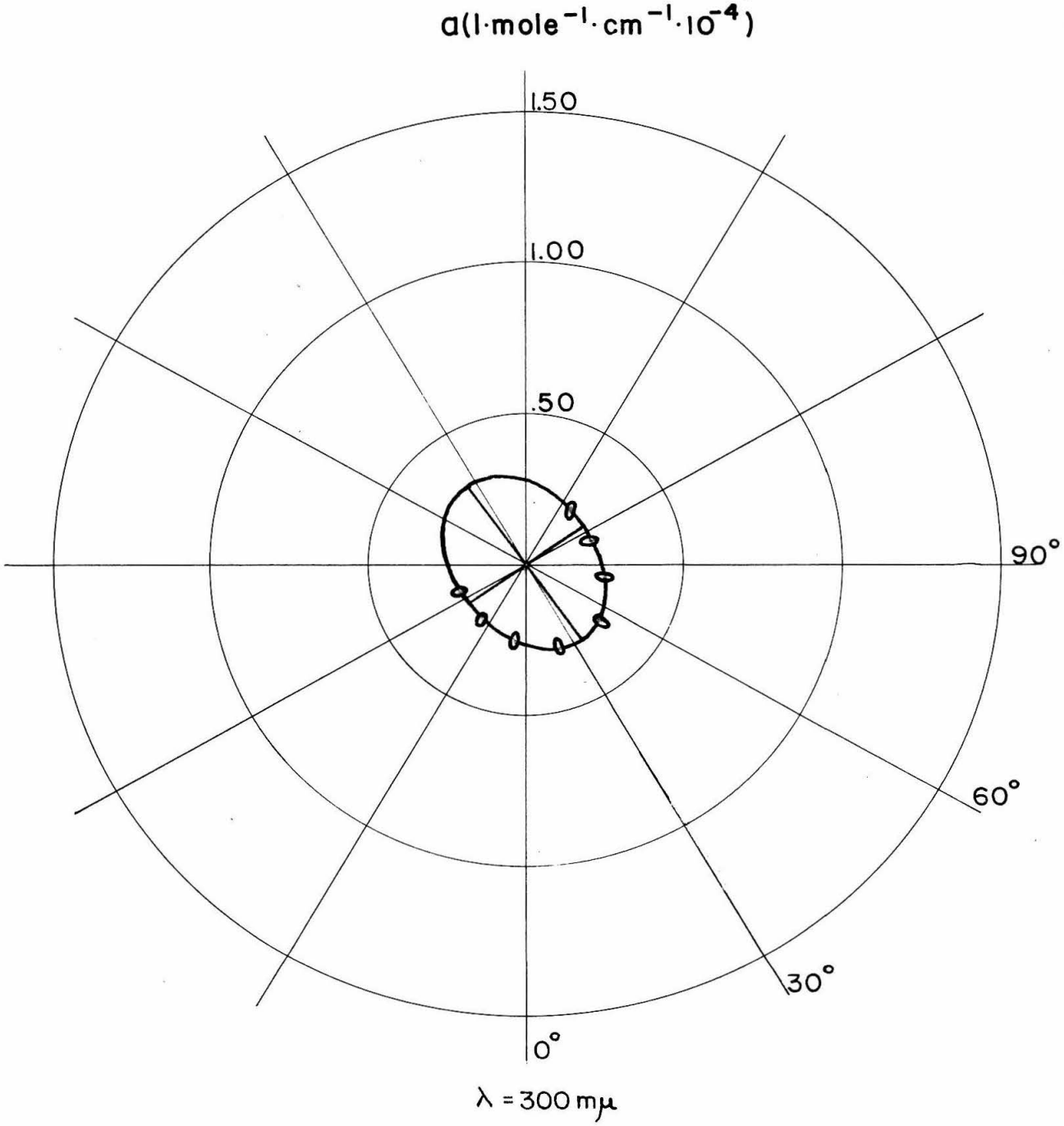
a(l·mole⁻¹·cm⁻¹·10⁻⁴)
1.50
1.00
.50
90°
60°
30°
0°
λ = 300 mμ

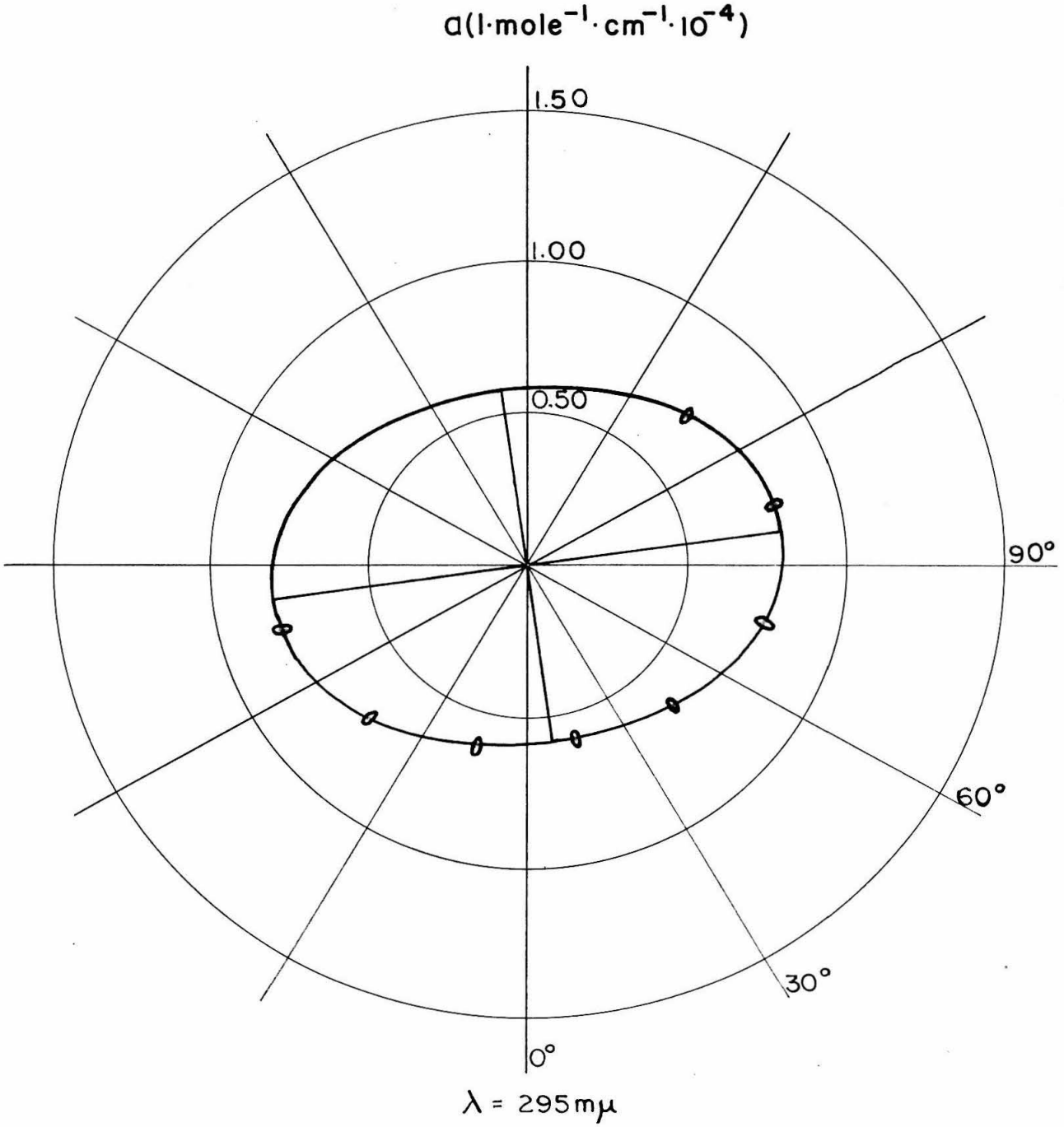
a(l·mole⁻¹·cm⁻¹·10⁻⁴)
1.50
1.00
0.50
90°
60°
30°
0°
λ = 295mμ

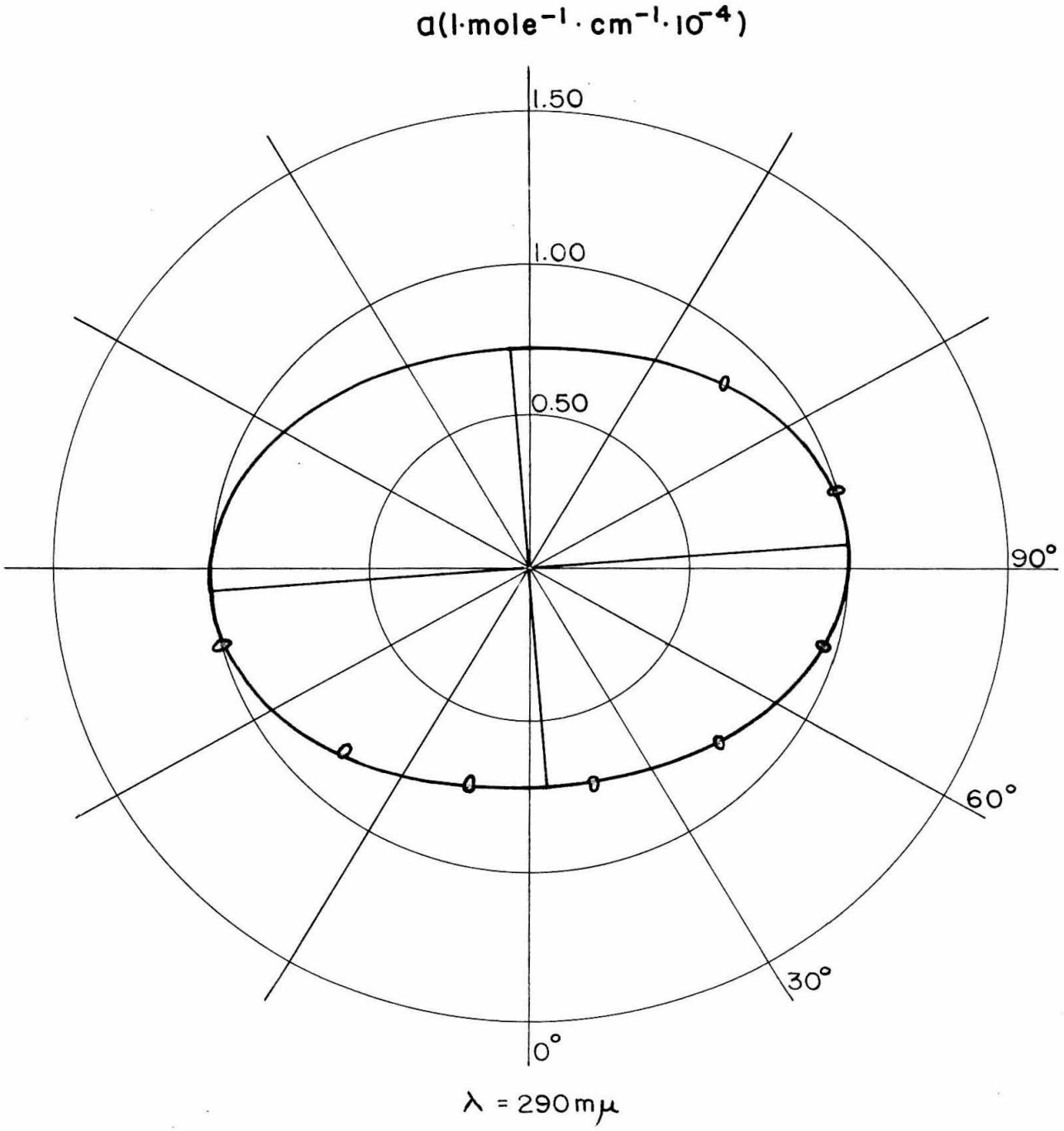
a(l·mole⁻¹·cm⁻¹·10⁻⁴)
1.50
1.00
0.50
90°
60°
30°
0°
λ = 290 mμ

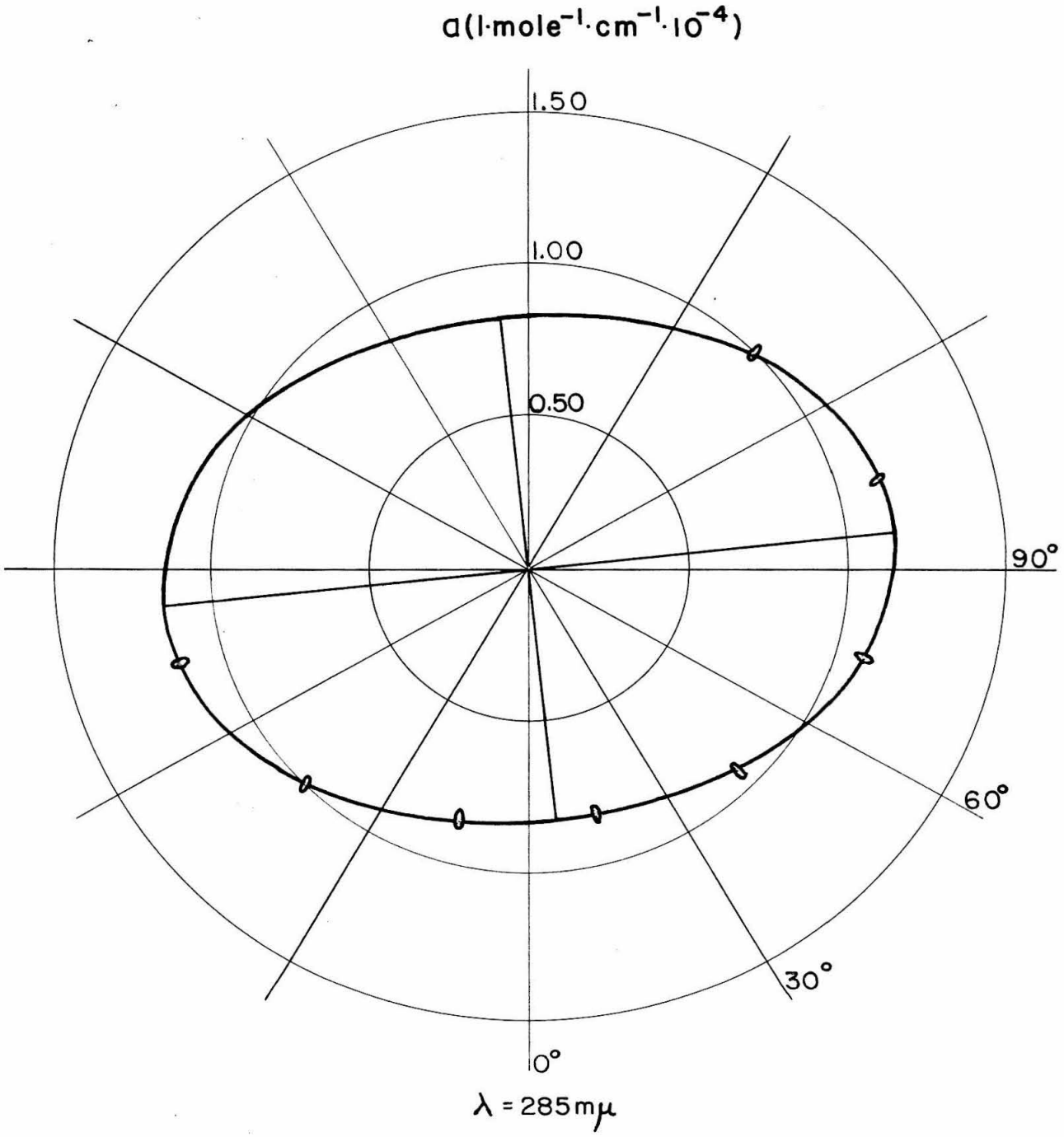
a(l·mole⁻¹·cm⁻¹·10⁻⁴)
1.50
1.00
0.50
90°
60°
30°
0°
λ = 285mμ

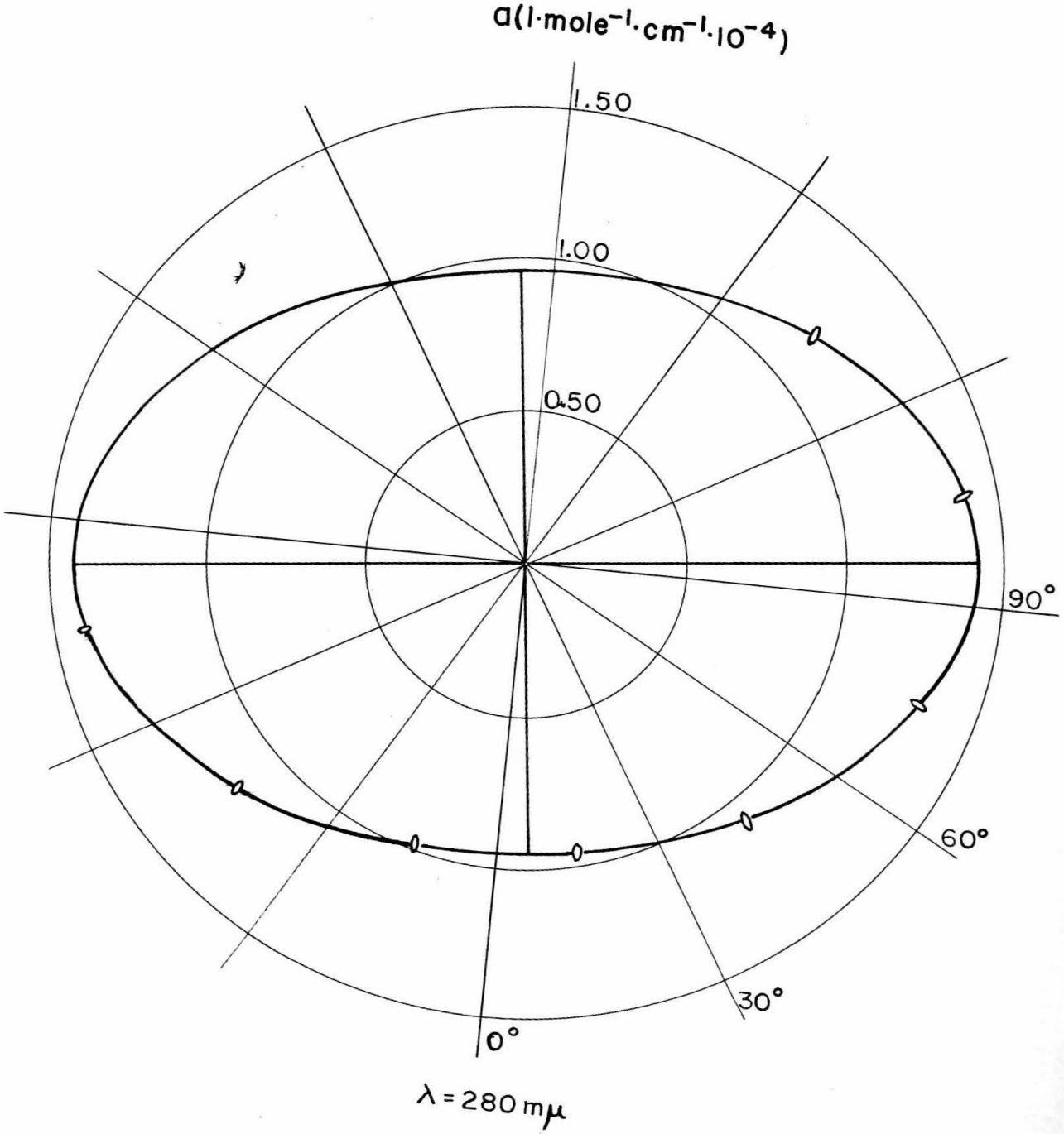
a(l·mole⁻¹·cm⁻¹·10⁻⁴)
1.50
1.00
0.50
90°
60°
30°
0°
λ = 280 mμ

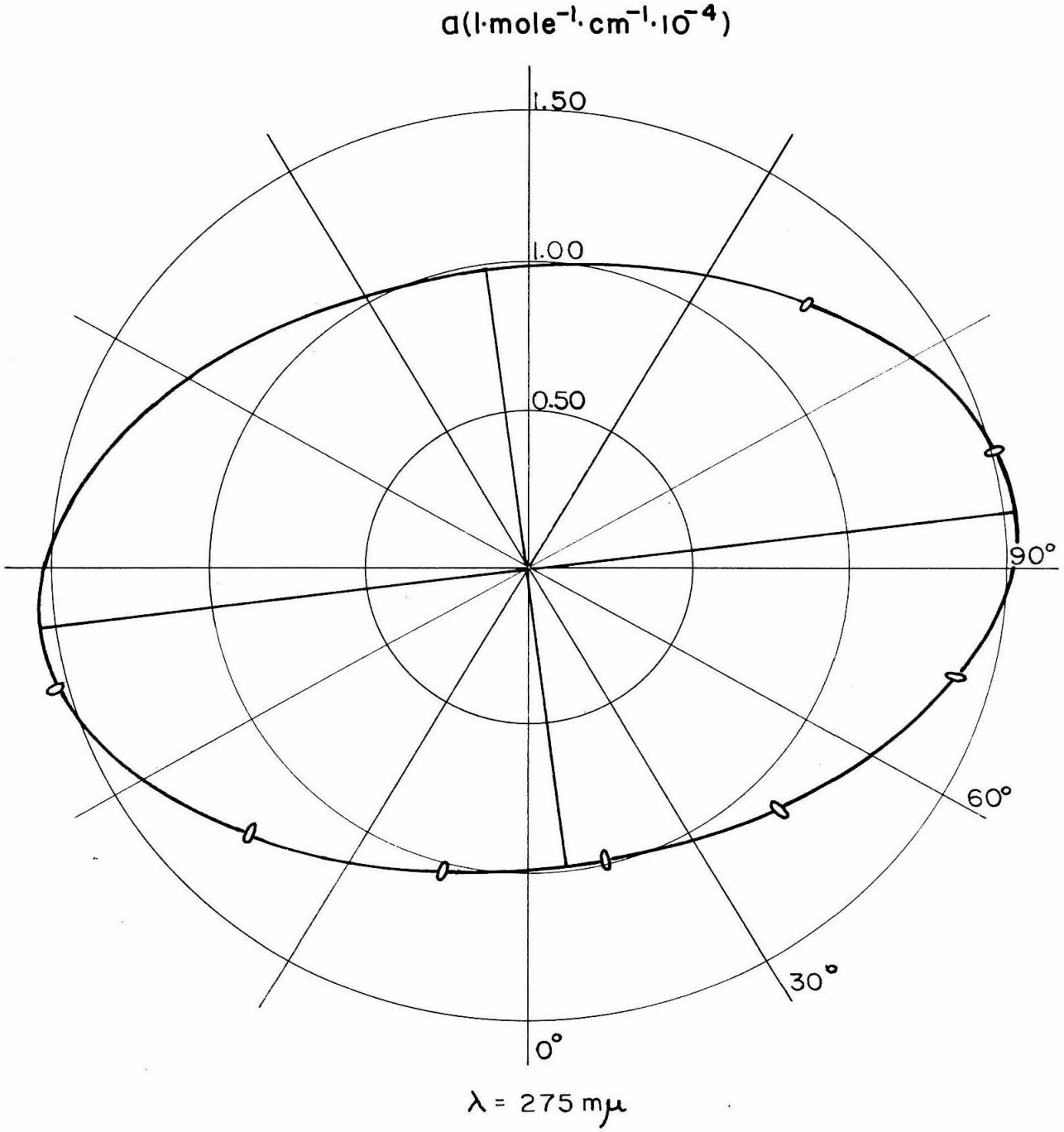
a(l·mole⁻¹·cm⁻¹·10⁻⁴)
1.50
1.00
0.50
90°
60°
30°
0°
λ = 275 mμ

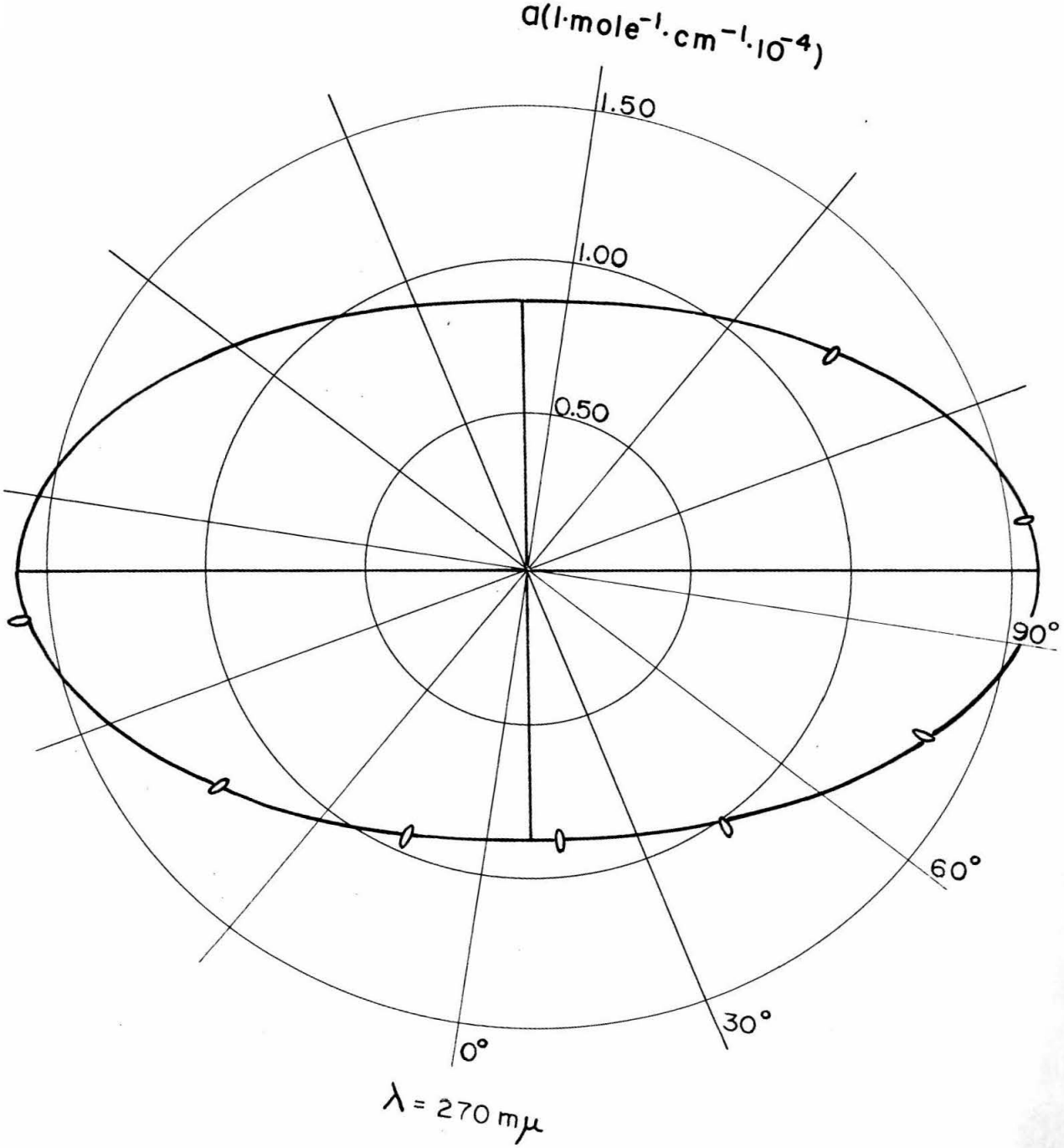
a(l·mole⁻¹.cm⁻¹.10⁻⁴)
1.50
1.00
0.50
90°
60°
30°
0°
λ = 270 mμ

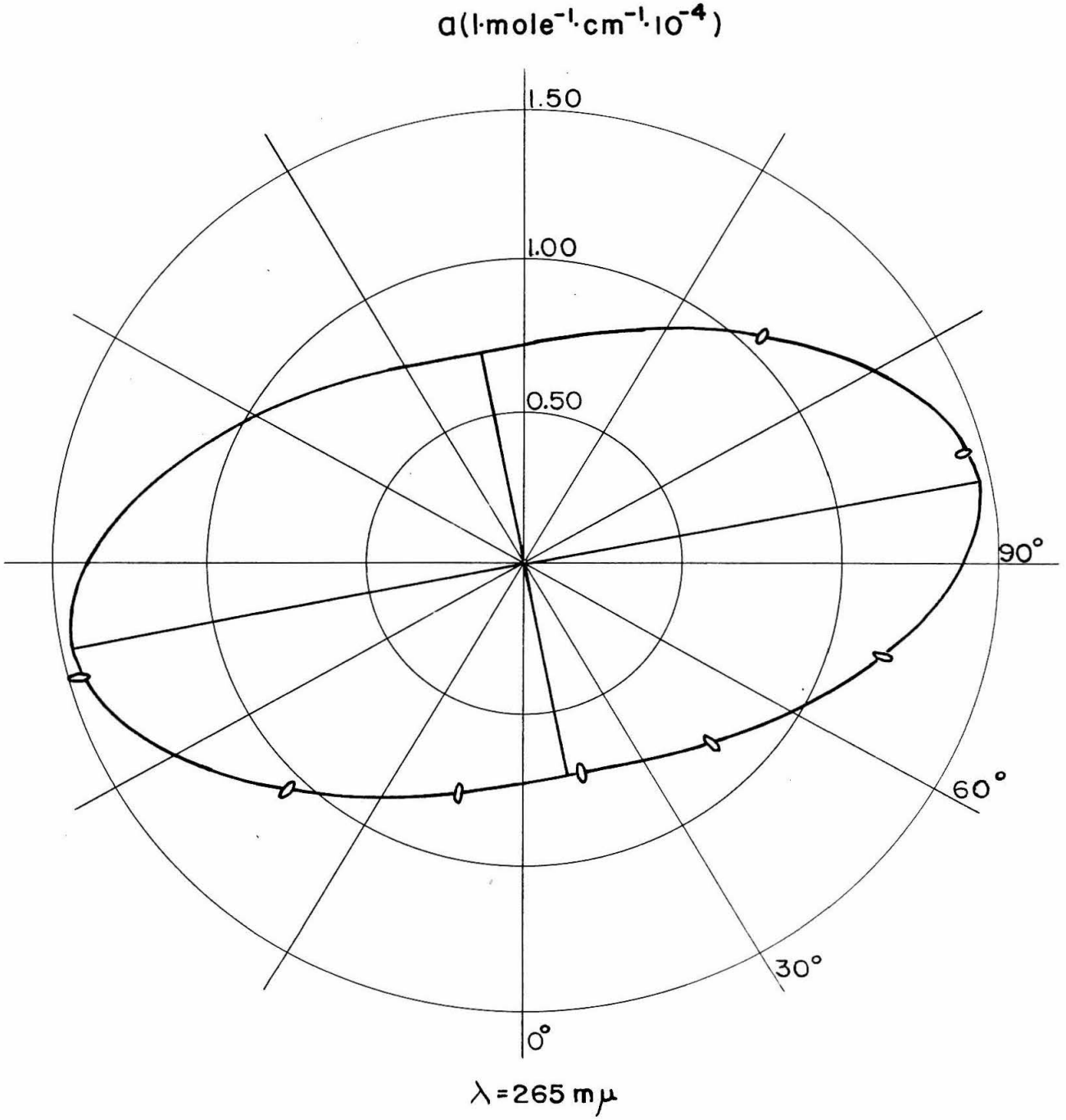
a(l·mole⁻¹·cm⁻¹·10⁻⁴)
1.50
1.00
0.50
90°
60°
30°
0°
λ=265 mμ

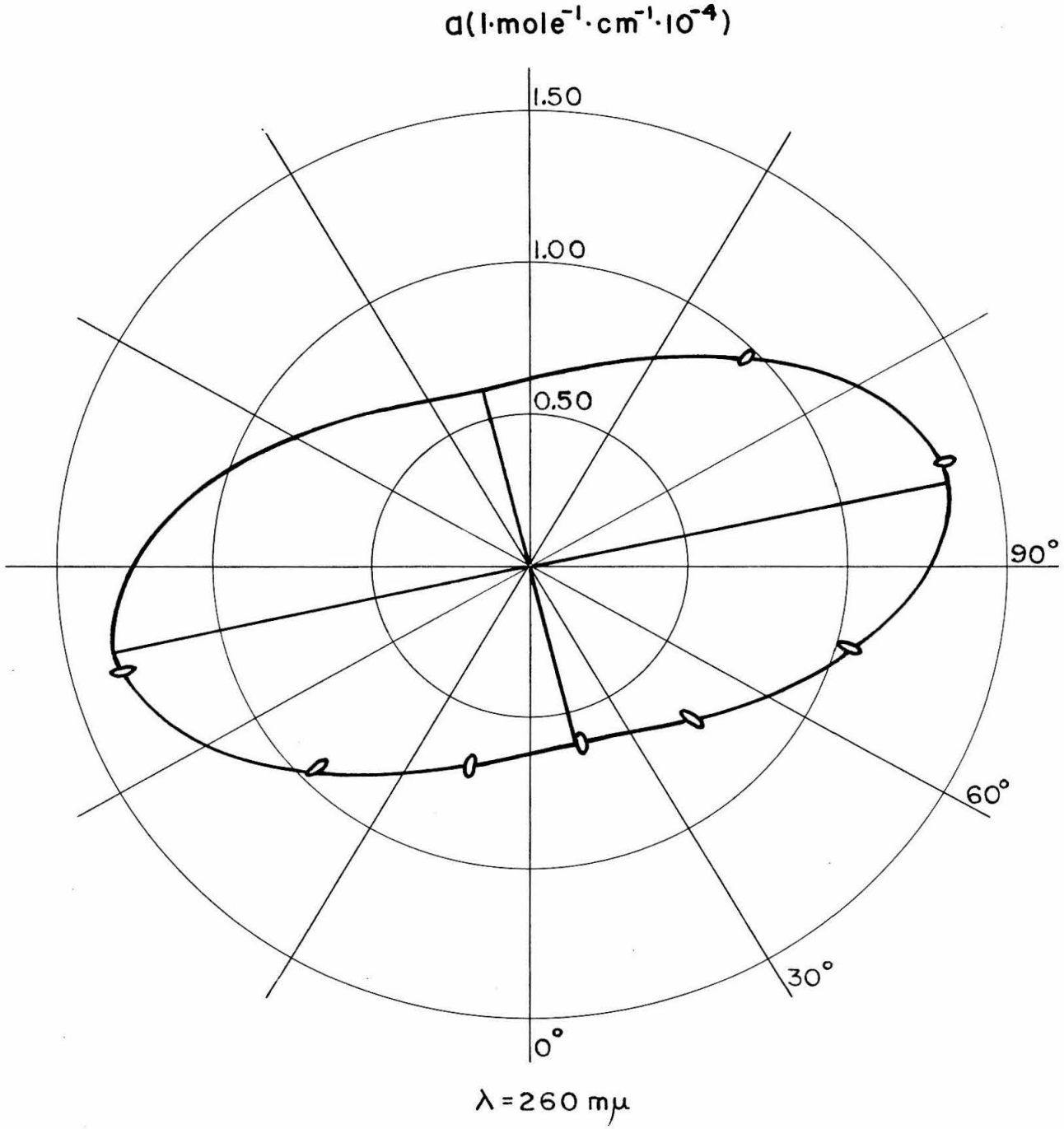
a(l·mole⁻¹·cm⁻¹·10⁻⁴)
1.50
1.00
0.50
90°
60°
30°
0°
λ=260 mμ

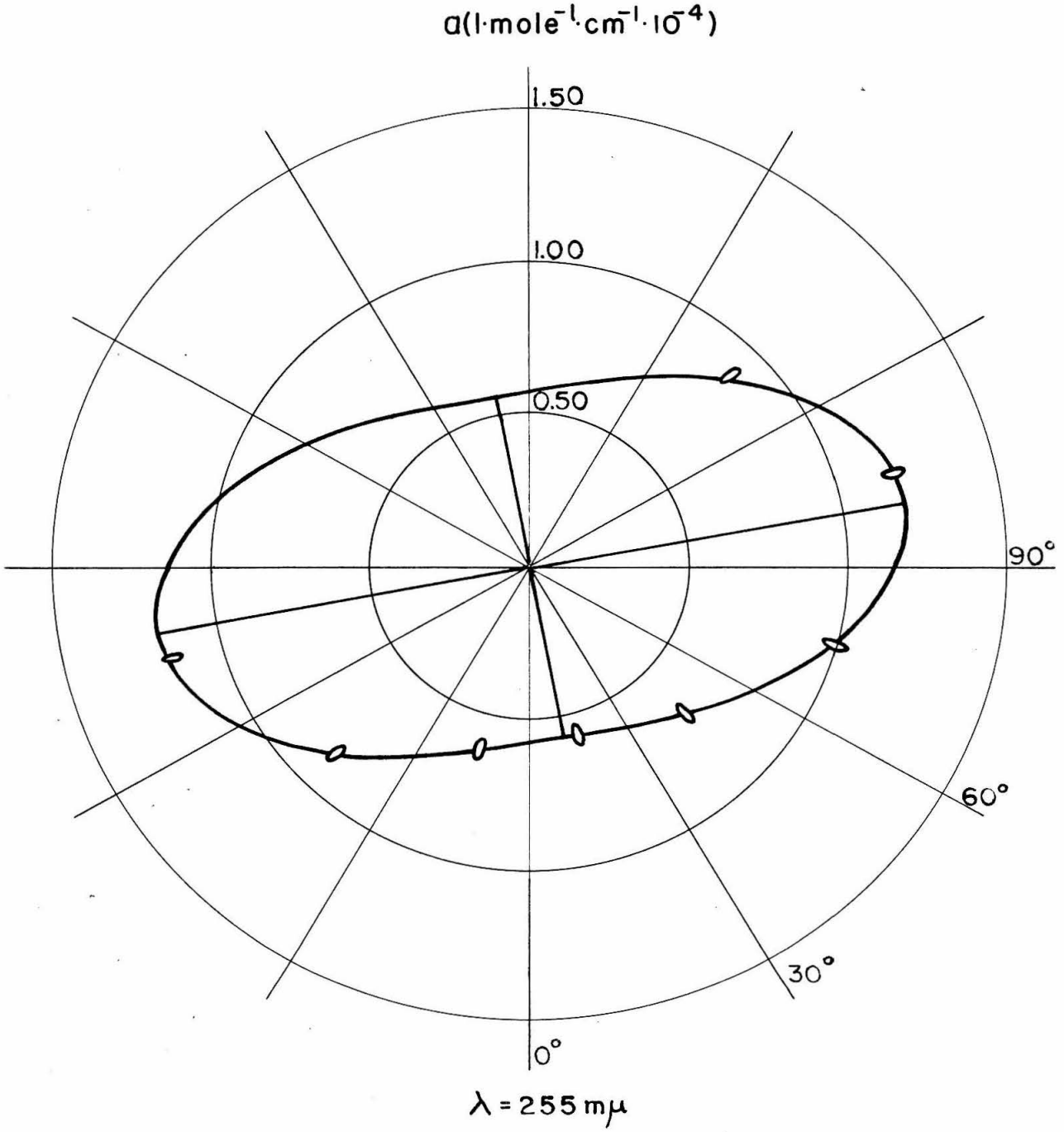
a(l·mole⁻¹·cm⁻¹·10⁻⁴)
1.50
1.00
0.50
90°
60°
30°
0°
λ = 255 mμ

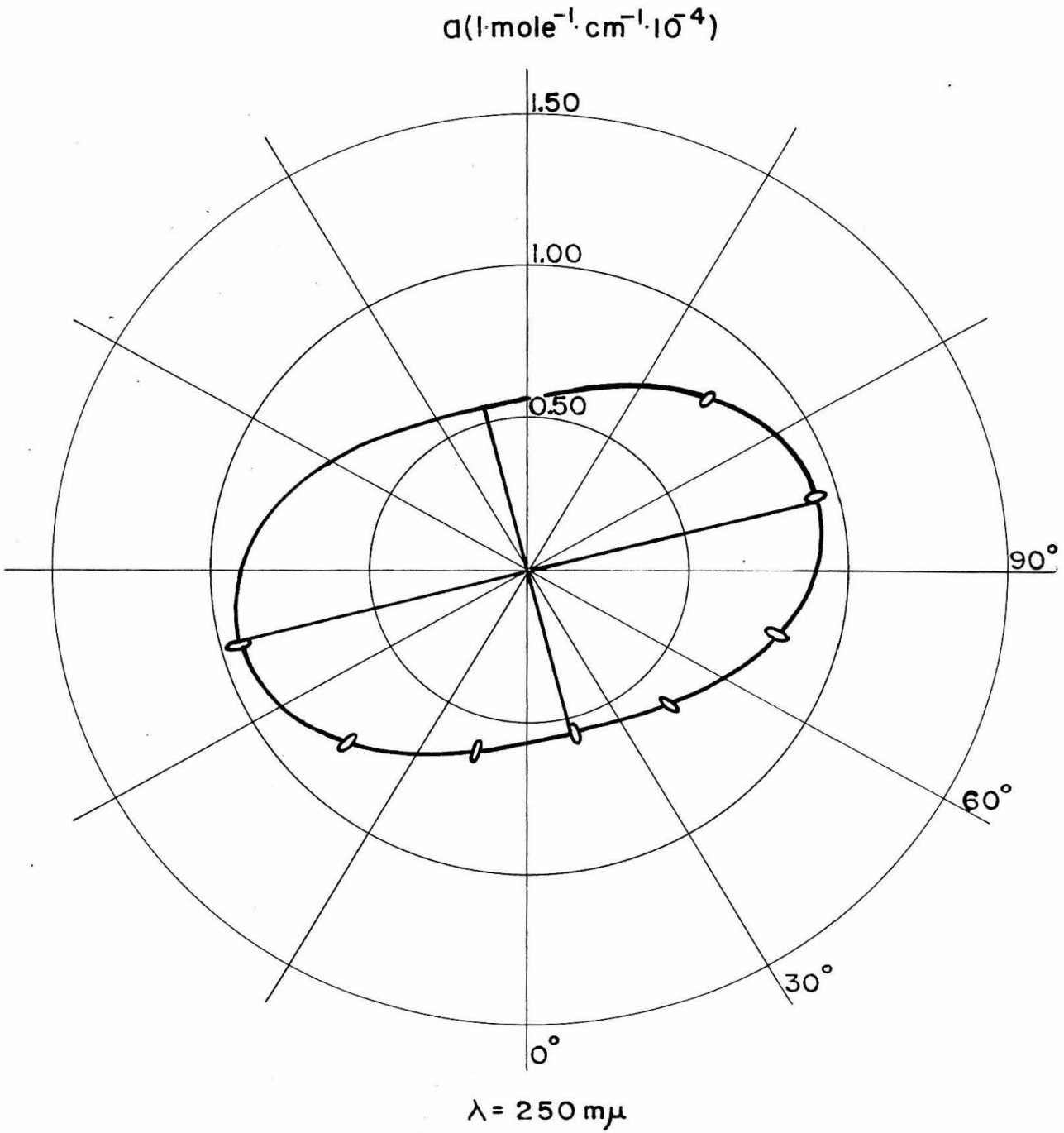
a(l·mole⁻¹·cm⁻¹·10⁻⁴)
1.50
1.00
0.50
90°
60°
30°
0°
λ = 250 mμ

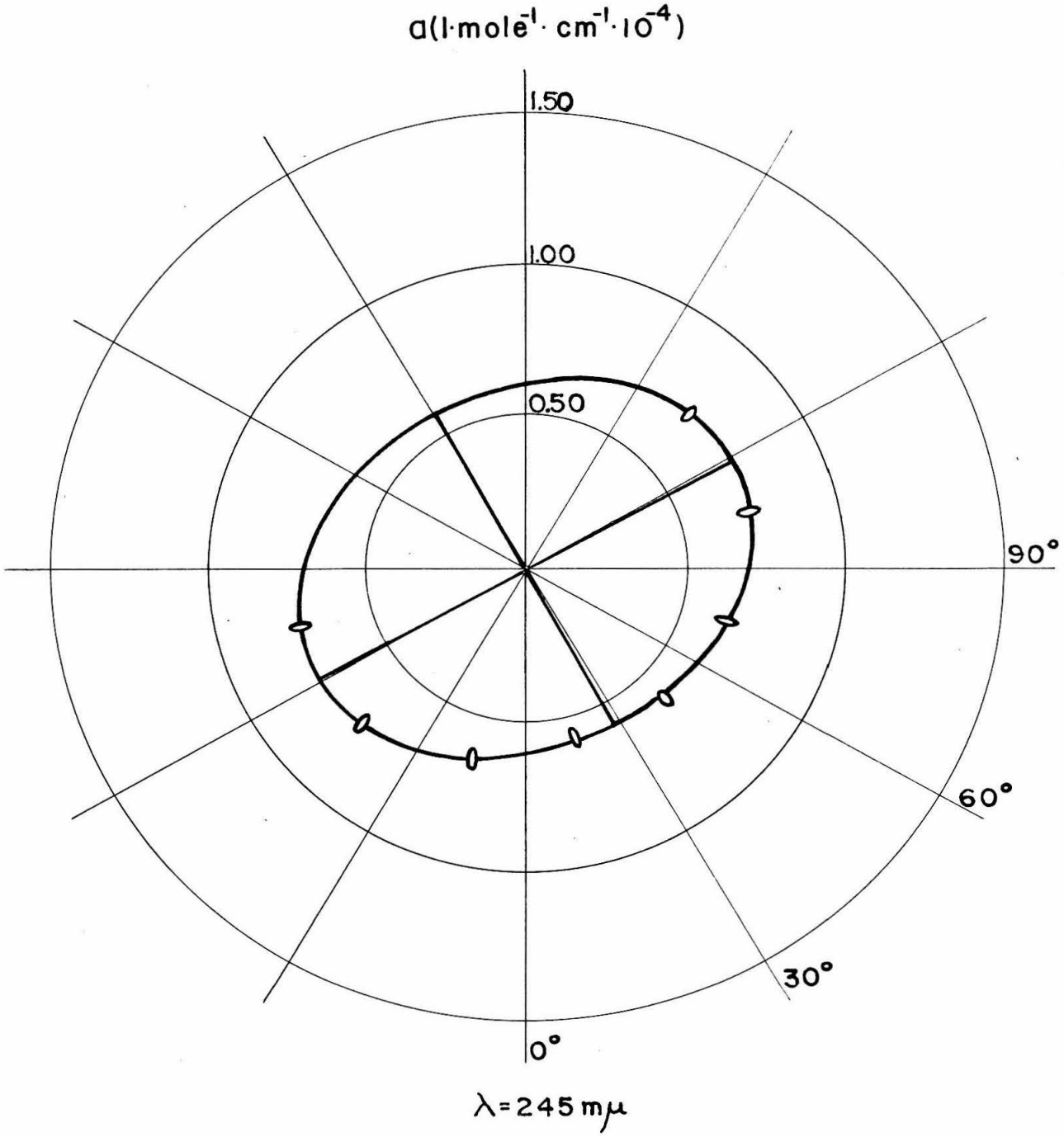
a(l·mole⁻¹·cm⁻¹·10⁻⁴)
1.50
1.00
0.50
90°
60°
30°
0°
λ=245 mμ

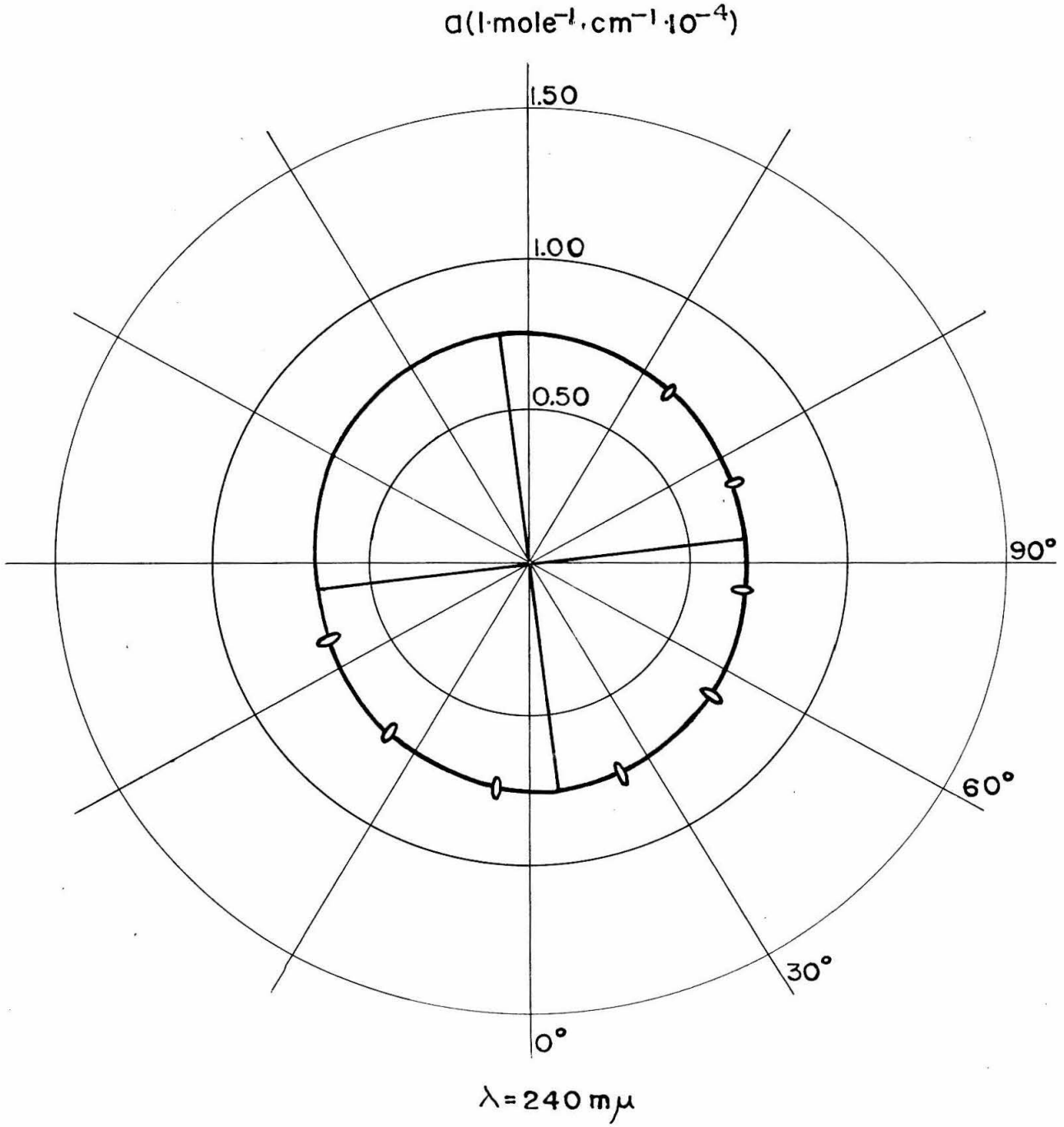
a(l·mole⁻¹·cm⁻¹·10⁻⁴)
1.50
1.00
0.50
90°
60°
30°
0°
λ=240 mμ

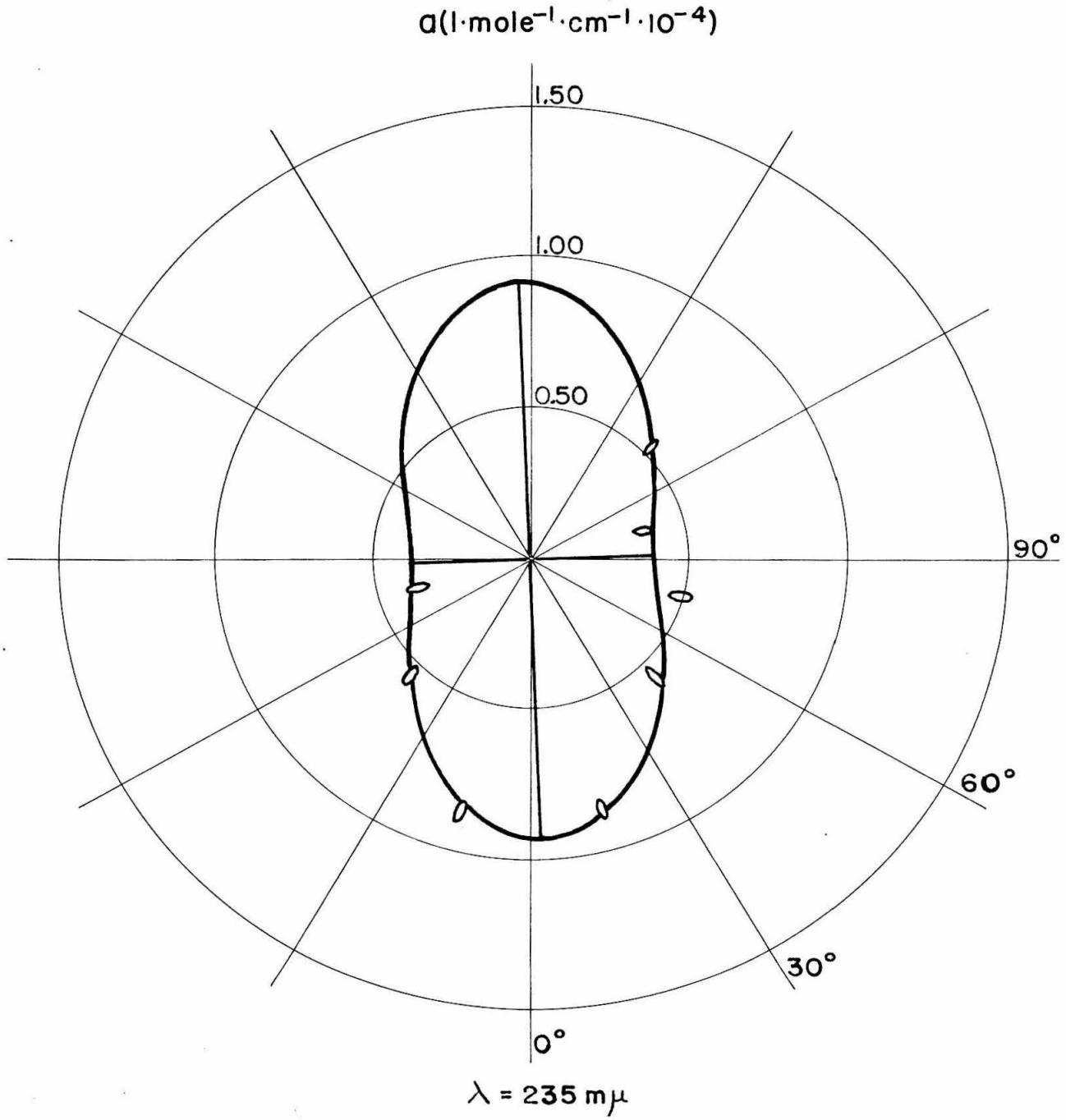
a(l·mole⁻¹·cm⁻¹·10⁻⁴)
1.50
1.00
0.50
90°
60°
30°
0°
λ = 235 mμ

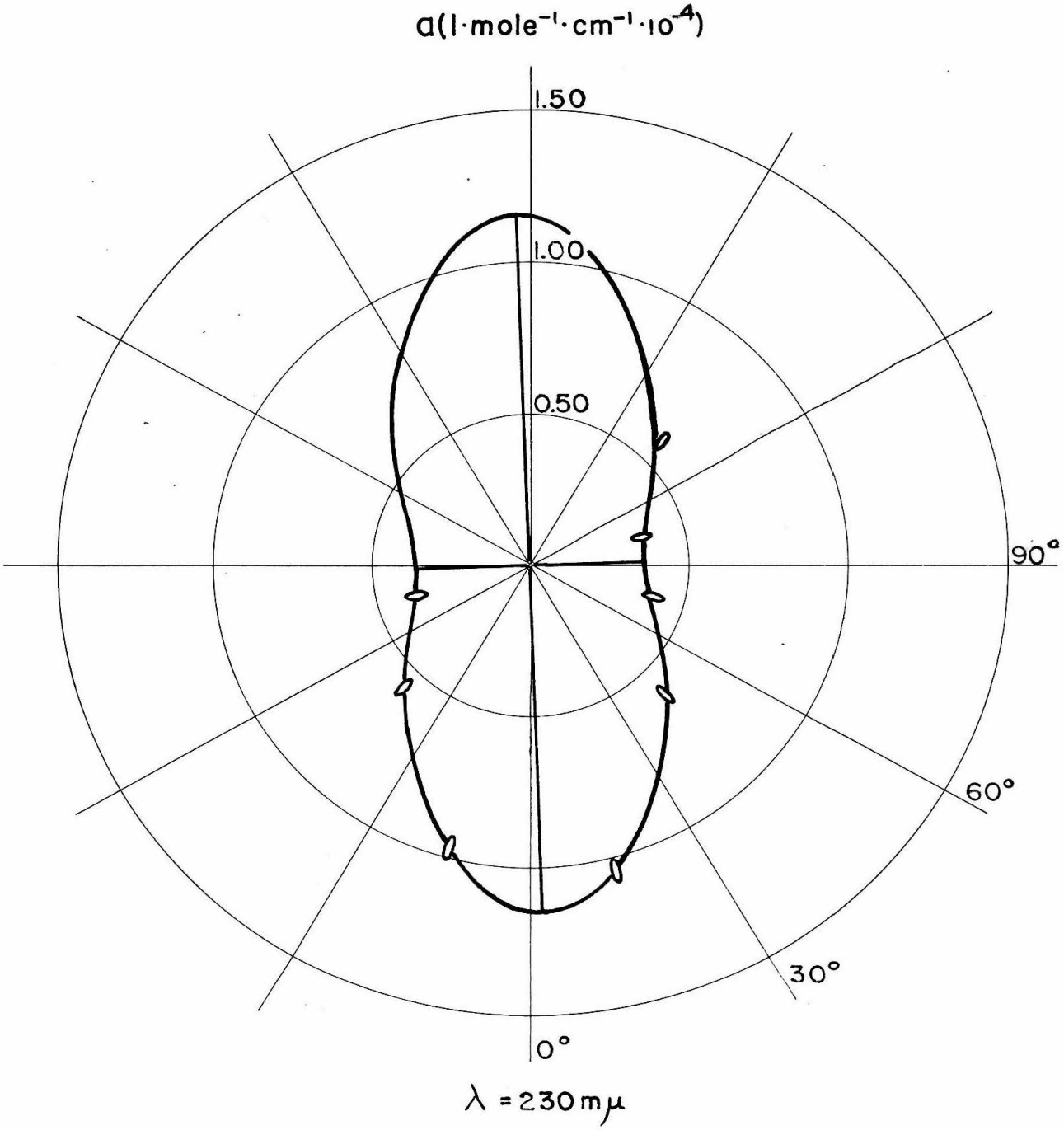
a(l·mole⁻¹·cm⁻¹·10⁻⁴)
1.50
1.00
0.50
90°
60°
30°
0°
λ = 230 mμ

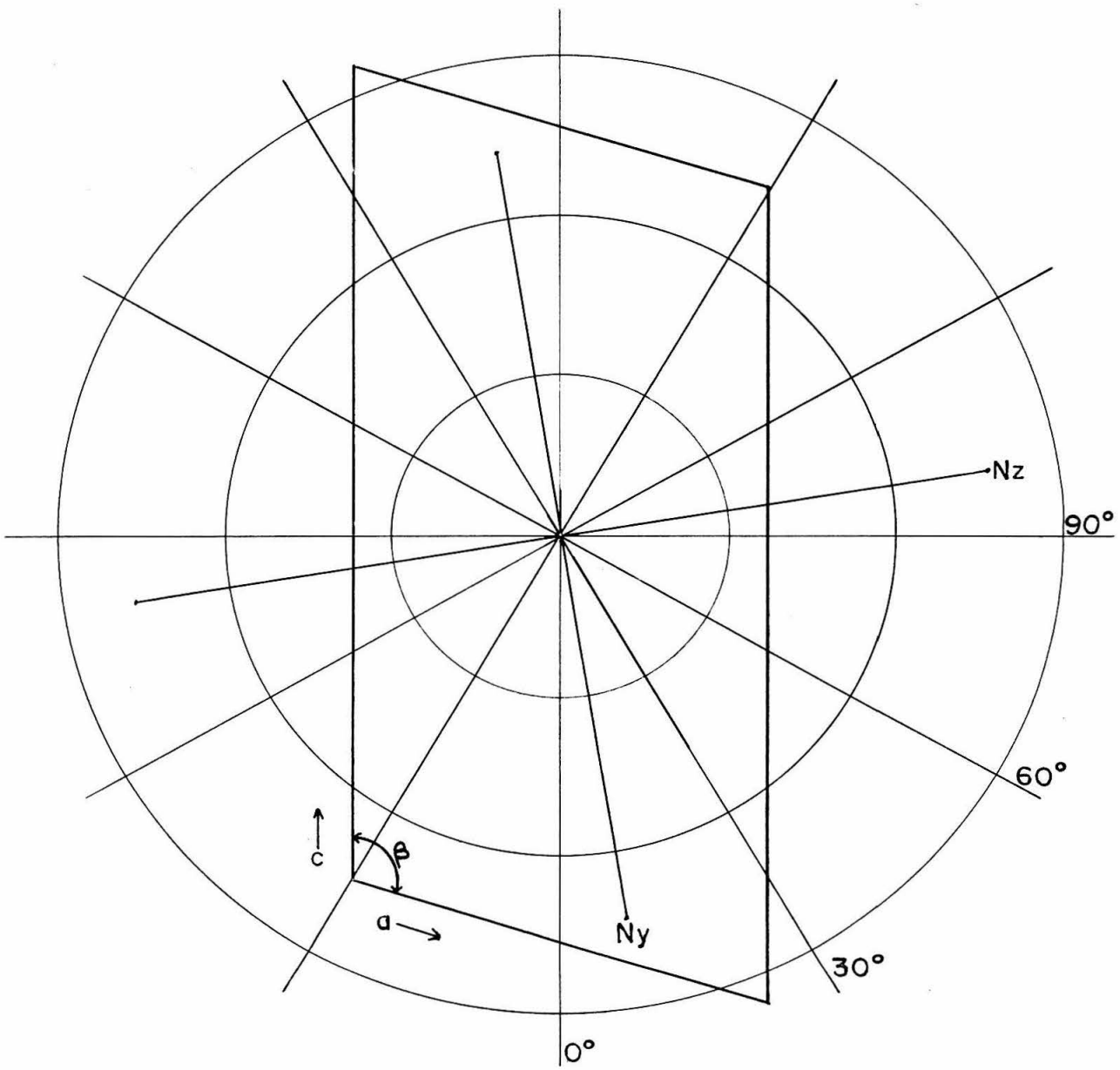

The (010) of the Hoogsteen dimer. The c-axis is parallel to the 0° radial line. N_Y and N_Z are the refractive index directions at 589 mμ.

APPENDIX C

Theory of Absorption for Plane Polarized Light in a Solid Angle by an Anisotropic Absorbing Plane.

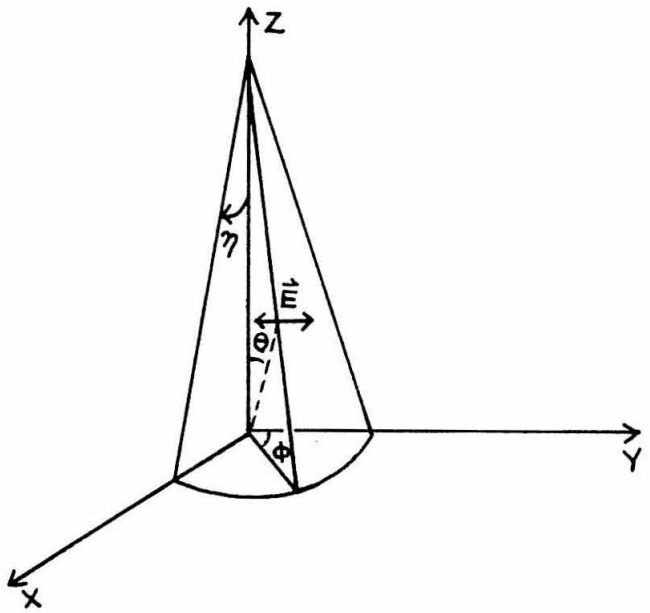

Absorbing plane is xz.

Plane of polarization is yz.

It is assumed that the eccentricity of the polarized light is unity and that the solid angle is uniformly filled with light.

Components of wave vector $\vec{K}$:

$(\sin\varphi \sin\theta,\ \cos\varphi \sin\theta,\ \cos\theta)$.

Components of electric field $\vec{E}$:

$(0,\ \alpha,\ \beta)$.

By orthogonality, $\vec{E} \cdot \vec{K} = 0$

$$\text{or } \alpha \cos\varphi \sin\theta + \beta \cos\theta = 0.$$

By normalization: $\alpha^2 + \beta^2 = 1$.

$$\therefore \alpha^2 = \frac{1}{1 + \cos^2\varphi \tan^2\theta} \quad \text{and} \quad \beta^2 = \frac{\cos^2\varphi \tan^2\theta}{1 + \cos^2\varphi \tan^2\theta}$$

The transmission observed is

$$I/I_o = \frac{\int_\omega e^{-\epsilon y t/\cos\theta\,\alpha^2} e^{-\epsilon z t/\cos\theta\,\beta^2} d\omega}{\int_\omega d\omega}$$

ϵy is the absorptivity in the y direction.

ϵz is the absorptivity in the z direction.

t is the thickness of the absorbing material.

$$I/I_o = \frac{\int_o^\eta \int_o^{2\pi} e^{-Ay\left(\frac{1}{\cos\theta}\cdot\frac{1}{1+\cos^2\varphi\tan^2\theta}\right)} e^{-Az\left(\frac{1}{\cos\theta}\cdot\frac{\cos^2\varphi\tan^2\theta}{1+\cos^2\varphi\tan^2\theta}\right)} \sin\theta\, d\theta\, d\varphi}{\int_o^\eta \int_o^{2\pi} \sin\theta\, d\theta\, d\varphi}$$

η is the angle between the central pole (z-axis) to the envelope of the solid angle.

For measurements of practical value η extreme is $\approx 10^{-1}$. Thus to a good approximation $\tan^2\theta = \theta^2$, $\sin\theta = \theta$ and $\cos\theta = 1$.

$\therefore \alpha^2 \sim 1$ and $\beta^2 \approx \theta^2\cos^2\varphi$.

We need therefore to evaluate

$$I/I_o = \frac{\int_o^{\eta}\int_o^{2\pi} e^{-Ay}\, e^{-Az\theta^2\cos^2\varphi}\,\theta\,d\theta\,d\varphi}{\int_o^{\eta}\int_o^{2\pi}\theta\,d\theta\,d\varphi}$$

$$= \frac{e^{-Ay}}{\pi\eta^2}\int_o^{\eta}\int_o^{2\pi} e^{-A_z\theta^2\cos^2\varphi}\,\theta\,d\theta\,d\varphi$$

Integrating over θ,

$$I/I_o = \frac{e^{-Ay}}{2\pi\eta^2 A_z}\int_o^{2\pi}\frac{1 - e^{-A_z\eta^2\cos^2\varphi}}{\cos^2\varphi}\,d\varphi$$

But

$$1 - e^{-A_z\eta^2\cos^2\varphi} = \sum_{n=0}^{\infty}(-1)^n\,\frac{(A_z\eta^2\cos^2\varphi)^{n+1}}{(n+1)!}$$

$$\therefore I/I_o = \frac{e^{-Ay}}{2\pi\gamma}\int_o^{2\pi}\sum_{n=0}^{\infty}(-1)^n\,\frac{(\gamma\cos^2\varphi)^{n+1}}{(n+1)!\cos^2\varphi}\,d\varphi$$

where $\gamma = A_z\eta^2$

or

$$I/I_o = \frac{e^{-Ay}}{2\pi}\int_o^{2\pi}\sum_{n=0}^{\infty}(-1)^n\,\frac{(\gamma\cos^2\varphi)^n}{(n+1)!}\,d\varphi$$

We note that,

$$\cos^{2n}\varphi = \frac{1}{2^{2n-1}}\left[\sum_{r=0}^{n-1} {}_{2n}C_r \cos 2(n-r)\varphi + \tfrac{1}{2}\,{}_{2n}C_n\right]$$

Integrating term by term,

$$\int \cos^{2n}\varphi\, d\varphi = \frac{1}{2^{2n-1}}\left[\sum_{r=0}^{n-1} \frac{{}_{2n}C_r}{2(n-r)} \sin 2(n-r)\varphi + \tfrac{1}{2}\,{}_{2n}C_n\,\varphi + \text{constant}\right]$$

This gives a simple, finite polynomial in $\sin 2(n-r)\varphi$. Moreover we note that

$$\sum_{n=0}^{\infty} \frac{(-1)^n \gamma^n}{(n+1)!} \frac{1}{2^{2n-1}} \sum_{r=0}^{n-1} \frac{{}_{2n}C_r}{2(n-r)} \sin 2(n-r)\varphi + \tfrac{1}{2}\,{}_{2n}C_n\,\varphi$$

converges. Thus we may interchange the summation and integration operations above.

$\therefore I/I_o =$

$$\frac{e^{-Ay}}{2\pi} \sum_{n=0}^{\infty} \frac{(-1)^n \gamma^n}{(n+1)!} \cdot \frac{1}{2^{n-1}} \sum_{r=0}^{n-1} \frac{{}_{2n}C_r}{2(n-r)} \sin 2(n-r)\varphi + \tfrac{1}{2}\,{}_{2n}C_n\,\varphi \Big|_0^{2\pi}$$

The sine terms vanish, so

$$I/I_o = e^{-Ay} \sum_{n=0}^{\infty} \frac{(-1)^n \gamma^n}{(n+1)!} \frac{{}_{2n}C_n}{2^n}$$

But

$$ {}_{2n}C_{n} = \frac{(2n)!}{(2n-n)!\,n!} = \frac{(2n)!}{(n!)^2} $$

$$ \therefore\ I/I_o = e^{-Ay \sum_{n=0}^{\infty} \frac{(-1)^n \gamma^n (2n)!}{2^n (n+1)!\,(n!)^2}} $$

REFERENCES

1. A. Bree and T. Thirunamachanbran, Mol. Phys., 5, 397-405 (1962).

2. Chargaff and Davidson, "The Nucleic Acids." Academic Press, New York, 1955, Vol. I (spectra in fly leaf).

3. D. P. Craig and S. H. Walmsley, Mol. Phys., 4, 113-124 (1961).

4. A. S. Davydov, "Theory of Molecular Excitons." (Translated from first Russian edition by M. Kasha and Max Oppenheimer, Jr.) McGraw-Hill Book Company, Inc., 1962. See Chapter III in particular.

5. H. DeVoe and I. Tinoco, Jr., J. Mol. Biol., 4, 500-517, 518-527 (1962).

5'. See p. 504 in above reference.

6. P. Drude, "The Theory of Optics." Dover Publications, Inc., New York, 1959, pp. 382-387.

7. M. A. El Sayed and G. W. Robinson, Mol. Phys., 4, 273-286 (1961).

8. V. Gilpin and W. McCrone, Anal. Chem., 22, 368 (1950).

9. C. Hintze, Handbuch der Mineralogie. Zweite Abtheilung Verlag von Veit und Comp., Leipzig, 1915, pp. 1277-1278.

10. K. Hoogsteen, Acta Cryst., in press.

11. K. Hoogsteen, Acta Cryst., 12, 822-823 (1959).

12. K. Hoogsteen, private communication.

13. M. Kasha, "The Nature and Significance of n-π* Transitions." Presented at the Symposium on Light and Life, Johns Hopkins University. Also see, J. Sidman, Chem. Rev., 58, 689-713 (1958).

14. L. E. Lyons, J. Chem. Phys., 20, 1814 (1952).

15. D. S. McClure, Canad. J. Chem., 36, 59-71 (1958).

16. See, e.g., H. McConnell, J. Chem. Phys., 20, 700-704 (1952).

17. J. R. MacDonald and M. K. Brachman, Rev. Mod. Phys., 28, 393-422 (1956).

18. S. F. Mason, J. Chem. Soc., 2071-2081 (1954).

19. S. F. Mason, J. Chem. Soc., 1240-1246 (1959).

20. G. S. Parry, Acta Cryst., 7, 313-320 (1954).

21. Cf. D. L. Peterson and W. T. Simpson, J. Am. Chem. Soc., 79, 2375-2382 (1957).

22. K. S. Pitzer, "Quantum Chemistry," Prentice-Hall, Inc., Englewood Cliffs, N. J., 1953, p. 266.

23. A. Pullman and B. Pullman, Bull. Soc. Chim., 766-772 (1958).

24. W. Rhodes, J. Am. Chem. Soc., 83, 3609-3617 (1961).

25. W. E. Seeds, Progr. Biophys. & Biophys. Chem., 3, 27-46 (1953).

26. W. T. Simpson and D. L. Peterson, J. Chem. Phys., 26, 588-593 (1957).

27. I. Tinoco, Jr., J. Chem. Phys., 33, 1332-1338 (1960).
and for erratum see J. Chem. Phys., 34, 1067 (1961).

28. Tinoco, Halpern and Simpson (1961). Polypeptide Symposium, Madison, Wis., in the press.

29. F. J. Wall et al., J. Am. Chem. Soc., 72, 4769-4773 (1950).

30. D. L. Wulff and G. Fraenkel, Biochim. Biophys. Acta , 51 332-339 (1961).

31. D. L. Wulff, private communication.

PROPOSITION I

The crystal structure for 9-methyladenine has not been determined. The unit cell dimensions and space group of the anhydrous, monoclinic crystal have been reported (1). (The unit cell dimensions are listed at the end of this proposition.) The crystal has a pronounced cleavage along the (001); this plane is believed to be the plane of the molecular layers (2).

The angular orientation for 9-methyladenine in the crystal is proposed below. My reasons for presenting this proposal are two-fold. I hope to entice someone to do the crystal structure of 9-methyladenine. The crystal structure determination would provide a test for the atomic positions given 9-methyladenine in the hydrogen bonded complex of 1-methylthymine and 9-methyladenine. The structure determination may, furthermore, provide some clue as to the relative stability of the hydrogen bonded complex of 1-methylthymine and 9-methyladenine compared to the single crystals of each, respective compound. The structure will also, hopefully, settle the question as to the transition moment direction for the strong component of the first ultraviolet absorption band in adenine. My second reason is to show that our transition moment direction assigned to 9-methyladenine can be used to construct a reasonable orientation of the 9-methyladenine molecules in the unit cell.

The dichroic ratio for absorption in the (001) has been determined for the first ultraviolet absorption band. (See the section on polarized absorption spectra of 9-methyladenine of this thesis.) Since the space group is $P2_{1/c}$ and there are four molecules per unit cell, the transition moment for one pair lies at an angle α from the b-axis, and for the other pair at an angle of $-\alpha$. From the dichroic ratio value of 5.1, the moment lies at an absolute angle of $24° \pm 2°$ with respect to the b-axis. From the analysis of polarized absorption spectra for a hydrogen bonded complex of 1-methylthymine and 9-methyladenine, the transition moment for 9-methyladenine was assigned to a direction of $168° \pm 4°$. By the Tinoco convention (3), the transition moment angle is measured from the C_5-C_4 bond in the purine compound and increases by rotation into the six membered ring. With the knowledge of the transition moment direction for the molecule and of the dichroic ratio in (001) of 9-methyladenine, two angular orientations for 9-methyladenine can be considered. One of these orientations should correspond to the true structure of the crystal.

From the polarization data obtained for 9-methyladenine studies the C_4-C_5 bond should lie at an absolute angle of $12° \pm 6°$ or $36° \pm 6°$ with respect to the b-axis. I have assumed that the two pairs of the four molecules per unit cell are hydrogen bonded from the N_7 to the 6-amino group. This hydrogen bonding scheme is the one reported by Broomhead in her determination of the adenine hydrochloride crystal structure (4).

By using Broomhead's center of symmetry for a hydrogen bonded pair, K. Hoogsteen's atomic coordinates for 9-methyladenine from the crystal of the adenine-thymine dimer (5), and assuming all molecules coplanar to the (001), I have calculated the atomic positions for the 9-methyladenine molecule for the two possible orientations. Both cases are presented below; one structure is preferable and suggests in a gross way the orientation of the 9-methyladenine molecules in the reported unit cell (1).

Figure 1 is a representation of one pair with the C_4-C_5 axis at an angle of 36°. The plane of the paper is (001). (The arrow over one molecule is believed to be the direction of the transition moment.) The other two molecules, not shown, of the unit cell are in a plane half way up the c-axis; this plane has a vertical separation of 3.60 Å from the (001). Although the unit cell is filled up by the molecules with adequate spacing, the hydrogen bonding for the 6-amino group is unacceptable. One proton of the amino group bonds to N_7 (by assumption) but the other proton has no nearby site for bonding. If one tries a hydrogen bonding scheme to the N_1 position (that is, reject the N_7 hydrogen bonding scheme), then the pair overfills the unit cell; the a-axis is too short to accommodate this latter configuration.

The second possibility for the angular orientation provides an attractive hydrogen bonding scheme. In Figure 2 the four molecules per unit cell are shown. Molecules 1, 2, and 2' are in the (001);

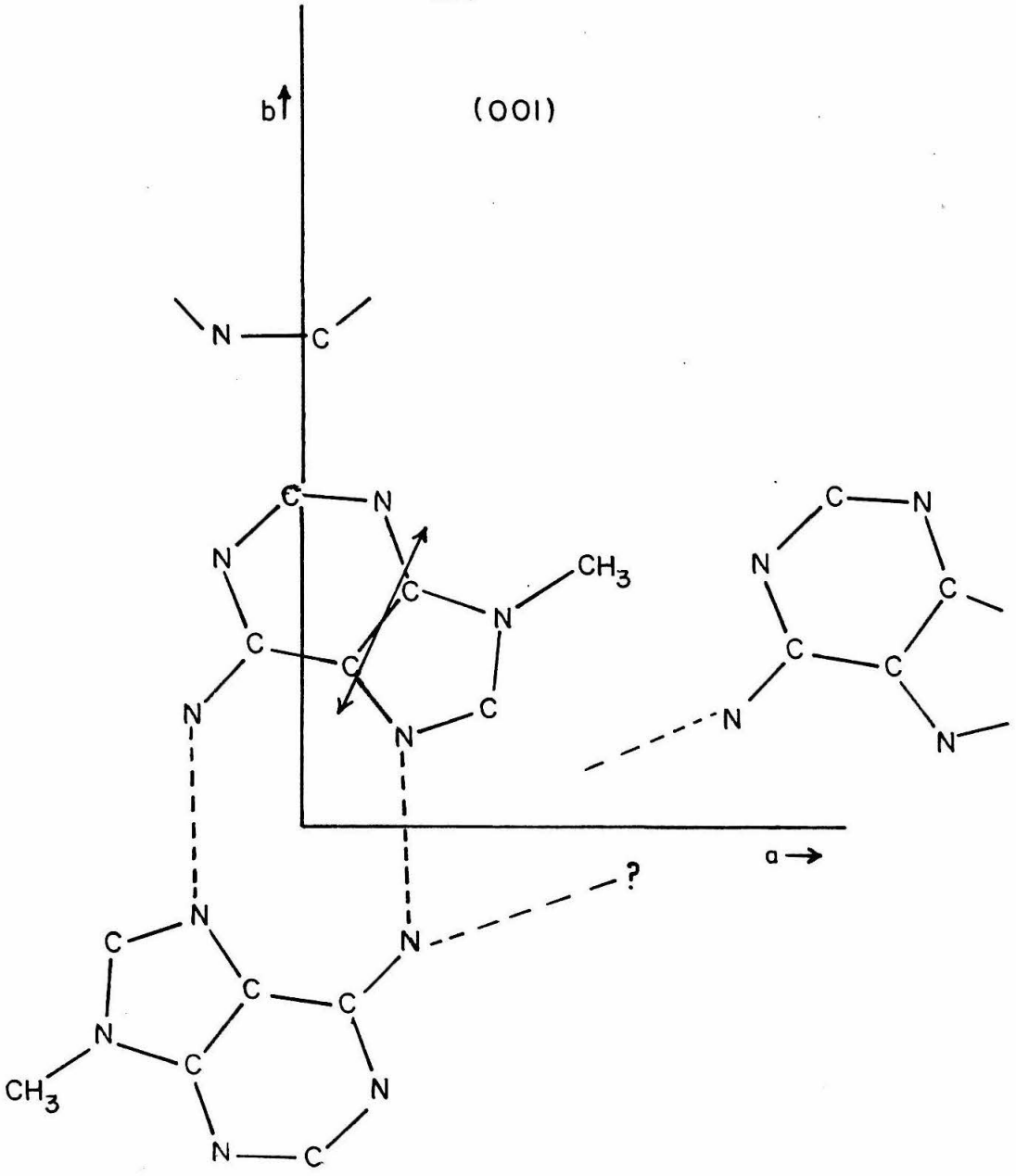

Figure 1. $< b \wedge C_4\text{-}C_5 = 36°$. The hydrogen bonding scheme is unacceptable.

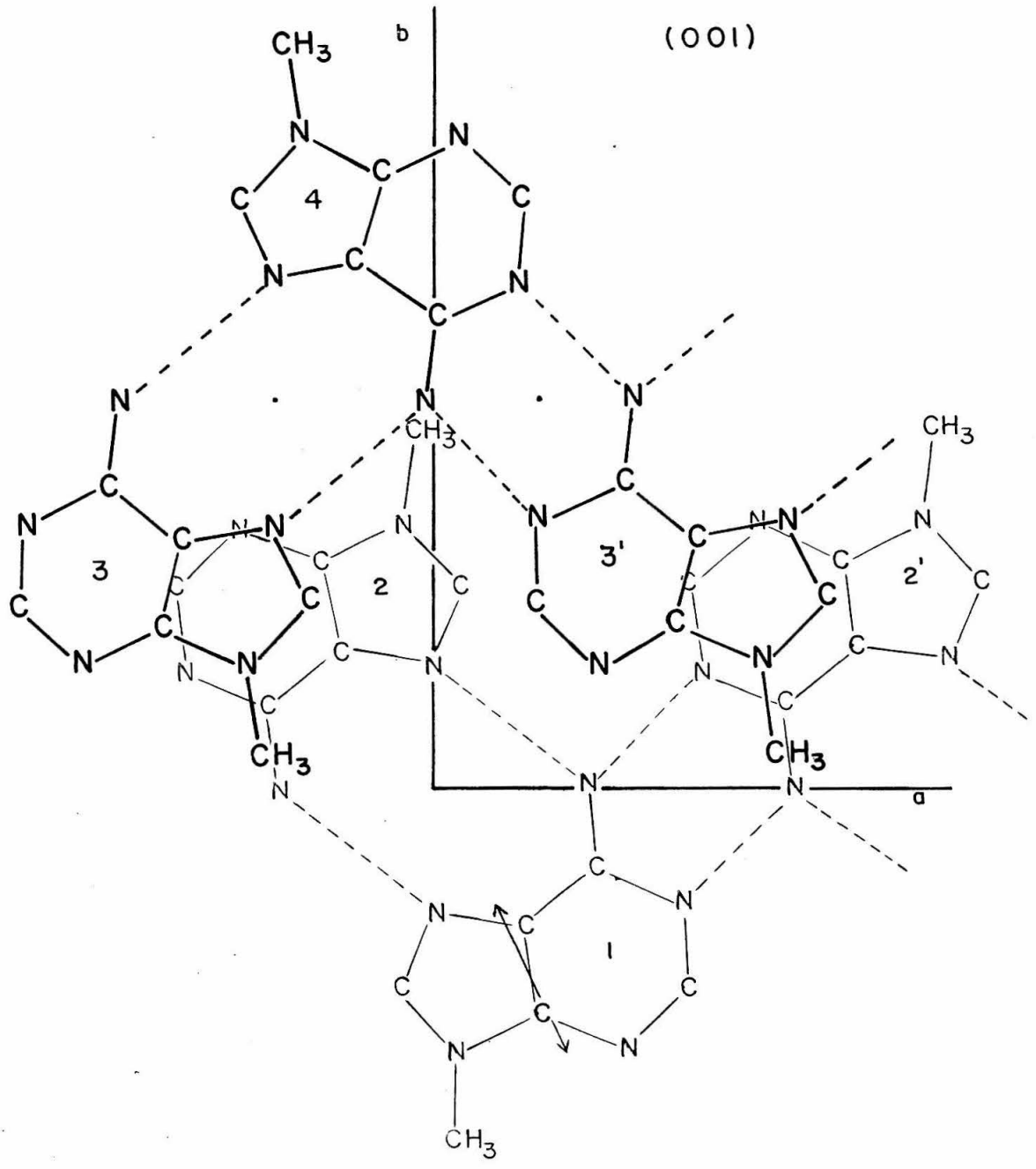

Figure 2. Proposed orientation of 9-methyladenine molecules in the unit cell. (See text for discussion)

molecules 3, 3', and 4, projected onto the plane of the paper, are above the (001), half way up the c-axis. The arrow on molecule 1 represents the transition moment.

The major feature of the proposed structure is the hydrogen bonding scheme. The 6-amino group is now in a favorable position to hydrogen bond to the N_1 of a 9-methyladenine in the adjacent cell. The two centers of symmetry on the a-axis provide the system with alternate types of hydrogen bonding between the molecules along the a-axis. If this is a correct scheme, then the crystal is an interesting structure to study in that there are two kinds of hydrogen bonding between the adenine molecules.

The present spacings of the molecules, as they are now shown in the unit cell, are not acceptable. The methyl group, attached to the N_9 in the purine ring, is too close to the methyl group in the next cell; the separation is $\sim 1\text{Å}$. Furthermore the N_{10} to N_1 hydrogen bond is only 2.5 Å. There is about a 6° error for the transition moment direction from my experimental measurements of the dichroic ratio and from the polarization analysis of the 1-methylthymine, 9-methyladenine hydrogen bonded complex. Rotation of the C_4-C_5 bond closer to the b-axis increases the separation of the neighboring methyl groups and also increases N_1 to N_{10} hydrogen bond distance. The center of symmetry taken from Broomhead's atomic coordinates may not be completely correct for this structure. By decreasing the N_{10}-N_7

hydrogen bonding distance, the methyl groups are separated further and the N_{10}-N_1 distance is also increased. The methyl groups, moreover, may be out of the plane of the molecules as well.

My polarization data cannot be used very well for constructing a more accurate structure than what is shown in Figure 2. It is useful, however, in establishing an approximate orientation of the 9-methyladenine molecules in the unit cell.

Unit cell dimensions for 9-methyladenine taken from K. Hoogsteen (1).

$a = 7.67 \pm .03$ Å

$b = 12.24 \pm .04$

$c = 8.47 \pm .03$

$\beta = 123°26' \pm 10'$

Space group: $P2_{1/c}$

Density: 1.471 $g \cdot cm^{-3}$ (meas)

$z = 4$

REFERENCES

1. K. Hoogsteen, Acta Cryst., 12, 822-823 (1959).
2. K. Hoogsteen, private communication.
3. H. DeVoe and J. Tinoco, Jr., J. Mol. Biol., 4, 518-527 (1962). (See p. 504 in preceding article)
4. J. Broomhead, Acta Cryst., 1, 324-329 (1948).
5. K. Hoogsteen, Acta Cryst., in press.

PROPOSITION II

It is proposed that orientations of macromolecules be looked for in the analytical ultracentrifuge by measuring the dichroism or birefringence. Hearst and Vinograd have studied the very interesting "speed" effect on the sedimentation behavior of macromolecular substances in an ultracentrifuge (1). The investigators report that for T-4 DNA at concentrations above 10 μg/ml, there is a pronounced dependence of the sedimentation coefficient on the angular velocity of the rotor. (These experiments for sedimentation equilibrium had $\bar{v}\rho$ approximately equal to 0.5; the investigators studied the sedimentation velocity in 0.15 M NaCl solutions.) For example, at a rotor speed of 20,410 r.p.m., the sedimentation coefficient for T-4 DNA solution at 15 μg/ml was 50 Svedberg units and at a rotor speed of 4,908 r.p.m., the sedimentation coefficient was 38 S. The authors report a similar, but less pronounced speed dependence for TMV virus; for this case the concentrations were several hundred μg/ml.

The dependence on rotor speed suggests that the molecules are being oriented by the effect of the centrifugal field. The effect of concentration also indicates that the macromolecular species need to be at a certain concentration before the speed dependence can be observed. Thus intermolecular interactions as well as the effect of the centrifugal field seem to be important factors for the speed dependence.

Dr. James Peterson has investigated several theories to account for the sedimentation phenomenon (2). Of the several mechanisms considered, none could successfully account for alignment of the rod-like particles in a centrifugal field. It is clear from Peterson's work that more experiments are required before one can proceed further on theoretical considerations. In particular the question of alignment should be answered. If the macromolecular species do orient in the presence of a centrifugal field, how do they orient? Are the rod-like particles oriented in the direction of the field, perpendicular to the field, or merely constrained to lie in a plane perpendicular to the axis of rotation of the rotor? For the first two possibilities, both dichroism and birefringence of the sample would develop with the field strength; for the last case one should observe a decrease in absorption compared to the isotropic solution.

It should be noted here that these kinds of experiments were considered (3) and were ruled out, because it was believed that the quartz windows were under too much strain at the high fields in an ultracentrifuge. The strain on the quartz windows, however, is not intolerable. Since the windows in ultracentrifuge cells are crystalline quartz cut perpendicular to the optic axis, rotary dispersion of the plane of polarization makes it impossible to extinguish polarized, non-monochromatic light with an analyzer. If one uses monochromatic light, the rotary dispersion is not a problem; the emerging monochromatic

light can be extinguished with an analyzer. The present quartz windows are ideal for dichroism or birefringence measurements. The rotation of the plane of polarization must be accurately measured so that the polarizer can be appropriately oriented. For quartz cut perpendicular to the optic axis, the plane of polarization will not be rotated, but very accurate alignment of the polarizer with one of the principal directions of the quartz is necessary. Otherwise the quartz will make the incident light elliptically polarized.

Dichroism experiments are simpler to construct than birefringence experiments, because the transmitted light does not have to be analyzed; only intensity must be measured. A control sample can be run in the centrifuge with a side wedge. Two slits can be appropriately placed in the focal plane of the optical system so that the control and sample can be measured under the same conditions. A photomultiplier device is perhaps a better detection system than photographic film, since the linearity of the former covers a much larger intensity range than the linearity of the latter.

REFERENCES

1. J. E. Hearst and J. Vinograd, Arch. Biochem. & Biophys., 92, 206-215 (1961).

2. J. Peterson, "The Hydrodynamic Alignment of Rod-Like Molecules in Centrifugal Fields," Ph. D. Thesis, California Institute of Technology, Department of Chemistry, 1963.

3. J. Vinograd, private communication.

PROPOSITION III

It is proposed that photochemical studies on 1-methylthymine be undertaken. It was reported in this thesis that 1-methylthymine suffered photodamage during transmission measurements. The photoproduct is very likely a 1-methylthymine dimer (1). The nearest neighbor in the crystal is situated above or below the molecule with the 5,6 double bonds over each other. If a cyclobutane ring forms between the two moieties, one would expect a 5,5'-6,6' type bonding with the pyrimidine rings trans to each other. (See Fig. 18, p. 85 of this thesis.) Such a structure corresponds to structure II proposed by Wulff and Fraenkel (2). This particular dimer can exist as a d or *l* compound, Since a 1-methylthymine can react with the nearest neighbor above or below equally well, one should expect a racemic mixture to form in the crystal.

1-Methylthymine can be crystallized as thin flakes on quartz plates. The developed face of the flakes is the (102), the plane of the molecules. By irradiating the crystals from above and below with an Hg germicidal lamp (or some other convenient ultraviolet source), one should get a reasonable yield of the photoproduct. Through fractional crystallization, the photoproduct can be separated from 1-methylthymine.

An easy way to indicate that the photoproduct is a thymine dimer

is to measure the ultraviolet absorption of the pure photoproduct. The band at 273 mμ should be absent. A molecular weight determination by freezing point depression and an elemental analysis would establish whether the compound is a dimer of 1-methylthymine or not.

By methylating the N_3 positions of the photoproduct, one can now compare this compound to the N,N'-dimethylthymine photoproducts I and II reported by Wulff. Such a comparison would help to settle the question of the four possible isomers which are consistent with Wulff's structural studies of the several photodimers.

If the structure proposed above is correct, then the photoproduct will be a racemic mixture. The pKa for both thymine and uracil is 9.5 (3). The photoproduct will probably have a comparable acidity. Therefore a strong base of pure d or ℓ form will be necessary to form diastereoisomers from the racemic mixture. Quinine methohydroxide or cinchonine methohydroxide may very well do the job (4). R. T. Major was able to resolve a racemic mixture of lactones with these reagents. With hydrochloric acid, one can remove the base and recover the respective d and ℓ photoproducts for further classification, i.e., measure the optical activity. Such an analysis would establish the photoproduct as isomer II or III in Wulff's work; the known crystal structure of 1-methylthymine makes it almost certain that the optically active compounds would be isomer II.

REFERENCES

1. Dr. D. L. Wulff, private communication.

2. D. L. Wulff and G. Fraenkel, Biochim. Biophys. Acta, 51, 332-339 (1961).

3. D. Shugar and J. J. Fox, Biochim. Biophys. Acta, 9, 199-218 (1952).

4. R. T. Major and J. Finkelstein, J. Am. Chem. Soc., 63, 1368-71 (1941).

PROPOSITION IV

It is proposed that dichroism studies of a single pyrazine crystal be undertaken to help clarify the nature of gained intensity for the lowest, symmetry forbidden, n-π^* transition of the molecule. M. A. El Sayed and G. W. Robinson investigated the lowest n-π^* transitions in pyrazine (1). The system provided the workers with an interesting study of intramolecular excitation transfer. The n-π^* transitions, which can occur at each end of the molecule, are orbitally degenerate. Interelectronic interactions remove this degeneracy; one transition is symmetry allowed, the other symmetry forbidden. The $^1B_{2g} \leftarrow {}^1A_g$ transition is symmetry forbidden (the point group for pyrazine is D_{2h}). For the symmetry forbidden transition there was some question as to how the transition gained most of its intensity. Most of the intensity for the symmetry forbidden transition lies in a band about 820 cm^{-1} above the (0, 0). (For the crystal, a weak transition about 500 cm^{-1} to the red of the (0, 0) allowed transition was thought to be the (0, 0) for the symmetry forbidden transition.) If this band at 820 cm^{-1} above the (0, 0) is polarized in-plane (of the molecule) then the intensity will be gained through mixing with a π-π^* transition. If the band is polarized out of plane, then most of the intensity will come from vibronic coupling between the symmetric and antisymmetric (n, π^*) components (1, 2).

With the pyrazine molecule in a crystalline environment, however, there is always the question of crystal perturbations. One cannot state with certainty that the polarized electronic intensity behavior for the molecule in the crystal is the same for the free molecule. But the polarization properties for the molecule in a crystalline environment are interesting in themselves.

The crystal structure of pyrazine has been determined (3). The orientations of the two molecules per unit cell in the orthorhombic crystal are pleasingly simple. The axis along the N_1, N_3 atoms in the ring is parallel to the a-axis. The two molecules have their respective planes at angles $\pm 22°3'$ with respect to the c-axis.

The crystals, which can be easily grown from a melt or by sublimation, can be cut to a thin section perpendicular to the a-axis. (I imagine 10 μ is a reasonable thickness for this weak transition.) The crystal will be cooled to 4° so that the bands will sharpen up somewhat. (It should be emphasized that an n-π^* transition is highly localized and is thus broadened considerably by crystal lattice vibrations. For the broadness of these absorption spectra see reference 1.) The absorption measured for light polarized along the b-axis is

$$A^{\parallel} b = a_x \cos^2 22°3' + a_y \sin^2 22°3'$$

where a_x is the absorption perpendicular to the molecular ring and a_y is the absorption in the plane of the ring at right angles to the N_1-N_3

axis. a_y and a_x are the molecular absorptions along the molecular coordinate system used for Robinson's study (1). Similarly,

$$A\|c = a_x \sin^2 22°3' + a_y \cos^2 22°3'$$

From these two absorption measurements we determine a_x and a_y.

Now we section another single crystal perpendicular to the b-axis. For light polarized along the a-axis, the molecular absorption, a_z, is determined directly. For light polarized along the c-axis,

$$A\|c = a_x \sin^2 22°3' + a_y \cos^2 22°3'$$

as before. This measurement provides a check on the earlier measurement. Therefore, from these polarization studies the distribution of intensity among the three components of the molecular coordinates is determined.

One possible difficulty with this experiment is a phase change in the crystal in going from 300°K down to 4°K. I do think, however, that the experiment is worth trying. Polarization studies of this type will add to the understanding of the intensity gained by the symmetry forbidden n-π^* transition, $^1B_{2g} \leftarrow {}^1A_g$.

REFERENCES

1. M. A. El Sayed and G. W. Robinson, Mol. Phys., 4, 273-286 (1961).
2. M. A. El Sayed and G. W. Robinson, J. Chem. Phys., 35, 1896-1897 (1961).
3. P. J. Wheatley, Acta Cryst., 10, 182-187 (1957).

PROPOSITION V

A number of polymers have rod-like properties. It would be interesting to study the "rod statistics" of these materials by breaking molecular bonds at defined places. Professor Norman Davidson has suggested that oriented polymers may be sectioned with an ultramicrotome. Such a suggestion leads to a variety of experiments for the statistical analysis of the rod-like properties of rigid, linear polymers. It is proposed that the analysis below be considered for these kinds of experiments.

For analyzing the system it is convenient to adopt the following model. We consider rods of length L and slice intervals of equal spacing s. We are given a set of lines infinitely long and spaced at equal intervals s. The number of lines in the z direction more than span the rod length L. We shall drop rods onto these cutting lines and determine the weight average and number average lengths collected below the lines. We always take $L > s$.

Case I: A paracrystalline polymer is assumed to be well oriented. All molecules are colinear, but the ends are staggered with equal probabilities. The molecules, moreover, are homogeneous in length. This case corresponds to dropping rods onto the cutting lines with rod axes parallel to the z direction and in the plane of the knife edges.

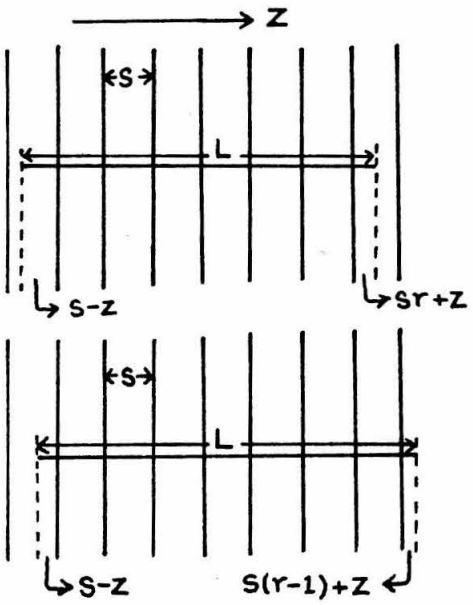

$L = ns + rs$ where n is an integer and r is a remainder.

Distribution of Pieces

	Number	Length
$0 \le z \le s(1-r)$	1	$s - z$
	$n-1$	s
	1	$sr + z$
$s(1-r) \le z \le s$	1	$s-z$
	n	s
	1	$s(r-1)+z$

$$\therefore \bar{l}_n = \frac{\int_o^{s(1-r)} [(s-z)+(n-1)s+(sr+z)]\,dz + \int_{s(1-r)}^{s} [(s-z)+ns+(s(r-1)+z)]dz}{\int_o^{s(1-r)} (n+1)dz + \int_{s(1-r)}^{s} (n+2)dz}$$

$$\text{or } \bar{l}_n = \frac{Ls}{L+s}$$

$$\bar{l}_w = \frac{\int_o^{s(1-r)} [(s-z)^2+(n-1)s^2+(sr+z)^2]\,dz + \int_{s(1-r)}^{s} [(s-z)^2+ns^2+(s(r-1)+z)^2]\,dz}{\int_o^{s(1-r)} [(s-z)+(n-1)s+(sr+z)]\,dz + \int_{s(1-r)}^{s} [(s-z)+ns+(s(r-1)+z)]\,dz}$$

$$= s\left(1 - \frac{s}{3L}\right)$$

If the molecules have a homogeneous density, then the lengths are proportional to the molecular weight. The molecular weights of

very high molecular weight material ($\sim 10^6$) are very hard to measure. By slicing the rods at different intervals s, one can determine weight average molecular weights by light scattering. $\bar{l}_{w/s} = l - s/_3 L$ is a linear function of s with slope $-l/_3 L$. Thus $\bar{M}_{w/s}$ versus s will give a value for the molecular weight. (The linear plot will extrapolate to give ρ, the linear density, and have a slope of $-\rho/_{3M}$.) By slicing the material at smaller intervals, one can use colligative properties to determine a number average molecular weight. From osmotic pressure measurements, for example, as a function of the slice interval, a plot of $1/\bar{M}_n$ versus $1/_s$ should extrapolate linearly to $1/_M$ at the ordinate intercept.

Perhaps an ideal system for attempting this experiment would be paracrystalline TMV virus. This virus can be prepared as a dried gel (1 mm x 0.5 mm x 0.5 mm) which has two dimensional orientation (1, 2, 3, 4). The TMV virus is a rigid rod, macromolecular structure. As a dry gel, the viruses are oriented parallel to each other, but the ends are randomly distributed along the fiber axis. The viruses are packed hexagonally in the dry gel state.

The expected root mean square value of lengths is

$$l_{r.m.s} = s\sqrt{\frac{L - s/3}{L + s}}$$

I shall now outline how this result was obtained. As before we

assume the lengths of all rods the same and $L/s = n + r$. For $0 \leq l \leq sr$, we have two pieces less than s and $(n - 1)$ pieces s long. For $sr \leq l \leq s$ we have two pieces less than s and n pieces s long. Thus the distribution is constant for pieces $0 \leq l \leq s$ and at s it becomes like a "δ-function." Therefore the unnormalized distribution function, $f(l)$, is

$$f(l) = \begin{cases} \frac{1}{s} \left(\frac{2r + 2(1-r)}{(2n + 3)} \right) \\ \frac{(1-r)(n-1) + rn}{2n + 3} \, \delta(1-s); \quad l = s \end{cases} \qquad 0 \leq l \leq s$$

By normalization,

$$\int_0^s f(l)\, dl = 1/N = C_1 s + C_2$$

where $C_1 = \frac{2}{s} \left(\frac{r + (1-r)}{2n + 3} \right)$ and $C_2 = \frac{(1-r)(n-1) + rn}{2n + 3}$

The mean square length is thus

$$l^2_{mean} = N \int_0^s l^2 \left[C_1 + C_2 \delta (1-s) \right] dl.$$

Electron microscopy micrographs for sliced TMV would provide one with a number average length; one could also determine the root mean square length.

The slicing experiments are also promising for the analysis of genetic markers on DNA, a rod-like polymer which contains genetic information. If one selects a DNA which can be genetically assayed

and aligns the DNA molecules (by pulling fibers, for example), then the theory for the analysis of genetic marker frequency as a function of slice interval is relatively simple. It is assumed that the genetic markers are very thin discs on the rod-like DNA, that when sliced the molecules break "cleanly" at a pair of sugar-phosphate linkages, and that the genetic markers are incorporated by a replicating system with equal efficiencies. Two simple models have been assumed.

I. For model I it is assumed that DNA has polarity in the genetic sense and that one end of the molecule is necessary for incorporation. A. D. Kaiser has studied the genetic behavior of λ -DNA from the bacteriophage λ , by breaking the λ -DNA molecule in half with a Hershey stirring system (5,6). One interpretation of his results is that one end of the molecule is necessary for incorporation; Kaiser sees only one half of the "genetic map" occurring for λ -DNA that has been broken in half. Presumably the other half lacked a necessary "head-piece" to become incorporated. We therefore envision a DNA with three genetic markers in the oriented fiber as follows:

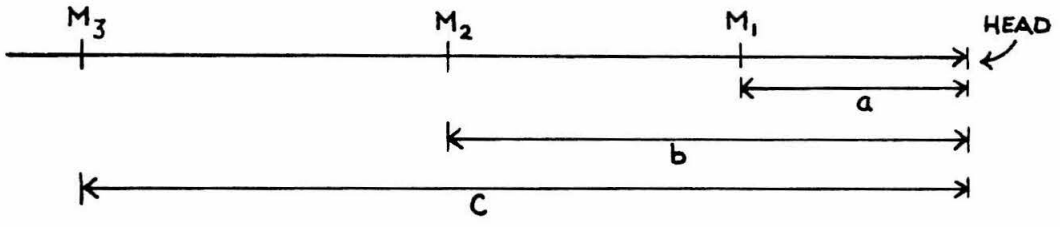

The "head" may be aligned in either direction along the fiber axis. The distance from the "head" to M_1 is a, to M_2 is b, and to M_3 is c. It is important that the "head" be attached to the marker; otherwise we assume no incorporation.

In a straight forward way it can be shown that the probability functions, normalized with respect to the total DNA, for the occurrence of markers as a function of s, the slice interval, are:

$$PM_1 = \begin{cases} 1-a/s & a \leq s \leq b \\ (b-a)/s & a \geq b \end{cases}$$

$$PM_1, M_2 = \begin{cases} 1-b/s & b \leq s \leq c \\ (c-b)/s & s \geq c \end{cases}$$

$$PM_1, M_2, M_3 = 1-c/s \qquad s \geq c$$

By following the frequency of genetic types (for this model we see only M_1, $M_1 + M_2$, and $M_1 + M_2 + M_3$) as a function of 1/s, we can determine the physical distances a, b, and c. Such a clean cut experiment would establish a map of genes on the DNA molecule by a physical criterion.

Recently, however, Simmons and Hogness have found that both pieces of half-broken λ -DNA will incorporate to show up with corresponding genetic traits, but one piece has only 3% of the activity of the other (6,7). Hence I present below a second model; it is assumed that all pieces of DNA can be assayed for genetic markers. By some method (a Hershey chromatographic column, for example) the sliced pieces

can be separated and relative efficiencies for genetic incorporation can be determined. The analysis below assumes that the relative efficiencies for genetic incorporation have been independently determined, and the frequency for genetic markers as a function of slicing interval s are correspondingly corrected to have unit efficiency for incorporation.

The DNA molecule, for the example here, has three markers, M_0, M_1, and M_2, which are separated by the respective distances a_1 and a_2. For the slice interval less than a_1, the smaller of the two spacings a_1 and a_2, the markers occur individually at a probability of 1/3 when normalized to the total occurrence of genetic traits.

At $a_1 \leq s \leq a_2$,

$$P_{M_2} = 1/3,\ P_{M_1} = P_{M_0} = a_{1/3s} \text{ and } P_{M_1 + M_2} = 2/3(1 - a_{1/s})$$

At $a_2 \leq s \leq a_1 + a_2$

$$P_{M_0} = a_{1/3s},\ P_{M_1} = 1/3\left(\frac{a_1 + a_2 - 1}{s}\right),\ P_{M_2} = a_{2/3s}$$

$$P_{M_2 + M_1} = 2/3(1 - a_{2/s}) \text{ and } P_{M_1 + M_0} = 1/3(1 - a_{1/s})$$

At $s \geq a_1 + a_2$

$$P_{M_1} = 0,\ P_{M_2} = a_{2/3s},\ P_{M_0} = a_{1/3s}$$

$$P_{M_1 + M_0} = 2/3\, a_{2/s},\ P_{M_1 + M_2} = 2/3\, a_{1/s} \text{ and } P_{M_1 + M_0 + M_2} = 1 - \frac{a_1 + a_2}{s}$$

A plot of the marker probabilities as a function of 1/s is:

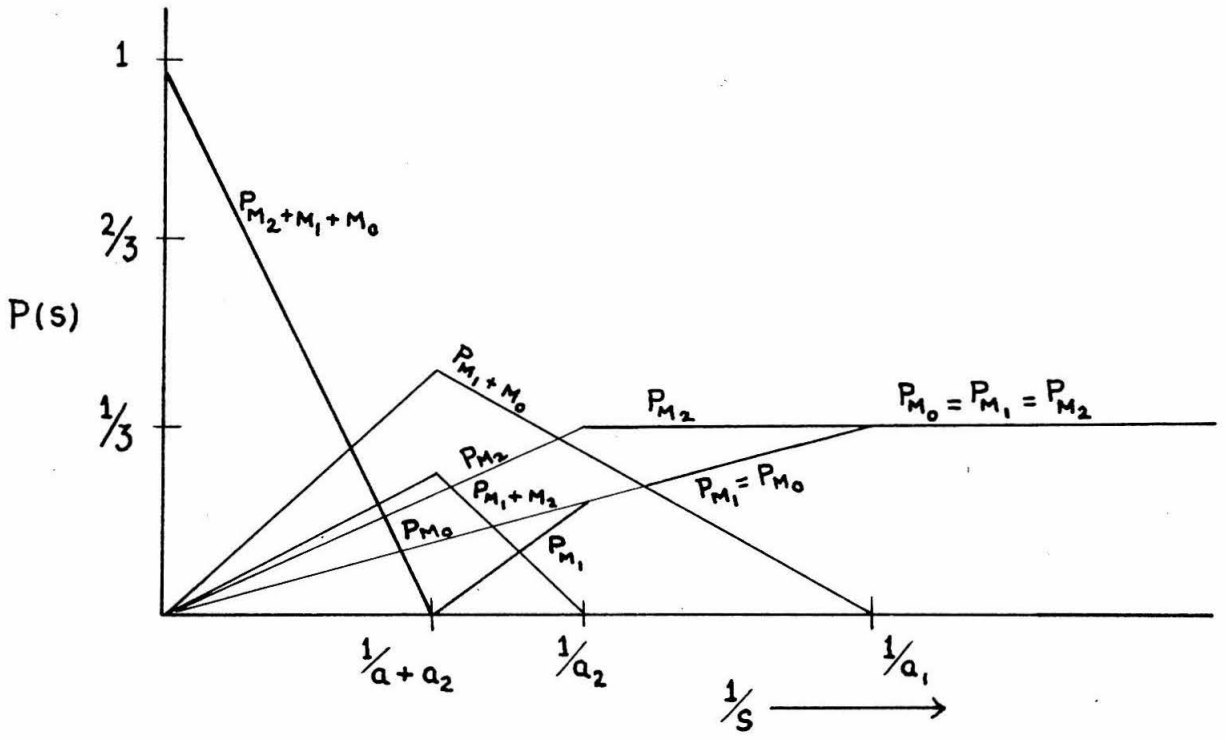

The various slopes of the linear plots and the discontinuity points suggest an ideal system for determining the physical separation of the several markers.

Case II. Rods of length l are dropped onto cutting edges at equal spacing s in a random fashion, i.e., all solid angles are equally probable. The polymer is now in a glassy state, but again the molecules are assumed to be rigid rods, all of length L. Consider projections of L's onto the z-axis.

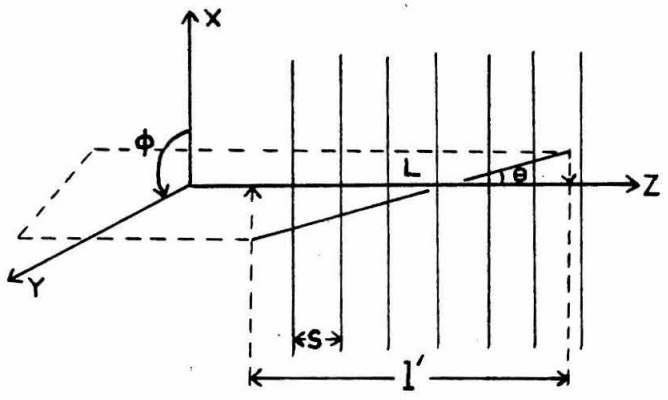

$L\cos\theta = l'/s = n+r$

For $\pi/2 \geq \theta \geq \cos^{-1} s/L$,

$n = 0$ and $\dfrac{L\cos\theta}{s} = r$

Distribution of Pieces

	Number	Length
(1) $\pi/2 \geq \theta \geq \cos^{-1} s/L$		
(a) $0 \leq z \leq s(1-r)$	1	$sr/\cos\theta$
(b) $s(1-r) \leq z \leq s$	1	$(s-z)/\cos\theta$
	1	$[z-s(1-r)]/\cos\theta$
(2) $\cos^{-1} s/L \geq \theta \geq 0$		
(a) $0 \leq z \leq s(1-r)$	1	$(s-z)/\cos\theta$
	n-1	$s/\cos\theta$
	1	$(sr+z)/\cos\theta$
(b) $s(1-r) \leq z \leq s$	1	$(s-z)/\cos\theta$
	n	$s/\cos\theta$
	1	$[s(r-1)+z]/\cos\theta$

$$\therefore \bar{l}_n = \frac{2\int_0^{2\pi} d\varphi \int_{\pi/2}^{\cos^{-1}s/L} \frac{\sin\theta\, d\theta}{\cos\theta} \left[\int_0^{s(1-r)} sr\,dz + \int_{s(1-r)}^{s} [(s-z)+z-s(1-r)]\,dz\right]}{2\int_0^{2\pi} d\varphi \int_{\pi/2}^{\cos^{-1}s/L} \sin\theta\, d\theta \left[\int_0^{(1-r)} dz + \int_{s(1-r)}^{s} 2dz\right]}$$

$$+ \frac{2\int_0^{2\pi} d\varphi \int_{\cos^{-1}s/L}^{o} \frac{\sin\theta}{\cos\theta} d\theta \left[\int_0^{s(1-r)} [(s-z)+(n-1)s+(sr+z)]\,dz + \int_{s(1-r)}^{s} (ns+rs)\,dz\right]}{2\int_0^{2\pi} d\varphi \int_{\cos^{-1}s/L}^{o} \sin\theta d\theta \left[\int_0^{s(1-r)} (n+1)\,dz + \int_{s(1-r)}^{s} (n+z)\,dz\right]}$$

$$= \frac{2Ls}{L+2s}$$

Similarly,

$$\bar{l}_w = s\left[(1/3)\, s/L + \tfrac{1}{2} + \log_e L/s\right]$$

The results indicate that a number average molecular weight experiment is better suited for simple intepretation. A plot of $1/\bar{M}_n$ versus $1/s$ should extrapolate linearly to $1/M$ with a slope of $\frac{1}{2}\rho$ where ρ is the linear density. The transcendental expression for the weight average length demands an exacting experiment and knowledge of L. For small slice intervals the dependence goes as $s \log_e L/s$ and for relatively large slice intervals the weight average dependence goes as $(1/3)\, s^2/L$.

Case III. Consider the realistic problem of a distribution of rods about the z-axis with a probability distribution function $p(\theta)$. The

azimuth about z is equally probable. One would expect some sort of density distribution about the z-axis (fiber axis) for pulled fibers of rigid rod macromolecules.

Suppose a fiber is pulled under equilibrium conditions. The rods experience a torque which is proportional to L sin θ . The energy to align the rod goes as -L cos θ . A Boltzmann-like distribution for the rods, therefore, is proportional to $e^{K \cos \theta}$, where K is a constant characteristic of the temperature and of the forces exerted on the molecular rods during fiber pulling.

$$\therefore p(\theta) = \frac{K}{4\pi(e^{K}-1)} \; e^{K|\cos\theta|}$$

is considered to be the normalized distribution function for the rods. The number average length becomes,

$$\bar{l}_n = \frac{Ls}{L\left[\frac{Ke^{K} - e^{K} + 1}{K(e^{K}-1)}\right] + s} = \frac{Ls}{Lf(K) + s}$$

The weight average expression is

$$\bar{l}_w = \frac{K}{e^{+K}-1}\, s \left\{ \left[1 + \tfrac{1}{3}(L/s)K\right]\left(\sum_{n=1}^{\infty} \frac{K^n[1 - (s/L)^n]}{nn!} + \log_e L/s \right) \right.$$

$$+ e^{Ks/L}\left(L/sK - \frac{L^2}{3s^2}\,\frac{(Ks/L - 1)}{K^2} - \tfrac{1}{3}\right)$$

$$\left. + \tfrac{1}{3}(s/L)e^{K} - L/sK - L^2/3s^2K^2 \right\}$$

A number average molecule weight experiment is desirable. The limits for f(K) are between 1 and $\frac{1}{2}$. $\lim_{K \to \infty} f(K) = 1$ where the rods are constrained to the z-axis. $\lim_{K \to 0} f(K) = \frac{1}{3}$ where the rods have equally probable solid angles. These two limits satisfy the expressions for Case I and Case II respectively. If one can independently determine the linear density of the polymer, then a plot of $1/\bar{M}_n$ versus $1/s$ will determine K, the constant characteristic to the distribution $p(\theta)$.

A more sharply peaked, normalized distribution function is

$$p(\theta) = \frac{1}{4\pi} \quad \frac{1}{e^{-a} - \sqrt{\pi a} + \sqrt{a}\,\Gamma(a)(-\frac{1}{2})} \quad e^{-\frac{a}{\cos^2\theta}}$$

where $$\Gamma(a)(-\tfrac{1}{2}) = \int_0^a y^{-\frac{1}{2}} e^{-y}\, dy$$

is an incomplete gamma function. The number average expression is

$$\bar{l}_n = \frac{Ls}{\left(\dfrac{e^{-a} - a\left\{-E_i(-a)\right\}}{e^{-a} - \sqrt{\pi a} + \sqrt{a}\,\Gamma(a)(-\frac{1}{2})} \right) \cdot L/2 + s}$$

where $\left\{-E_i(-a)\right\} = \int_a^\infty z^{-1} e^{-z}\, dz$

is a tabulated exponential integral.

The predicted weight average is a considerably more complicated expression.

$$\bar{l}_{w/s} =$$

$$\frac{\frac{1}{6}\left\{-E_i(-a)\right\} - \left(\frac{aL^2}{6s^2} + \frac{1}{6}\right)\left\{-E_i(-a\sqrt{L/s})\right\} + \left(L/s - \frac{s}{6L(a)^{\frac{1}{2}}}\right)\left[a\sqrt{L/s}\,(-\tfrac{1}{2})\right]}{e^{-a} - \sqrt{\pi a} + \sqrt{a}\left[a\,(-\tfrac{1}{2})\right]}$$

$$+ \frac{(L/s)^{\frac{3}{4}} e^{-a\sqrt{L/s}} - L/s\sqrt{\pi a} - 1/6\,(L/s)^{3/2}\, e^{-a\sqrt{L/s}}}{e^{-a} - \sqrt{\pi a} + \sqrt{a}\left[a\,(-\tfrac{1}{2})\right]}$$

The number average experiment is the obvious choice. The point here is that slicing experiments cannot determine a unique distribution for the rods in a fiber. One must understand a specific mechanism for orientation before he can put confidence into the slicing experiment as a means for determining a distribution parameter.

REFERENCES

1. J. D. Bernal and J. Frankuchen, J. Gen. Physiology, 25, 111-146 (1941).
2. J. D. Watson, Biochim. et Biophys. Acta, 13, 10-19 (1954).
3. D. L. D. Caspar, Nature, 177, 928 (1956).
4. R. E. Franklin, Nature, 175, 379 (1955); ibid., 177, 929 (1956).
5. A. Hershey and E. Burgi, J. Mol. Biol., 2, 143-152 (1960). (This is reference to breakage by stirring.)
6. A. D. Kaiser, J. Mol. Biol., 4, 275-287 (1962).
7. A. D. Kaiser, ibid., 285. J. Weigle, private communication.

PROPOSITION VI

The six parameter problem for the resolution of two Gaussians is presented below. The three parameter problem for the resolution of two equal Gaussians has been solved and a computer program written for the least squares analysis of the problem. It is proposed that the latter analysis be employed for the treatment of data from density gradient, sedimentation equilibrium experiments which have been used to look for strand separation of DNA.

The general problem of the resolution of two Gaussians is of interest to people carrying out density gradient, sedimentation equilibrium experiments. It has been shown that macromolecules of homogeneous density and molecular weight will band with a Gaussian distribution about a buoyant density position in a three component system (1). The band width is proportional to $1/(M)^{\frac{1}{2}}$ where M is the molecular weight of the macromolecule. The question of two species has often come up in density gradient studies. (In many cases there is also the problem of more than two species.) For certain conditions the resolution of two Gaussians with arbitrary amplitudes and band widths has been considered and solved (2). Two criteria for resolution were considered. One condition was that the respective maxima of the two Gaussians be distinct; the other that the distribution has at least four inflection points; i.e., one Gaussian manifests itself as a shoulder.

Although a system is "unresolved" by our criteria, if one has a system in which he knows that there are two species, then the general resolution of the respective Gaussians is in principle solvable.

I have considered the problem in detail and present the results below. I will outline the general six parameter problem (two amplitudes, two band widths, and two positions) and show how it is solvable in principle, but in practice I have not been able to find a convenient solution. A solution for the case of equal band widths, but different amplitudes and positions is outlined below. It is very likely that a better method can be found. The case of equal amplitudes and band widths, but different positions, has been solved and a generalized least squares analysis carried out. I have written an IBM 7090 computer program for this last case and will gladly leave it with anyone who is interested in the problem. The last case is particularly useful for density gradient studies of "strand-separation" for DNA. If one treats DNA with a strong base, at pH 11, most of the thymine and guanine in the molecule will be titrated (3). The hydrogen bonded structure will be disrupted. To the extent that each of the two strands has a different density, the strands will move to their corresponding densities. The single Gaussian distribution for the native molecule will now broaden and become a sum of the two Gaussians characteristic for each strand. Each strand should be essentially the same in molecular weight and the ultraviolet absorption for each should be almost identical. Thus the two new

Gaussians have equal band widths and equal amplitudes. In order to carry out a least squares analysis for this experiment, the original DNA must be very homogeneous and breakage of the strands by action with base must be minimal. T-7 DNA is highly homogeneous (4) and could very well be an ideal material to look for strand separation with the kind of analysis discussed above.

The non-interacting Gaussians are written as

$$G(x) = A_1 e^{-\frac{(x-a_1)^2}{2\sigma_1^2}} + A_2 e^{-\frac{(x-a_2)^2}{2\sigma_2^2}} .$$

One way to generate six independent equations for the six parameters, a_1, a_2, σ_1, σ_2, A_1, and A_2, is to evaluate integrals of the type

$$\int_{-\infty}^{\infty} x^n G(x)\, dx \qquad \text{for } n = 0 \text{ to } n = 5 .$$

Define

$$I_n = \frac{1}{\sqrt{2\pi}} \int_{-\infty}^{\infty} x^n G(x)\, dx$$

Then,

$$I_0 = A_1\sigma_1 + A_2\sigma_2$$

$$I_1 = a_1A_1\sigma_1 + a_2A_2\sigma_2$$

$$I_2 = A_1\sigma_1 (\sigma_1^2 + a_1^2) + A_2\sigma_2 (\sigma_2^2 + a_2^2)$$

$$I_3 = A_1a_1\sigma_1 (3\sigma_1^2 + a_1^2) + A_2a_2\sigma_2 (3\sigma_2^2 + a_2^2)$$

$$I_4 = A_1\sigma_1 (3\sigma_1^4 + 6\sigma_1^2a_1^2 + a_1^4) + A_2\sigma_2 (3\sigma_2^4 + 6\sigma_2^2a_2^2 + a_2^4)$$

$$I_5 = A_1a_1\sigma_1 (15\sigma_1^4 + 10\sigma_1^2a_1^2 + a_1^4) + A_2a_2\sigma_2(15\sigma_2^4 + 10\sigma_2^2a_2^2 + a_2^4)$$

It is difficult to solve these six equations simultaneously for the six parameters. Another form for the sum of the two Gaussians may be written

$$G(x) = P_1 Q_1^{\,x} R_1^{\,x^2} + P_2 Q_2^{\,x} R_2^{\,x^2}$$

Then $G(0) = P_1 + P_2$

$$G(1) = P_1 Q_1 R_1 + P_2 Q_2 R_2 \qquad G(-1) = \frac{P_1 R_1}{Q_1} + \frac{P_2 R_2}{Q_2}$$

$$G(2) = P_1 Q_1^{\,2} R_1^{\,4} + P_2 Q_2^{\,2} R_2^{\,2} \qquad G(-2) = \frac{P_1 R_1^{\,4}}{Q_2^{\,2}} + \frac{P_2 R_2^{\,4}}{Q_2^{\,2}}$$

It is also difficult to solve for P's, Q's, and R's from these equations. By using the first three simple equations of each kind, one might hope for an easy solution. But the transcendental relationship between P's, Q's, and R's and the A's, σ's, and a's does not afford a simplification. The general relationship

$$\int_{-\infty}^{\infty} (x-x_o)^n G(x)dx = I_n - n x_o I_{n-1} + \frac{n(n-1)}{2!} x_o^{\,2} I_{n-2}$$

$$+ \cdots \frac{+(-1)^r n!}{(n-r)!\,r!} x_o^{\,r} I_{n-r} + \cdots + I_o x_o^{\,n}$$

may be useful. A choice of x_0 can make one of the integrals with an odd power of $x' = (x-x_0)$ vanish. It is not obvious, however, which of the three odd power integrals will afford a simplification by choosing an

x_0 such that

$$I'_{2n+1} = \int_{-\infty}^{\infty} (x-x_0)^{2n+1} G(x)\, dx = 0, \text{ for } n = 0, 1, \text{ or } 2.$$

This last possibility has not been belabored.

For the case of $\sigma_2 = \sigma_1$, a considerable simplification is introduced. The integral expressions now become

$$I_0 = (A_1 + A_2)\sigma$$

$$I_1 = (A_1 a_1 + A_2 a_2)\sigma$$

$$I_2 = [A_1 a_1 (3\sigma^2 + a_1^2) + A_2 (\sigma^2 + a_2^2)]\sigma$$

$$I_3 = [A_1 a_1 (3\sigma^2 + a_1^2) + A_2 a_1 (3\sigma^2 + a_2^2)]\sigma$$

$$I_4 = [A_1 (3\sigma^4 + 6\sigma^2 a_1^2 + a_1^4) + A_2 (3\sigma^4 + 6\sigma^2 a_2^2 + a_2^4)]\sigma$$

We may also use the relationships

$$I_1(x_0) = I_1 - x_0 I_0$$

$$I_2(x_0) = I_2 - 2x_0 I_1 + x_0^2 I_0$$

$$I_3(x_0) = I_3 - 3x_0 I_2 + 3x_0^2 I_1 - x_0^3 I_0$$

$$I_4(x_0) = I_4 - 4x_0 I_3 + 6x_0^2 I_2 - 4x_0^3 I_1 + x_0^4 I_0$$

where

$$I_n(x_0) = \int_{-\infty}^{\infty} (x - x_0)^n G(x)\, dx .$$

We choose $x_0 = \dfrac{a_1 + a_2}{2}$, <u>i.e.</u>, $(a_1 - x_0) = -(a_2 - x_0)$.

Then

$$I_1(x_0) = (A_1 - A_2)a\sigma \text{ , where } a = a_1 = -a_2.$$

$$I_2(x_0) = (A_1 + A_2)\sigma^3 + (A_1 + A_2)a^2\sigma$$

$$= I_0(\sigma^2 + a^2)$$

$$I_3(x_0) = (3\sigma^2 + a^2)(A_1 - A_2)a\sigma$$

$$= I_1(x_0)\,(3\sigma^2 + a^2)$$

If x_0 can be determined, then the solution for a, σ, A_1, and A_2 is immediate. From $I_2(x_0)$ and $I_3(x_0)$ we may easily get expressions for a^2 and σ^2. We then substitute into $I_4(x_0) = I_0(3\sigma^4 + 6a^2\sigma^2 + a^4)$ for a^2, σ^2 expressions. The result is

$$4I_4(x_0)I_1^2(x_0)I_0 = 3[I_3(x_0)I_0 - I_2(x_0)I_1(x_0)]^2$$

$$+ 6[I_3(x_0)I_0 - I_2(x_0)I_1(x_0)][3I_2(x_0)I_1(x_0) - I_3(x_0)I_0]$$

$$+ [3I_2(x_0)I_1(x_0) - I_3(x_0)I_0]^2$$

By substituting the $I_n(x_0)$'s with the polynomial expansions in x_0 and I_n's, we get a sixth order polynomial in x_0. With the appropriate root, then, the parameters a, σ, A_1, and A_2 can be determined.

The analysis of the two Gaussians with equal amplitudes and band widths is now presented. Since the two Gaussians are equal, the center of gravity position $\bar{x}$ will be the origin of the system such that

$$G(x') = A\left[e^{-(x' + a)^2/2\sigma^2} + e^{-(x' - a)^2/2\sigma^2}\right]$$

where $x' = x - \bar{x}$. Therefore, we first locate the origin $\bar{x}$.

$$\bar{x} = \frac{\int_{-\infty}^{\infty} xG(x)\,dx}{\int_{-\infty}^{\infty} G(x)\,dx}$$

and define the new coordinate $x' = x - \bar{x}$.

We next solve for a first approximation of the parameters A, a, and σ.

$$I_0 = A\sigma$$

$$I_2 = A\sigma(\sigma^2 + a^2) = I_0(\sigma^2 + a^2)$$

$$I_4 = A\sigma\left[3(\sigma^2 + a^2)^2 - 2a^4\right] = I_0\left[3(I_2/I_0)^2 - 2a^4\right]$$

$$I_n = \frac{1}{\sqrt{2\pi}} \int_{-\infty}^{\infty} x'^n G(x')\,dx'$$

$$\therefore \quad a_0 = \sqrt[4]{\tfrac{1}{2}\left[3(I_2/I_0)^2 - I_4/I_0\right]}$$

$$\sigma_0^2 = I_2/I_0 - \sqrt{\tfrac{1}{2}\left[3(I_2/I_0)^2 - I_4/I_0\right]}$$

$$A_0 = I_0 \Big/ \sqrt{I_2/I_0 - \sqrt{\tfrac{1}{2}\left[3(I_2/I_0)^2 - I_4/I_0\right]}}$$

The subscripts zero refer to first order approximations.

With the parameters approximated to first order, we now

proceed to a generalized least squares analysis (5).

A convenient form for the overall distribution function G(x) is

$$y = PR^{x'^2}(Q^{-x'} + Q^{+x'})$$

where

$$P = Ae^{-a^2/2\sigma^2}; \quad Q = e^{a/\sigma^2}; \quad R = e^{-1/2\sigma^2}.$$

To first approximation

$$P_0 = A_0 e^{-a_0^2/\sigma_0^2}$$

$$Q_0 = e^{a_0/\sigma_0^2}$$

$$R_0 = e^{-1/2\sigma_0^2}$$

Let n be the number of measured ordered pairs, $(X_i Y_i)$ $(i = 1, 2, \ldots, n)$.

Then $F^h = y_h - PR^{x_h^2}(Q^{-x_h} + Q^{+x_h}) = 0; \quad h = 1, 2, \ldots n,$

where y_h and x_h are the calculated points for the determined parameters P, Q, and R. Let

$$x_i = X_i - Vx_i$$

$$y_i = Y_i - Vy_i$$

$$P = P_0 - p$$

$$Q = Q_0 - q$$

$$R = R_0 - r$$

Now we Taylor expand F^h about x_i, y_i, P, Q, and R. Then

$$\sum_i \frac{\partial F^h}{\partial y_i} \cdot Vy_i + \sum_i \frac{\partial F^h}{\partial x_i} \cdot Vx_i + \frac{\partial F^h}{\partial P} \cdot p + \frac{\partial F^h}{\partial Q} \cdot q$$

$$+ \frac{\partial F^h}{\partial R} \cdot r = F^h$$

We approximate

$$F^h \approx Y_i - P_0 R_0^{X_i} (Q_0^{-X_i} + Q_0^{+X_i}) \equiv F_0^h$$

By least squares,

$$\delta = \Sigma W \cdot res^2$$

or $$\frac{1}{2}\delta S = \Sigma W V \delta V = 0 .$$

The variations of the residuals, δV, must satisfy the n Taylor expansions above. By using La Grange's multipliers we solve for p, q, and r. The solutions are:

$$p = (\Sigma F_0^i \frac{\partial F^i}{\partial P} / L_i) \Delta_{1,1}^{-1} + (\Sigma F_0^i \frac{\partial F^i}{\partial Q} / L_i) \Delta_{1,2}^{-1} + (\Sigma F_0^i \frac{\partial F^i}{\partial R}) \Delta_{1,3}^{-1}$$

$$q = (\Sigma F_0^i \frac{\partial F^i}{\partial P} / L_i) \Delta_{2,1}^{-1} + (\Sigma F_0^i \frac{\partial F^i}{\partial Q} / L_i) \Delta_{1,2}^{-1} + (\Sigma F_0^i \frac{\partial F^i}{\partial R}) \Delta_{1,3}^{-1}$$

$$r = (\Sigma F_0^i \frac{\partial F^i}{\partial P} / L_i) \Delta_{3,1}^{-1} + (\Sigma F_0^i \frac{\partial F^i}{\partial Q} / L_i) \Delta_{3,2}^{-1} + (\Sigma F_0^i \frac{\partial F^i}{\partial R}) \Delta_{3,3}^{-1}$$

where $$L_i = \frac{\frac{\partial F}{\partial x}(X_i, Y_i, P_0, Q_0, R_0)}{W_{X_i}} + \frac{\frac{\partial F}{\partial y}(X_i, Y_i, P_0, Q_0, R_0)}{W_{Y_i}}$$

and Wx_i and Wy_i are the weights for the corresponding points X_i, Y_i. The Δ^{-1}_{ij} are the inverse matrix elements of the matrix

$$\Delta = \begin{vmatrix} \Sigma \frac{1}{L_i} \left(\frac{\partial F_i}{\partial P}\right)^2 & \Sigma \frac{\partial F_i}{\partial P} \frac{\partial F_i}{\partial Q} / L_i & \Sigma \frac{\partial F_i}{\partial P} \frac{\partial F_i}{\partial R} / L_i \\ \Sigma \frac{\partial F_i}{\partial Q} \frac{\partial F_i}{\partial P} / L_i & \Sigma \left(\frac{\partial F_i}{\partial Q}\right)^2 / L_i & \Sigma \frac{\partial F_i}{\partial Q} \frac{\partial F_i}{\partial R} / L_i \\ \Sigma \frac{\partial F_i}{\partial R} \frac{\partial F_i}{\partial P} / L_i & \Sigma \frac{\partial F_i}{\partial R} \frac{\partial F_i}{\partial Q} / L_i & \Sigma \left(\frac{\partial F_i}{\partial R}\right)^2 / L_i \end{vmatrix}$$

The standard deviations of the parameters a, σ, and A are calculated from the inverse matrix elements in the usual way.

For the computer program I have assumed that a first approximation is adequate for the least squares analysis. If a second approximation is needed, then the data are probably too crude for the detailed analysis above.

REFERENCES

1. Cf. John E. Hearst and Jerome Vinograd, Proc. Nat. Acad. Sci., 47, 999-1025 (1961).
2. W. Huber, R. Stewart and J. Vinograd, unpublished work.
3. J. Morris, J. Vinograd, N. Davidson and W. Dove, Proc. Nat. Acad. Sci., in press.
4. J. Vinograd, private communication.
5. W. E. Deming, Statistical Adjustment of Data. John Wiley & Sons, Inc., New York, 1943, pp. 49-58.